Towards a

Unified Theory of Sensor Pattern Noise

An analysis of Dark Current, Lens effects and Temperature Bias in CMOS Image Sensors.

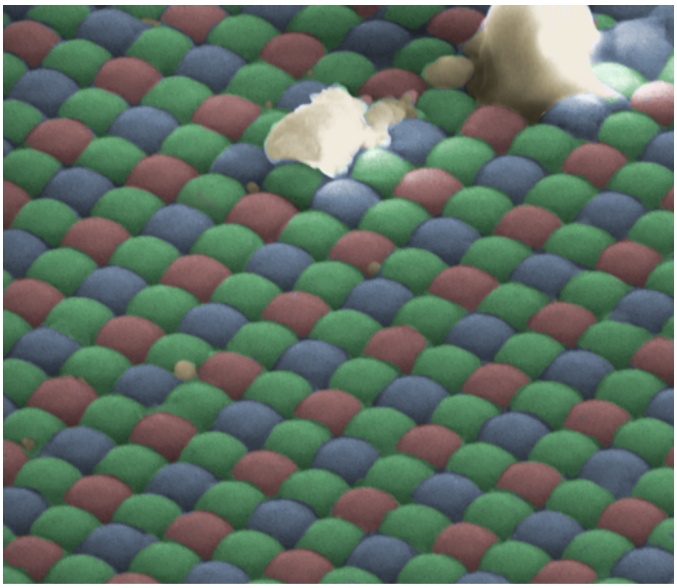

Mr. Richard Henry Edwin Matthews

Bachelor of Engineering (Electrical and Electronic, Honours),
University of Adelaide, 2014

Thesis submitted for the degree of
Doctor of Philosophy
in
Electrical and Electronic Engineering
University of Adelaide

8 March 2019

THE UNIVERSITY
of ADELAIDE

Title Page Image: A Sony IMX2019PQ image sensor displays dust build up under a scanning electron microscope at 9982x magnification (Colourised). Photo credit to Richard Matthews using the facilities, and the scientific and technical assistance, of the Australian Microscopy and Microanalysis Research Facility at Adelaide Microscopy, the University of Adelaide.

"Wherever he steps, whatever he touches, whatever he leaves, even unconsciously, will serve as a silent witness against him. Not only his fingerprints or his footprints, but his hair, the fibers from his clothes, the glass he breaks, the tool mark he leaves, the paint he scratches, the blood or semen he deposits or collects. All of these and more, bear mute witness against him. This is evidence that does not forget. It is not confused by the excitement of the moment. It is not absent because human witnesses are. It is factual evidence. Physical evidence cannot be wrong, it cannot perjure itself, it cannot be wholly absent. Only human failure to find it, study and understand it, can diminish its value."

- Paul L. Kirk

Contents

Citation Listing **ix**

Abstract **xi**

Declaration **xiii**

Acknowledgements **xv**

List of Figures **xvii**

List of Tables **xviii**

Symbols and Definitions **xxi**

1 Introduction **1**
1.1 Context 1
1.2 Motivation 2
1.3 Aim and Scope 3
1.4 Significance 4
1.5 Overview 6

2 Background **9**
2.1 Image Sensor Fundamentals 9
2.2 Sensor Pattern Noise Extraction Process 20

3 Literature Review **23**
3.1 The Blind Camera Identification Problem 23
3.2 Forensic Implications of the Physical Image Pipeline 25
3.3 Forensic Implications of the Digital Image Pipeline 31
3.4 Forensic Implications of the Image Environment 32
3.5 Conclusion 33

4 Rethinking Image Sensor Noise for Forensic Advantage: An Exploratory Study 35
4.1 Abstract . . . 35
4.2 Introduction . . . 36
4.3 Basic operation of an Image Sensor . . . 37
4.4 Rethinking the noise model for Forensic Advantage . . . 39
4.5 Micrometer Imagery . . . 48
4.6 Conclusion . . . 51

5 Reverse Engineering the Raspberry Pi Camera V2: A study of Pixel Non-Uniformity using a Scanning Electron Microscope 55
5.1 Abstract . . . 55
5.2 Introduction . . . 55
5.3 Related Work . . . 56
5.4 Research Methodology . . . 58
5.5 Data Collection and Analysis . . . 60
5.6 Discussion . . . 68
5.7 Conclusion and Future Work . . . 69

6 An Analysis of Optical Contributions to a Photo-Sensor's Ballistic Fingerprints 73
6.1 Abstract . . . 73
6.2 Introduction . . . 74
6.3 Background . . . 76
6.4 Methods . . . 81
6.5 Results and Discussion . . . 83
6.6 Conclusion . . . 90

7 Thermal Effects of Dark Current on Blind Source Camera Identification 95
7.1 Abstract . . . 95
7.2 Introduction . . . 96
7.3 Related Work . . . 97
7.4 Research Methodology . . . 101
7.5 Data Collection and Analysis . . . 104
7.6 Discussion . . . 110
7.7 Conclusion and Future Work . . . 112

8 Discussion 115
8.1 Introduction . . . 115
8.2 Applied Signal Processing Theory - A new model for Pixel Non Uniformity . . . 115
8.3 Forensic Indicators from Process Variations . . . 118

8.4 Specific Forensic Indicator Findings 119
8.5 Conclusion 121

9 Conclusion **123**

Bibliography **124**

Citation Listing

This is a thesis conducted by mixed publication and dissertation style. Figures and Tables are faithfully reproduced as they would appear in a published work. However, acknowledgements have been condensed into a single section at the start of this work, a single bibliography is provided at the end and references to future work, where conducted as a separate study, but, included in this thesis, have been edited for clarity and flow.

The following publications appear in this work:

Chapter 5	Matthews, R., Sorell, M., & Falkner, N. (n.d.). A Visual Analysis of Pixel Non Uniformity using a Scanning Electron Microscope.
Chapter 6	R. Matthews, M. Sorell, & N. Falkner, "An Analysis of Optical Contributions to a Photo-Sensor's Ballistic Fingerprints," *Digital Investigation*, vol. 28, pp 139-145, 2019. [Online]. Available: https://doi.org/10.1016/j.diin.2019.02.002
Chapter 7	Matthews, R., Sorell, M., & Falkner, N. (n.d.). Thermal Effects of Dark Current of Blind Source Camera Identification.

The following publications are also based on this work, but do not appear in the text:

i Matthews, R. H., Sorell, M., & Falkner, N. (2019) Isolating lens effects from source camera identification using sensor pattern noise, Australian Journal of Forensic Sciences, DOI: 10.1080/00450618.2019.1569133

ii Matthews, R. H., Sorell, M., & Falkner, N. (2018). Isolating Lens Effects from Source Camera Identification using Photo-Response Non-Uniformity Noise. In 24th International Symposium of the Australian and New Zealand Forensic Science Society. Perth, Australia.

iii Matthews, R. H., Sorell, M., & Falkner, N. (2018). Thermal Effects of Dark Current on Blind Source Camera Identification. In Proceedings of the 4th Interdisciplinary Cyber Research Workshop 2018 (pp. 37-41). online: Tallinn University of Technology.

iv Matthews, R., Sorell, M., & Falkner, N. (2017). Isolating Lens Aberrations within Fixed Pattern Noise. In Proceedings of the 3rd Interdisciplinary Cyber Research Workshop 2017 (pp. 21-24). online: Tallinn University of Technology.

Abstract

Matching images to a discrete camera is of significance in forensic investigation. In the case of digital images, forensic matching is possible through the use of sensor noise present within every image. There exist misconceptions, however, around how this noise reacts under variables such as temperature and the use of different lens systems. This study aims to formulate a revised model of the additive noise for an image sensor to determine if a new method for matching images to sensors could be created which uses fewer resources than the existing methods, and takes into account a wider range of environmental conditions. Specifically, a revised noise model was needed to determine the effects of different lens systems and the impact of temperature on sensor noise.

To determine the revised model, an updated literature search was conducted on the background theory relating to CMOS sensors, as the existing work focuses on CCD imaging sensors. This theory was then applied using six off the shelf CMOS imaging sensors with integrated lens systems. An image sensor was examined under scanning electron microscopy and through the use of Energy-dispersive x-ray spectroscopy the non-uniform structure of individual pixels was visually observed within the sensor. The lens systems were removed and made interchangeable through the use of a 3D printed camera housing. Lens effects were assessed by swapping lens systems between the cameras and using a pinhole lens to remove all optical effects. The temperature was controlled using an Arduino controlled Peltier plate device, and dark current images were obtained at different temperatures using a blackout lens.

It was observed that dark current could be used to identify the temperature of the image sensor at the time of acquisition, contrary to the statements in existing literature that sensor pattern noise is temperature invariant. It was shown that the lens system contributes approximately a quarter of the signal power

used for pattern matching between the image and sensor. Moreover, through the use of targeted signal processing methods and simple ”Goldilocks” filters processing times could be reduced by more than half by sacrificing precision without losing accuracy.

This work indicates that sensor pattern noise, while already viable for forensic identification of images to a specific camera, can also be used for identification of an image to a specific lens system and an image sensors temperature. It has also shown that a tool using sensor pattern noise may have a viable future as a forensic method of triage when confronted with large image data sets. Such additional information could prove effective for forensic investigators, intelligence agencies and police when faced with any form of crime involving imaging technology such as fraud, child exploitation or terrorism.

Declaration

I certify that this work contains no material which has been accepted for the award of any other degree or diploma in my name in any university or other tertiary institution and, to the best of my knowledge and belief, contains no material previously published or written by another person, except where due reference has been made in the text. In addition, I certify that no part of this work will, in the future, be used in a submission in my name for any other degree or diploma in any university or other tertiary institution without the prior approval of the University of Adelaide and where applicable, any partner institution responsible for the joint award of this degree.

The author acknowledges that copyright of published works contained within this thesis resides with the copyright holder(s) of those works. I give permission for the digital version of my thesis to be made available on the web, via the University's digital research repository, the Library Search and also through web search engines, unless permission has been granted by the University to restrict access for a period of time.

I acknowledge the support I have received for my research through the provision of an Australian Government Research Training Program Scholarship.

Mr Richard Matthews B.Elec(Hons) GradIEAust

Date:

Acknowledgements

There is a vast list of people without whom this thesis would not have been written, and to whom I am forever indebted.

Firstly, to Tegan for encouraging and persevering alongside me during this three and a half year journey while also looking after her own studies. Without your love and daily support this would not have been possible.

To my Supervisors Dr Matthew Sorell and Associate Professor Nickolas Falkner for their late night emails, lengthy discussions, numerous glasses of wine and countless hours of advice both here and in Estonia. The mentoring and friendships developed over the last four years have cemented my love for the academy.

To Cate Jerram for her final edits on the draft.

To my Children. May this inspire you also.

For the assistance provided by Ian Linke and his team in the ECMS and School of Electrical and Electronic Engineering Workshops, particularly those of Alban O'Brien. Through technical challenges it was still possible to manufacture the equipment needed for the work to be done.

And to Professor Matt Roughan for his insight and suggestion to use a pinhole lens.

Finally, formal acknowledgements is extended to the follow organisations for the work or sponsorship received in crafting this thesis.

- The OptoFab node of the Australian National Fabrication Facility, utilising NCRIS and (NSW) state government funding for provision of laser drilling services.
- The supercomputing resources provided by the Phoenix HPC service at the University of Adelaide.
- The facilities, the scientific and technical assistance, of the Australian Microscopy and Microanalysis Research Facility at Adelaide Microscopy, the University of Adelaide.
- The Australian Federal Government, this work was sponsored through the provision of an Australian Government Research Training Program Scholarship.

List of Figures

2.1 Modern Digital Camera. 11
2.2 The “Bucket Brigade” analogy of the CCD Senor. 12
2.3 A breakdown of the CCD sensor. 13
2.4 A breakdown of the APS CMOS sensors. 13
2.5 FSI fabrication process. 14
2.6 BSI fabrication process. 15
2.7 Difference between TSV and DBI 16
2.8 Stacked image sensors 16
2.9 Graphical example of an OPC sensor in comparison to a FIS. . . 18
2.10 OPC readout circuitry. 19

3.1 The Image Pipeline 26
3.2 Sony IMX219 Dual Anstigmat Lens 30

4.1 The structure of a Pinned Photo Diode CMOS Image Sensor . . 38
4.2 Shared Pixel Concept 38
4.3 The Image Pipeline 40
4.4 New Additive Noise Model 41
4.5 Shared Pixel CIS with CFA and Microlens 42
4.6 Lens effects vs Pinhole for a Single Row 44
4.7 Pinhole reference pattern compared with a Lens reference pattern 46
4.8 Platinum deposit on CIS 49
4.9 Excavated CIS 49
4.10 Micrometer imagery of Sony IMX219PQ 50

5.1 SEM Microscope Excavation Process 59
5.2 A horizontal cross-section of the IMX219PQ sensor 61
5.3 A secondary cross-section of the IMX219PQ sensor. 62
5.4 The equivalent circuit for the IMX219PQ pixel unit. 62
5.5 The length of six transfer gates. 63
5.6 SEM Microscope Excavation Process 65
5.7 Sectioning the top lens layer of the Image sensor IC. 66
5.8 Four photodiodes compared for length 67

6.1 The noise model proposed in our work 75
6.2 Lukáš *et al* noise model 77
6.3 Noise Residue Model 80
6.4 Overlapping Edge Removal Method 82
6.5 All Cameras with Dark Current 83
6.6 Pinhole Image Sets with Dark Current 84
6.7 All Cameras without Dark Current 86
6.8 Pinhole Image Sets without Dark Current 86
6.9 Signal power break down as a column graph 89

7.2 Gaussian High Pass Filter in DCT Domain 102
7.3 Gaussian High Pass Filter in DCT Domain 103
7.4 Comparison of Wavelet and DCT method 105

List of Tables

4.1 Camera One Dark Current Correlation 47
4.2 Camera Two Dark Current Correlation 47
4.3 Camera Three Dark Current Correlation 47

5.1 Transfer Gate Length 63
5.2 Photodiode length 66
5.3 Isolation Length 67

7.1 Run Times of Filter Methods 104
7.2 Identified Temperature of Image Sets 110

Symbols and Definitions

A Word on Language from the Author

In writing this thesis I have endeavoured to use the first person in line with current views on passive voice within academic writing. When the pronoun "we" is used it is used in the context of referring to you and I going on a journey together through the relevant chapter. The exception to this is of course the work that has been written in manuscript style with my PhD supervisors as initial peer reviewers and co-authors. These papers, where indicated, have been submitted, published or are awaiting publication to relevant academic journals. In these chapters the use of "we" is used to indicate my co-authors and I.

In following with the current thoughts on the matter, I have made the decision to use the phrase Child Exploitation Material in this work to refer to Child Sexual Exploitation Material and Child Sexual Abuse Material. All of these phrases are used interchangeably. These phrases are preferred over the usage of "Child Pornography" or "Pedo-Pornography" as they assist in highlighting the gravity of the crimes that are committed [1].

As mentioned previously, this is a thesis conducted by mixed publication and dissertation style. Figures and Tables are faithfully reproduced as they would appear in a published work. However, acknowledgements have been condensed into a single section at the start of this work, a single bibliography is provided at the end and references to future work, where conducted as a separate study, but, included in this thesis, have been edited for clarity and flow.

ABBREVIATION		DEFINITION
3D	-	Third Dimension
A/D	-	Analogue to Digital
ADC	-	Analogue to Digital Converter
APS	-	Active Pixel Sensor
BSI	-	Backside Illumination
B	-	Blue
CCD	-	Charge Couple Device
CDS	-	Correlated Double Sampling
CFA	-	Colour Filter Array
CIS	-	CMOS Image Sensor
CMOS	-	Complementary Metal-Oxide-Semiconductor
CSAM	-	Child Sexual Abuse Material
CSEM	-	Child Sexual Exploitation Material
CSI	-	Crime Scene Investigation
CTE	-	Charge Transfer Efficiency
DBI	-	Direct Bond Interconnect
DCRAW	-	A program used to process RAW format images
DCT	-	Discrete Cosine Transform
DNA	-	Deoxyribonucleic Acid
DSLR	-	Digital Single Lens Reflex, also dSLR
DSN	-	Dark Signal Noise
DSNU	-	Dark Signal non-Uniformity
EXIF	-	Exchangeable Image File Format
FD	-	Floating Diffusion
FIJI	-	FIJI is just ImageJ
FIS	-	Frontside Illumination
FPN	-	Fixed Pattern Noise due to dark current. See DSN, DSNU
G	-	Green
IC	-	Integrated Circuit
IUT	-	Image Under Test
JPEG	-	Joint Photographic Experts Group
LED	-	Light Emitting Diode
LOS	-	Lens Optical System
MAP	-	Maximum A-Posteriori
OPC	-	Organic Photoelectric Conversion
OPF	-	Organic Photoelectric Film
PCB	-	Printed Circuit Board
PCE	-	Peak Correlation Estimate
PNU	-	Pixel Non-Uniformity
PPD	-	Pinned Photodiode
PRNU	-	Photo Response Non-Uniformity

Pt	-	Platinum
R	-	Red
RST	-	Reset
SEM	-	Scanning Electron Microscope
SF	-	Source Follower
SLR	-	see DSLR
SN	-	Sense Node
SNR	-	Signal-to-Noise ratio
SPN	-	Sensor Pattern Noise
SWGDE	-	Scientific Working Group on Digital Evidence
TiO_2	-	Titanium Dioxide
TIFF	-	Tagged Image File Format
TX	-	Transfer

SYMBOL		DEFINITION	UNITS
c	-	speed of light $c = 3.19 \times 10^8$	ms^{-1}
D_{e^-}	-	Dark Current	numeric
e^-_{ph}	-	Photon generated electrons	numeric
e^-_{DARK}	-	Dark Current generated electrons	numeric
E_G	-	detector band gap	eV
E_{ph}	-	Photonic energy	Joules
E_t	-	impurity band gap	eV
f	-	spatial frequency	cycles/mm
h	-	Planck's constant $h = 6.626 \times 10^{(-34)}$	Js^{-1}
$\mathbf{I}$	-	a noise free image	pixels
J_D	-	Dark current density	A/cm^2
k	-	Boltzmann's constant, $k = 1.38 \times 10^{-23}$	J/K
λ	-	wavelength	μm
$\mu_{e^-_{dark}}$	-	average number of dark current electrons	numeric
$\mu_{e^-_{ph}}$	-	average number of photon induced electrons	numeric
μ_{max}	-	average max number of electrons	numeric
μ_{e^-}	-	average photon induced electrons	numeric
μ_{ph}	-	Average photons	numeric
N	-	Number of images	numeric
$< n_{1/f} >$	-	1/f noise	rms electrons
$< n_A >$	-	Amplifier noise	rms electrons
$< n_{ADC} >$	-	ADC quantisation noise	rms electrons
$< n_{DARK} >$	-	dark current noise	rms electrons
n_{DARK}	-	dark current electrons	numeric
$< N_{DIGITAL} >$	-	digital pipeline noise	rms electrons
$N_{e^-_{PH}}$	-	number of photon generated electrons	numeric
$N_{e^-_{DARK}}$	-	number of Dark current electrons	numeric
$< N_{FPN} >$	-	fixed pattern noise	rms electrons
$< N_{IMAGE} >$	-	Image process noise	rms electrons
$< N_{LOS>}$	-	lens noise	rms electrons
N_{max}	-	maximum number of electrons	numeric
$< n_{PE} >$	-	photon shot noise	rms electrons
n_{PE}	-	photo electric electrons	numeric
$< N_{PRNU} >$	-	PRNU	rms electrons
$< N_{RANDOM} >$	-	Random Noise	rms electrons
$< n_{RESET} >$	-	Reset noise	rms electrons
$< n_{shot} >$	-	Shot noise	rms electrons
$< N_{SPN} >$	-	Sensor Pattern noise	rms electrons
n_{WELL}	-	charge well capacity	numeric
$< n_{w_{ref}} >$	-	hf components of an image reference pattern	rms electrons
$< n_{w_{IUT}} >$	-	hf components of an image under test	rms electrons

P_{signal}	-	Signal power	dB
P_{total}	-	Total power	dB
q	-	Charge of an electron $q = 1.6 \times 10^{-19}$	coulombs
T	-	Temperature	°C
σ_e	-	dark current shot noise	dB
σ_{ph}	-	photon shot noise	dB
t_{int}	-	Integration time	Seconds
V_{cc}	-	Supply Voltage	Volts
W_{corr}	-	Pearson Correlation coefficient	numeric
W_{IUT}	-	Image residue for an Image Under Test	pixels
W_{res}	-	Noise residue for an image	pixels
W_{ref}	-	Image reference pattern	pixels
$\mathbf{Y}$	-	output of an image sensor	pixels

Chapter 1

Introduction

1.1 Context

Cybercrime - crimes directed at computers, networks, software and data - is a growing threat globally but principally in the Indo-Pacific region where many countries lack legislative or technical capabilities to fight it [2]. Allowing public confidence to be undermined in the digital domain will result in an estimated loss of US$1.02 trillion in global economic growth [3]. Of particular concern to the Indo-Pacific region is where computer equipment is used to facilitate existing offences including those involving Child Sexual Exploitation Material (CSEM) [4]. [1] There is no reliable data on the number of victims or offenders who are currently engaged in the trade of this material [1] [5]. As such it makes it impossible to assess if the problem is growing.

To combat this problem work has commenced on developing global indicators to identify victims of CSEM using the images produced [1]. While the continued investigatory efforts have turned towards victim-centric goals, prosecution of crimes involving CSEM is still of vital importance. As such, it is essential that images of offending can be linked to identified victims and also

[1] Child Sexual Exploitation Material - All material of a sexualised nature depicting children including Child Sexual Abuse Material (CSAM) which is correctly used to describe material documenting abusive acts towards children of a sexual nature or focusing on the genitalia of a child.

to identifiable offenders. “Offenders would be deterred through the knowledge that governments have the know how to investigate them.” [5]

For researchers faced with the task to develop new tools and methods to assist Governments in building cases against offenders their efforts can be defined in clear directions based on the needs of investigators. For those in the field confronted with an urgent and growing caseload, there is a need for the quick categorisation and quarantine of images with the minimum of resources; the triage problem. Investigators must also establish the provenance of an image and link it to a particular suspect. This must be done to the different standard of proof required in a particular court of laws and varies around the world.

Establishing the provenance of an image can be done in many ways. The common goal is to link evidence (a photograph) back to a suspects camera, or specifically the image sensor, with a high degree of certainty. This has been referred to as the Camera Identification Problem [6]. However, the current methods of solving the Camera Identification Problem rely on the use of techniques that are not widely understood, are vulnerable to counter forensic techniques or have insufficient research behind them to meet the needs of a Daubert hearing [7]. Focusing only on the use of Sensor Pattern Noise methods, they typically involve the use of specific computing resources, are time and resource intensive and have only been researched extensively to image sensors known as Charge Coupled Devices (CCD) as opposed to the more common sensors now seen on the market, the Active Pixel Sensor (APS) CMOS. The existing method also relies upon large datasets to draw statistically significant conclusions, of which such large data sets are not normally available in the field.

1.2 Motivation

A proposed solution to these problems would be to create a database of cameras based on a unique signal like a watermark which is present within each image.

This signal is made from noise present within each image referred to as Sensor Pattern Noise (SPN). A similar solution has been proposed before but by using only a subset of this noise know as Photo-Response Non-Uniformity (PRNU) Noise [8]. These terms are discussed in further detail below.

Such a database when combined with social media, could be used in the same manner as fingerprint databases around the world to trace and identify criminals. When an image is uploaded to a cloud-based service provider or image host the fingerprint could be extracted. This would then be compared against the database. If it is matched against a fingerprint of interest, new intelligence about the location of the upload would be added to a case file. Someone in possession of such a camera could then be questioned by authorities as to why they had a camera known to have been used in the commissioning of CSEM or CSAM.

However, what are the issues with such an approach? By insisting each camera manufacturer record the sensor pattern noise fingerprint before it leaves the factory, a provenance chain can be established. However, if the process to document the fingerprint is resource intensive then manufacturers are unlikely to comply. Furthermore, just as the ballistic fingerprint for a firearm changes with the firearm's use, if a camera's SPN fingerprint changes over time, then such storage would be a waste of resources and lead to high false detection rate. What is therefore needed is a method for generating a fingerprint based on the SPN methods that are stable across time, uses limited resources and is invariant to environmental conditions.

1.3 Aim and Scope

The aim of this thesis is therefore to develop a new method for linking images back to a source camera based on the sensor pattern noise methods of [6] that uses considerably fewer resources. Specifically, is it possible to create a reference

pattern from a single image taken with an APS CMOS?

To answer this question several hypothesises will be explored:

- Is dark current contaminating SPN fingerprints?
- Can a more accurate fingerprint be obtained by removing lens aberrations from SPN correlations?
- Can Dark current in isolation be used as a PRNU alternative?

1.4 Significance

For an image to be linked back to a camera, there are several processes available for forensic scientists to utilise. One such method involves the analytical study of an images pattern noise using a representation of a unique signature known as the Pixel Non-Uniformity (PNU) noise to obtain a correlation value of how similar the image is to this reference pattern. It is a widely accepted that noise can be introduced through many different sources as a digital image is taken. Conventional sources of noise include quantisation, half-toning, channel noise, shot noise and compression errors [9] [10].

During the manufacturing process of a digital imaging sensor slight changes to structures within the silicon that is used to make up the sensor are responsible for differences in how each photosite will respond to excitation from light. These minor differences are responsible for a contribution of additive noise that falls under the category of Photo-Response Non-Uniformity (PRNU) noise [10] or more specifically Pixel Non-Uniformity Noise (PNU) [6] [11] [12]; acknowledging that there is a slight misunderstanding with this term within the literature as defined in Holst [10]. As a parallel it took 69 years from the arguable discovery of the fingerprint in a criminal context before it was used in a court of law. Likewise, 33 years of research passed from the discovery of DNA before its first successful use in a criminal trial. As it will be shown in Chapter 3, the PRNU

method has only been under research for a decade and as such is still open for many advances before it will be awarded certainty in the criminal context. As such it is still a relatively new technique and is always open to interpretation and study.

While some ten years of research has been undertaken on using PRNU as a tool to solve the Camera Identification Problem, there is little knowledge of the thermal characteristics of this noise. There is additionally minimal evidence to suggest how this noise may change over time. Research conducted suggests that positive matches remain after the passage of time however, contrary to the conclusions currently drawn this does not infer the stability of the fingerprint since other metrics are being included in the reference pattern which contaminates the sensor pattern noise; such as compression artefacts or dark current [13, 14]. In fact, it has been shown that with the addition of more defect pixels over time to the pattern the approximate age of an image can be determined, thus assisting in determining timelines [14].

Holst shows that the noise contributed by the sensor's dark current, the current output by the sensor in the absence of illumination, is temperature dependant [10]. It has been suggested within the literature that PRNU is ideally independent of temperature [6] [11]. This is because the effects of dark current may be subtracted from the output through direct removal of a dark frame [10]. However, the cause of dark current is inherently attributed to the same physical electrical characteristics as PRNU with the difference being the the illumination of the sensor. This suggests that simple removal by dark frame may not eliminate all traces. Additionally, sensors that employ advanced designs with multiple transistors to reduce noise will still exhibit dark current within these additional transistors as each PN junction will cause additional thermal effects. Currently, the impact of this, and other sources of random noise are removed through frame averaging requiring the use of large data sets($N > 50$).

Some work has been done in the area of lens aberrations and how they may be manipulated for image provenance purposes [15]. The work of Knight, Moschu and Sorell is particularly important as this yielded inconclusive results in determining if a particular lens was culpable in the provenance of a specific image [16]. There is also a wealth of information regarding the types of aberrations that can occur within the lens. These are primarily referred to as the Seidel Aberrations after the work of Ludwig von Seidel [17] [18]. The central research question posed in our work has not been addressed in the literature though. Additionally, the literature has not isolated the pattern noise from the lens using a pinhole aperture. This is novel and will enable us to verify the works existing. It will also allow a signal analysis to be performed to isolate dark current as a reference pattern.

1.5 Overview

To address these aims, several studies have been conducted. Firstly, a new model of SPN was established by taking into account each of the overlooked areas highlighted above. This is described in Chapter 4 and shows how the new theory of unifying SPN as a tool will progress as an extension of the existing literature. In Chapter 5, we examine a CMOS image sensor under a scanning electron microscope (SEM) to provide a visual understanding to benefit a lay juror as to where PNU arises from. In Chapter 6 the lens aberration effects will be isolated from the SPN using a pinhole to establish an overall signal-to-noise analysis of each component contributing to SPN beginning the process of breaking the SPN down. In Chapter 7, the effect of temperature on CMOS sensors will be examined, contrasted and compared under controlled conditions that are specifically designed to exacerbate the dark current present to emphasise the effects of dark current shot noise. In Chapter 8 we contextualise the work in the wider field of digital forensics before providing a summary in chapter

9 explaining how these studies proffer a tangible solution to the problem as described and define future directions for the work.

Chapter 2

Technical Background

2.1 Image Sensor Fundamentals

There are two types of image sensor that dominate the market. These are the Charge Couple Devices (CCD, discussed in Section 2.1.1) and Active Pixel Sensor CMOS Image Sensors (APS, discussed in Section 2.1.2). In this chapter we use APS to refer to the active pixel sensor CMOS image sensor and CMOS to refer to the complimentary metal oxide silicon fabrication process. It is noted that the abbreviation CIS (CMOS image sensor) is also relevant and interchangeable [10]. Other sensor architectures exist, such as the Organic Photoelectric Conversion (OPC) sensor (discussed in Section 2.1.3) and the *foveon* sensor - based upon the same principle of colour film which uses the wavelength property of light to sample different colours at increasing depths. However, these sensor have not become as ubiquitous as the APS sensor for imaging. Even the CCD sensor has lost its popularity. A brief analysis of image sensors available on the market at time of writing (November 2018) sees very few cameras or camera modules which employ the *foveon* sensors available for purchase. Scientific applications are dominated by the CCD due to wider dynamic range and other advantages, however most devices now use APS sensors due to the ubiquitous

nature of the mobile phone camera. CCD sensors are still seen in some professional level dSLR cameras but even these are starting to become dominated by the APS. Sensors other than the APS and CCD are therefore considered outside the scope of this work due to limited forensic relevance.

The operating principle for the two dominant types of architectures on the market are the same. CCD and APS sensors, both being solid state devices, convert discrete photons into discrete electrons using a block of semiconductor material. This block of material is divided into two types, P type material on one side and N type material on the other to form a PN junction. This junction is the building block for most semiconductor circuits including image sensors and the associated readout circuitry.

2.1.1 CCD

Several advancements in technology were needed in order for Steven Sasson and Gareth Lloyd's invention to become what is now known as the digital camera. In their 1977 patent application, "Electronic Still Camera" [19] Sasson and Lloyd describe the first electronic device that is the embodiment of what we know as the digital camera today. Their device contained an "inexpensive information recording medium", dark current removal filters, high-speed A/D (analogue-to-digital) converter, buffer memory, permanent memory and finally a way to display an image onto a screen. This is similar to the structure we see for modern consumer digital cameras. What was novel about their design was the use of a Charge Coupled Device (CCD) for the image sensor, as designed by Smith and Boyle several years earlier [20] and previously envisaged by Michael Francis Tompsett [21].

The main design feature of the CCD that enabled Sasson's design is the way in which it reads out charge. The circuit for the CCD is shown in Figure 2.3. In each individual photo-diode an analogue charge is stored due to the interaction of photons striking the depletion region of a PN silicon junction. These photons

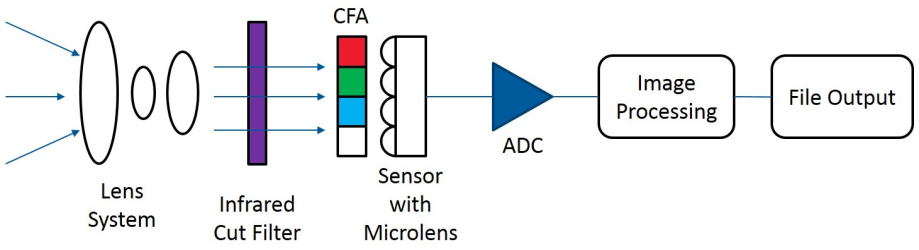

Figure 2.1: Modern Digital Camera.

are filtered according to the Bayer colour filter array (CFA) to ensure a colour image can be obtained [22]. Each pixel is then read out in a serial fashion via a concept similar to that of a bucket brigade device. The charge contained in each PN junction is transferred from pixel to pixel, with near perfect charge transfer efficiency, until they reach a bus. This bus is connected to an analogue to digital (A/D) converter and each charge is read out as a quantized digital signal. The limitation of such technology stems from the requirement for near perfect charge efficiency over macroscopic distances within the silicon structure of the device. This requirement limits the maximum physical size of a CCD.

A water analogy of how a CCD works is shown in Figure 2.2 using droplets of water instead of photons to fill jars (the depletion region of the photo-diode) on a moving conveyor belt before being measured on a digital scale (A/D converter). Each jar takes the previous position of the next jar in sequence representing the perfect charge transfer efficiency. In reality, instead of a conveyor belt each jar is tipped into each other jar in sequence. Some water would remain due to friction and other such forces within the glass jar acting upon the water. This represents the small loss of charge as each individual pixel would experience. The amount of water lost is a minuscule amount compared to the overall capacity. This is the imperfect charge transfer. Should this be extrapolated over a large surface area with many jars it becomes apparent that the amount of water left in each jar would eventually result in no water being placed on our read out conveyor. The same thing occurs within the silicon PN photodiode and hence is the cause

for the size restriction of the CCD.

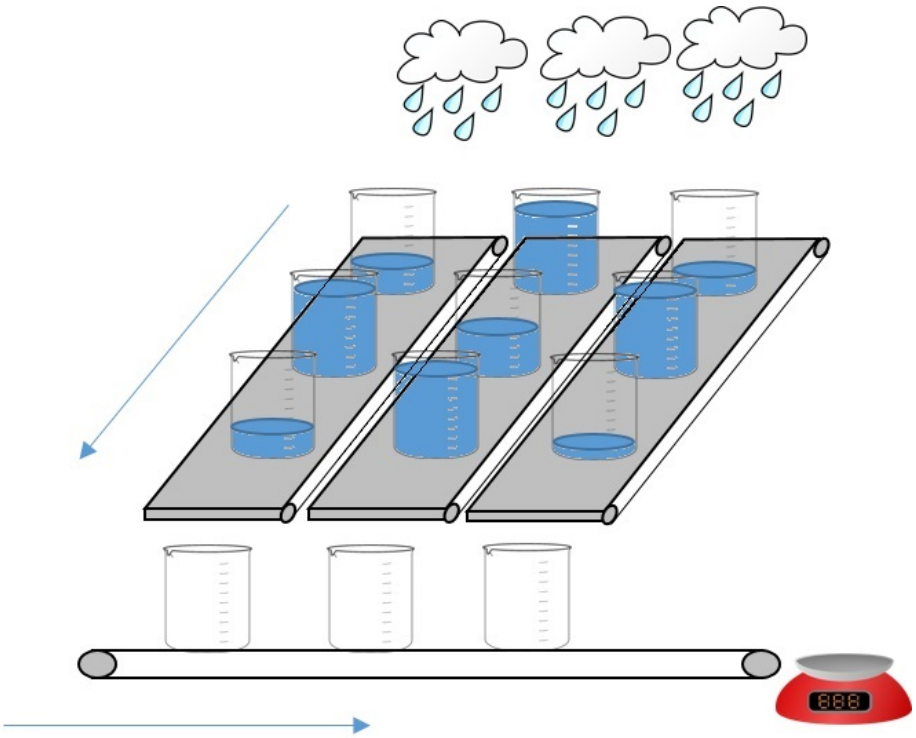

Figure 2.2: Bucket brigade analogy adapted from Janesick [23]. Each jar fills with "water" along the array. Once the "rain" finishes the conveyors move one bucket at a time on to the conveyor below which in turn shifts each jar onto a set of scales to be weighed. The scale emulates our analog to digital convertor, the rain our light, the jars our photosites within the CCD and our horizontal conveyor the bus.

Sasson established that a 0.01 megapixel camera (about 100 x 100 pixels) was not capable of outputting an image of comparable quality to analogue prints [24]. Consumers would need at least a sensor capable of measuring light to 1 megapixel (about 1000 x 1000 pixels) before the quality of analogue prints could be matched. Using Moore's law, a relationship where the number of transistors that can fit onto an integrated circuit approximately doubles every two years, he calculated that it would take approximately 30 years before the technology would mature to a usable format [24]. This estimation was approximately correct with digital cameras not becoming popular until the early 2000's.

2.1.2 APS CMOS

Just as the CCD was reaching consumer levels a new technology was being formulated. In 1994 an imaging device based on CMOS (monolithic complementary mental oxide semiconductor) technology came about thanks to the work of Fossum *et al* [25].

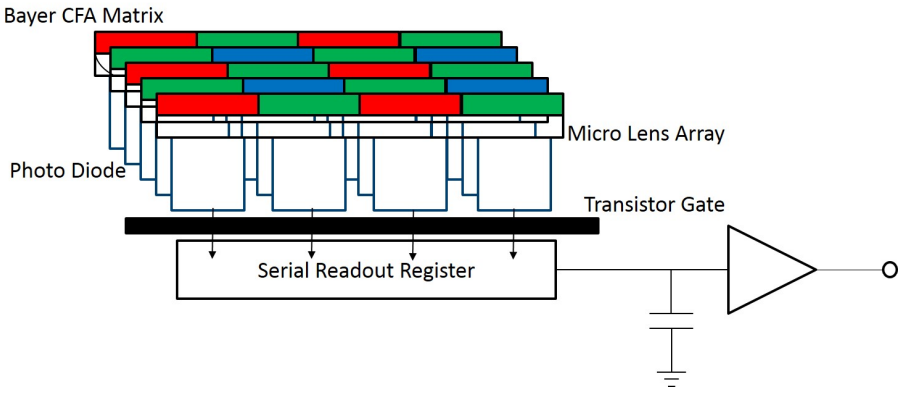

Figure 2.3: A breakdown of the CCD sensor. Note the readout method is the bucket brigade system as mentioned earlier.

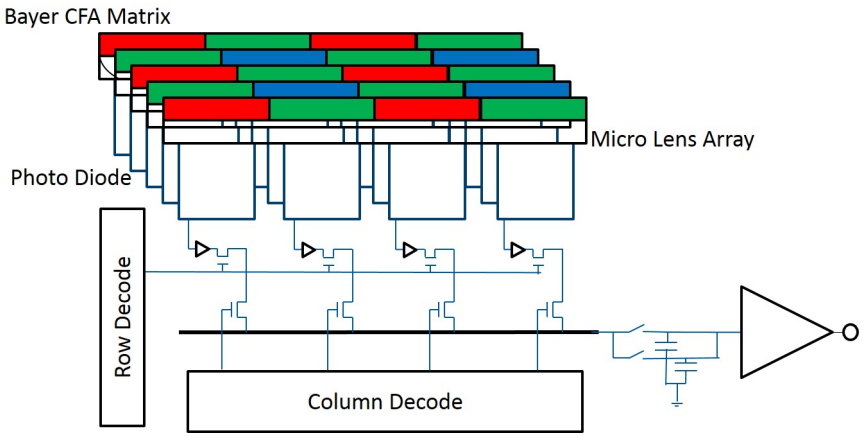

Figure 2.4: A breakdown of the APS CMOS sensors. The readout method is via row and column select transistors.

The key difference of the APS from the CCD is the way in which charge is transferred. Figure 2.4 shows the basic circuit structure. To avoid the limitations introduced by the need for perfect transfer of charge within the silicon

of the CCD, the APS concept integrates transistors into the pixel area of the imaging detector array which buffer the signal and drive the readout interface. Charge from each pixel is then carried across wires rather than through the silicon structure of the device. This results in less power needed to read out the individual pixels within the device and consequently the physical fill-factor can be increased for each pixel. Once microlenses are included on the array the fill-factor of the device increases up to 80% when compared to CCD sensors [26]. As Fossum reviewed the technology he noted that "a new imaging sensor technology that preserves the positive attributes of the CCD yet eliminates the need for charge transfer could quickly eclipse the CCD [26]." He was right. The demand for cameras in consumer electrical devices now means that the humble digital camera is ubiquitous, especially in platforms such as the mobile phone.

To make an image sensor using CMOS processes however takes several steps. This process uses standard CMOS fabrication processes, unlike the process used to manufacture a CCD. The complete CMOS process is beyond the scope of this work. A simplified version is described here. Using a CMOS process a diode region is implanted into a silicon wafer. 4 layers of metal wires are layered on top ensuring a light channel is centred above the diode. Finally, a CFA and micro lens is formed to complete the sensor. This creates a frontside illuminated (FSI) sensor. This is demonstrated in Figure 2.5.

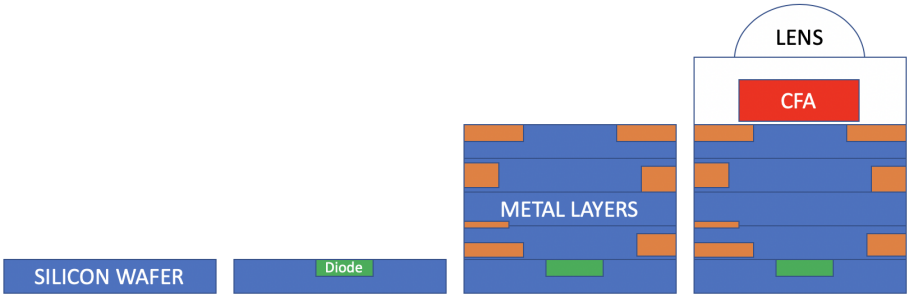

Figure 2.5: The frontside illumination sensor fabrication process using CMOS. The diode is visible at the bottom of the structure with the metal wire layers above the diode.

FSI sensors however have quality issues relating to the incident light hitting

the metal layers and reflecting into incorrect, neighbouring photodiodes or not being measured at all. To address this, light channels of dielectric material or physical shielding were implemented; however, this was not completely resolved until the introduction of the Backside illuminated (BSI) sensor. The BSI sensor fabrication process involved reversing the order of the circuitry and the diode so that the light first hits the photodiode. This is achieved by processing both sides of the silicon wafer in a double sided operation (Figure 2.6). This results in less reflection, scattering and light loss occurring within the metal layers of the sensor, however the manufacturing process requires the silicon wafer to be flipped, thinned and processed on both sides.

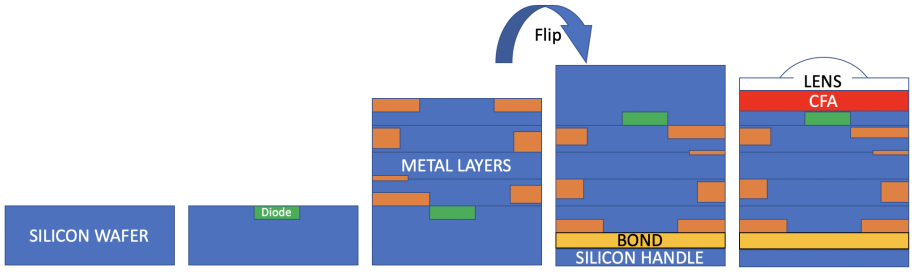

Figure 2.6: The backside illumination sensor fabrication process using CMOS. The diode is visible at the top of the structure with the metal wire layers below the diode. The process is similar to that of the FSI sensor however involves etching operations on both sides of the wafer and hence, flipping the wafer and bonding to a new silicon handle.

To achieve processing on both sides, however, a 3D or stacked chip was required to be developed. The top layer of the image sensing wafer is required to be bonded to an additional wafer to execute the further CMOS steps required to fabricate the lens and CFA. This is achieved using a direct oxide bond and through silicon via (TSV) interconnects around the perimeter to allow connection to the underlying circuit. A draw back of this process is that it requires high volume manufacturing to be cost effective [27]. Stacking via direct wire bonding or direct bond interconnect (DBI) resolves some of the issues which leads to this higher cost and offers an alternative by bonding without out the need for TSV. A graphical contrast between TSV and DBI is shown in [28, Fig.

1] reproduced below as Figure 2.7.

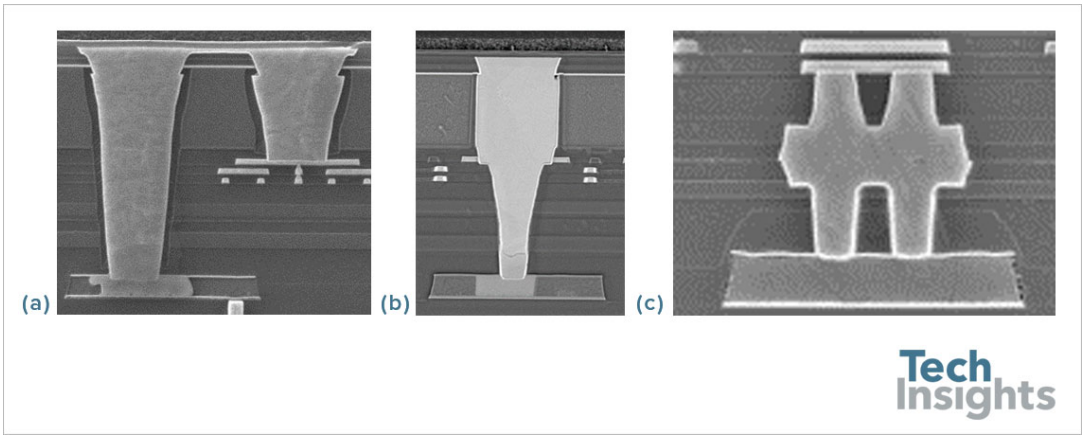

Figure 2.7: An example provided by TechInsights showing the difference between TSV (a), (b), and DBI technology (c) required for the stacking of multiple CMOS wafers to create smaller but 3D IC packages.

The use of DBI also allows the increased use of the stacked wafers below the original wafer. This leads to numerous CMOS wafers integrated vertically in the sensor allowing advanced image processing to be performed on chip. Such vertical integration significantly decreases the size of the overall sensor.

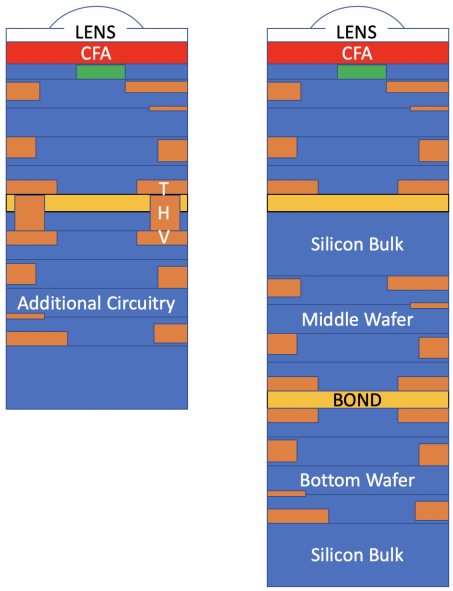

Figure 2.8: Using DBI and direct oxide bonding we can increase the number of wafers bonded to the image sensor. This leads to fully integrated image processing packages on chip.

One of the main benefits from CCD to APS is the ability to read out individual pixels as distinct from entire lines or sections at a time. This assists with operations such as binning where groups of pixels are summed and averaged to be read out as a single pixel. Such operations reduce noise due to averaging. Additionally, noise cancellation techniques such as correlated double sampling can be employed with ease on chip through the use of additional stacked wafers containing additional circuitry. Other benefits include the lower production cost since standard CMOS fabrication processes can be used, and lower power consumption.

The advances from CMOS fabrication processes on image sensors are critical for image sensor size shrinking and the inclusion of more powerful image sensors in mobile applications. The forensic implications from CCD to APS from the approach of pixel non-uniformity are limited. When stacking circuitry the connections to the remaining parts of the circuit are either on the peripheral of the sensor or buried under the photo sensing section of the diode. Hence there is minimal impact on the photo-detecting region of the sensor, if any. The advances in image stacking technology does mean, however, that a reduction in noise is apparent through an increase in the signal to noise ratio since these advances enable more photons to enter the individual photo-detecting regions. Other advances have also been made to increase the number of photons entering the diode region. Such advances include the use of wider shields and dielectric isolation between pixels to prevent optical cross talk referred to as deep trench isolation (DTI). The length of the photo-diode can also be increased to optimise the near-infra red sensitivity.

2.1.3 Future Developments

Scientific CCDs remain a critical application space due to their wider dynamic range than APS [10,29]. In future this may be challenged by advances in photon detection methods such as the collaboration between Fuji Film and Panasonic

in the area of organic films. This collaboration announced in 2013 [30] relies on the principle of the photoelectric effect to generate an image and is referred to as an Organic Photoelectric Conversion (OPC) sensor or an Organic Photoelectric Film (OPF) sensor. Both are used interchangeably in this text. An example of this structure is given in [30, Fig. 1] reproduced here as Figure 2.9. This method of photon detection results in approximately 20% more dynamic range [30] than APS.

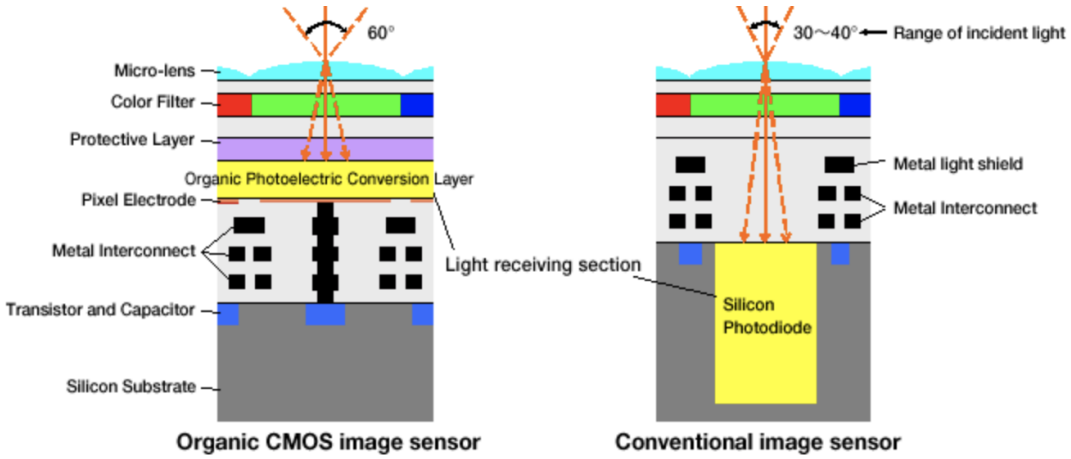

Figure 2.9: Graphical example of an OPC sensor in comparison to a FIS.

Aside from the photo detection relying on the photoelectric effect as opposed to the inner photoelectric effect of a photodiode, the readout circuitry is also simplified for the OPC sensor. The charge storage component in an OPC is a smaller circuit compared to the CMOS counterpart. This is due to the removal of the photodiode and associated transfer node needed to move the detected electrical charge from the photodiode to the charge storage node for read out. In the OPC sensor charge is read directly from the organic film to the charge storage node below. This is illustrated in [30, Fig. 8] and reproduced in Figure 2.10.

Such sensors have been realised in 2018 [31]. It is too early to determine if they will be adopted by the market since no information regarding cross talk is discussed. Since the design still uses a Bayer matrix it is feasible for photons

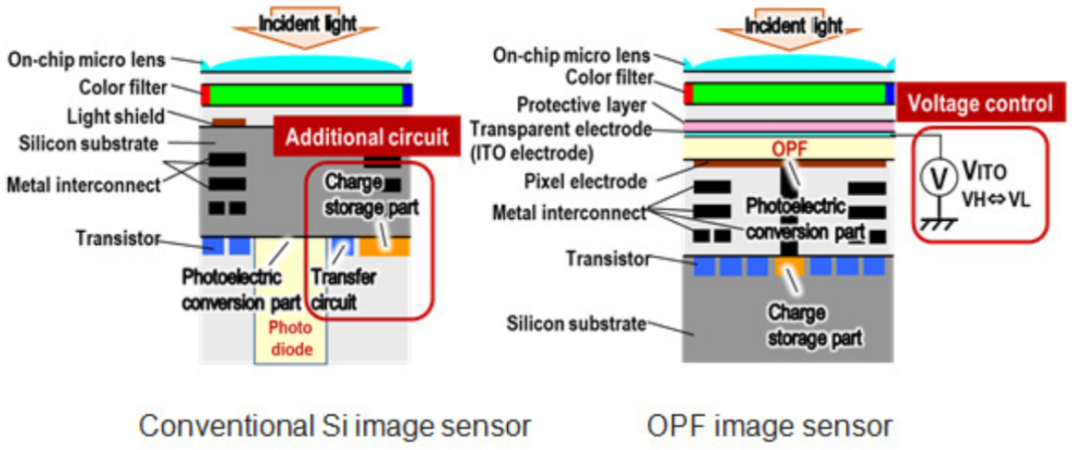

Figure 2.10: Aside from the photo detecting element, the charge storage and read out elements also differ within the OPC sensor.

which have a high incident angle to strike the OPC layer and be realised as the wrong colour. This is of course a principle advantage of the BIS structure with deep trench isolation as discussed above and as such may prevent adoption. There are also additional issues due to reset noise since the charge storage element is physically connected to the organic layer within the sensor. As a result, in pixel noise cancellation is required to be used [31]. It is unclear if the advanced noise cancellation methods employed would be effective in reducing crosstalk or other sources of noise other than the stated reset noise.

Panasonic and Fuji Film also claim that the OPC sensor is able to sample significantly more photons to produce a much wider dynamic range [30, 31]. It is unclear how this would affect the signal to noise ratio within a standard image. Experiments will need to be conducted to determine if SPN methods are still applicable on this emerging camera technology. Should SPN methods not work (or work with less precision) this would confirm the hypothesis that a significant source of PNU is due to the non-uniformity within the PN region of a photodiode. However, should SPN methods still work, this would demonstrate that PNU can be at least partially attributable to the remaining elements of the sensor that are universally similar to CMOS and CCD sensors.

OPC sensors may revolutionise the mobile imaging market or they may be susceptible to the same fate as the foveon sensor. Given the recent application of this technology in a sensor format, it will be some time before forensic investigators are given the opportunity to determine its effects, if any.

2.2 Sensor Pattern Noise Extraction Process

We model the output of an image sensor $\mathbf{Y}$ as a noise-free image $\mathbf{I}$ multiplied by a noise signal $\mathbf{k}$.

$$\mathbf{Y} = \mathbf{I} \odot \mathbf{k} \tag{2.1}$$

The noise signal $\mathbf{k}$ when isolated and properly filtered is assumed to be the sensor pattern noise (SPN) of an image. Should $\mathbf{k}$ not be isolated or be incorrectly filtered then other elements from the noise model will still be present.

The method for extracting SPN is based on an assumption that all noise above a spatial frequency f is unique to a sensor. Using this assumption we can thus isolate the signal using any high-pass filter technique. In our work we use the wavelet coring method as the filter first proposed in [12] but as modified in [16] for Bayer RAW images. This involves using a wavelet based filter to obtain a noise free image I decimated into individual colour filter arrays (CFA). The noise is estimated in each CFA sub-array before recombining. The SPN estimation based on this high-frequency assumption is then obtained by subtracting the filtered image from the original sensor output.

$$\mathbf{k} = \mathbf{I} \odot \mathbf{k} - \mathbf{I} \tag{2.2}$$

In reality there are additional sources of error present within our estimation. We discuss these further in section 4.4. We now let S_1 be the SPN, S_2 be the artefacts due to the optics and S_3 be the contribution of all other random

variables modelled with a Gaussian distribution within image noise residues $N_1, N_2, \ldots, N_N$. We assume S_1, S_2 and S_3 to be independent and additive. Modelling the high-frequency components of our image above the cut-off frequency as $f(I)$ our noise residue is defined as:

$$W_{res} = S_1 + S_2 + S_3 + f(I) \tag{2.3}$$

We define our reference pattern W_{ref} as the average of N noise residues taken from flat field images where N is greater than 50 .

$$W_{ref} = \frac{1}{N} \sum_{i=1}^{N-1} W_{res_i} + W_{res_{i+1}} \tag{2.4}$$

This averaging is critical to ensure the effects of S_3 approach zero due to the Gaussian distribution. As more images are included in the average, the elements of $f(I)$ can be amplified so it is important to reduce the effects of $f(I)$ to minimise a source of possible error. We can do this in our original reference pattern calculation by using smooth flat field images, in RAW format and isolate to each Bayer filter element.

Upon correlation W_{corr} with an uncorrelated image under test W_{IUT} outside of the previously defined set of images with the reference pattern we obtain:

$$W_{corr} = W_{ref} \otimes W_{IUT} \tag{2.5}$$

$$= (S_{1_{ref}} + S_{2_{ref}} + n_{w_{ref}}) \otimes (S_1 + S_2 + n_{W_{IUT}}) \tag{2.6}$$

where n_{wref} and $n_{W_{IUT}}$ are the uncorrelated high-frequency components of the image obtained from the reference pattern and the image respectively that are still present after wavelet coring.

Assuming a priori that the image is within the same set of images taken from the initial camera (ie. $S_{1_{ref}} = S_1$) and taking the expectation of our result:

$$\begin{aligned} E\{W_{corr}\} =& S_1^2 + S_2^2 + 2 \cdot n_{w_{ref}} \cdot n_{W_{IUT}} + 2 \cdot S_1 \cdot S_2 \\ &+ S_1 \cdot n_{W_{IUT}} + S_2 \cdot n_{W_{IUT}} + S_1 \cdot n_{W_{ref}} \\ &+ S_2 \cdot n_{W_{ref}} \end{aligned} \tag{2.7}$$

Given that the noise signals S_1 and S_2 are assumed independent, we can further simplify as cross terms with these independent signals are all uncorrelated and will be zero:

$$E\{W_{corr}\} = S_1^2 + S_2^2 + 2 \cdot n_{w_{ref}} \cdot n_{W_{IUT}} \tag{2.8}$$

We can further simplify this final term as the contribution from the high-frequency bias from the image content as n_V.

$$E\{W_{corr}\} = S_1^2 + S_2^2 + n_V \tag{2.9}$$

In Chapter 6 we will use Equation 2.9 to perform a SNR analysis of the noise residues obtained via the standard wavelet process using a tool box provided by Goljan *et al* [8]. This process is further explained in Section 6.3 where a robust experimental analysis is performed to isolate dark current and lens effects from SPN. This will enable the isolation of the contribution of lens artefacts and dark current on our reference pattern.

Chapter 3

Literature Review

Here I establish the field of knowledge for the submitted papers which are presented in Chapters 5, 6 and 7. This is continued in Chapter 4 where further context of this chapter is presented in a manuscript style highlighting the proposed benefits of rethinking the sensor pattern noise model as described below.

3.1 The Blind Camera Identification Problem

Image forensics can be broken down into two main objectives: establishing the credibility of an image; or establishing its origin. Establishing an image's credibility refers to understanding an image as a true and accurate reflection of the scene. However, with the advent of image manipulation techniques, both digital and analogue, establishing how credible an image is requires great skill. This is often simplified as detecting an image forgery, however it is more than just a simple digital forgery given that images can be staged. The second objective of establishing an images origin concerns itself with establishing the history of a particular image. Which camera was responsible for the image's capture is the primary question where an answer is often sought, however, there are other pertinent questions to be answered in the age of information sharing. This includes understanding which social media platforms an image may have been shared

thorough, where the image has been stored, what file format the image has been processed as and which image programs have been used to view the image. We concern ourselves with only one of these problems, that is the identification of the camera responsible for taking the image originally. This is known in the literature as the camera identification problem.

3.1.1 SPN and Blind Camera Identification

There has now been close to two decades of research into the field of "ballistic" fingerprinting of image sensors for forensic identification to solve the camera identification and verification problem using sensor pattern noise, a combination of dark current [32] and photo-response non-uniformity noise (PRNU) [12]. The camera identification problem focuses on identifying which camera is responsible for photographing a particular image having a priori knowledge that the camera is within the set of cameras under test (closed set). The camera verification problem is a complicated version of this problem and requires identifying if a photograph was taken by a camera in possession of an investigator without a priori knowledge (open set) of its involvement. In this manner, forensic investigators and law enforcement have seen sensor pattern noise to be a capable tool for image provenance investigations [33] and image forgery detection alike. Since the principal extraction method for the sensor pattern fingerprint is via a high-pass filter, it is unclear how the lens, through high-frequency Seidel aberrations, contributes to the fingerprint.

Sensor pattern noise has been widely tested across a variety of imaging platforms. It has been shown to be effective in identifying images from still image cameras [12], scanners and photocopiers [34, 35], video cameras [36] and fingerprint sensors of similar design [37].

While much work has been done to solve the Camera Identification Problem legal professionals wishing to use these methods may face problems regarding its admissibility due to stringent requirements of the Daubert standard requiring

known error rates and general acceptance to have been reached within the scientific community [7,38]. What compounds this problem is that much of the literature has focused on identifying Charged Coupled Devices (CCD) as opposed to the more recent invention of the Active Pixel Sensors based on Complimentary Metal-Oxide Semiconductor technology (APS). This is an issue because APS now dominates the market due to their lower cost and better performance [10].

Whilst much work has been done on improving the estimation of the PRNU signature contained within the noise residue [39] it still remains an approximation. From the fingerprint extraction process described in detail in Section 2.2 it is clear that additional signals remain, including trace artefacts from the lens. These sources of interference are primarily related to the image capture process referred to as the image pipeline (Figure 3.1).

To analyse sources of noise, the pipe can be broken down into three main categories with a fourth category related to the environment the camera is operating in. The breakdown of each area of noise in this way creates a dedicated area of research where each resultant source of noise must be tracked and documented within the SPN model. These areas are the physical image pipe, the digital image pipe, the image scene itself and the environment. We describe these areas below and explore their noise contribution mathematically in Section 6.3. Each section of the pipe is relevant for the analysis of the origin or credibility of an image.

3.2 Forensic Implications of the Physical Image Pipeline

The physical image pipeline comprises the lens optical system (LOS) including any filters applied, the sub lens system, the image sensor and any associated electronics required to turn the analogue signal into a digital signal ready for processing by the digital image pipeline. This includes quantisation by any

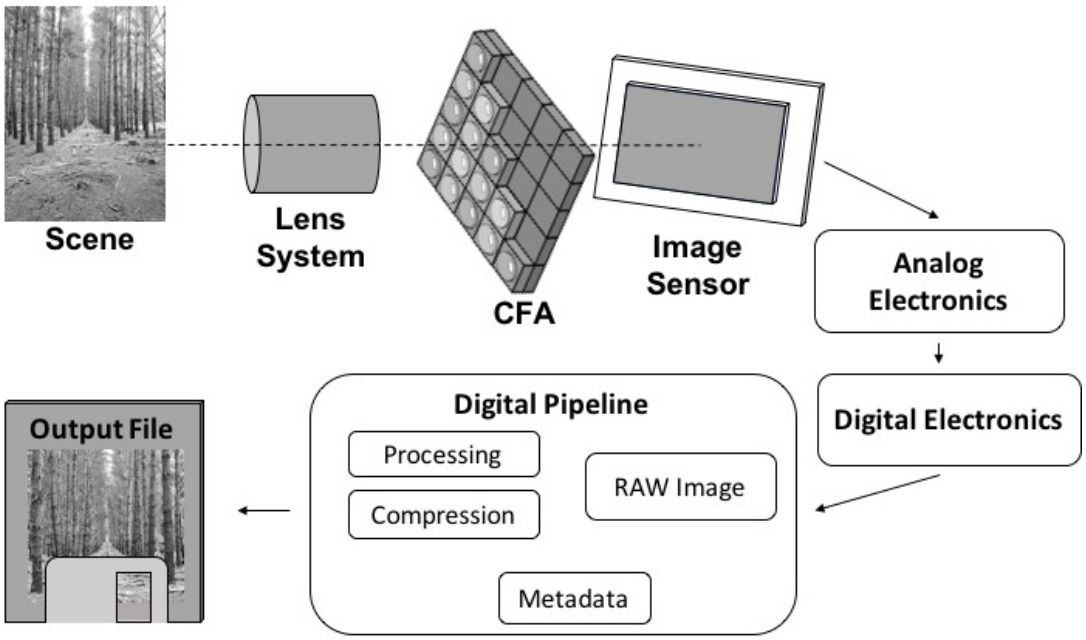

Figure 3.1: The image capture process referred to as the image pipeline contains two discrete sections, the analogue and the digital. Each element within the pipeline can be exploited to solve the camera identity problem. The analogue pipe consists of the lens optical system including the colour filter array and micro lens system, the image sensor and the analogue readout electronics. The digital pipe commences from the output of the analogue to digital converters (ADC) and involves all the in camera digital processes, the discrete digital signal transverses before finally being saved as an image file.

analogue to digital to converters.

3.2.1 Image Sensor Specific

There are several types of image sensors on the market. Whilst these vary in popularity overtime, two main competitors have emerged as ubiquitous throughout the industry. Charged-coupled devices (CCD) were the first widely adopted sensor type. However, these large and expensive devices have since been surpassed in popularity by the Active Pixel CMOS (CMOS) image sensors due to the ease of manufacture and small form size. Much of the theory that was applicable to CCDs should be directly applicable to CMOS sensors however, it is hypothesised that there are some differences that are yet to be fully realised in the research literature. The image sensor can be regarded as the only unique el-

ement of the camera involved in the image capture process since lenses are often able to be interchanged. This means considerable literature has been focused on the study of Pixel Non-Uniformity (PNU) noise, that is the non-uniform output of discrete pixels since this forms a unique signature for a camera [12]. PNU can be described as a combination of pixel defects (pixels that are saturated or under exposed) and noise due to dark current (DSN) and photo response non-uniformity (PRNU) [10].

Hot and Dead Pixels

As the number of pixels increase on the array so too does the chance of a manufacturing defect. These defects within the sensor are static regions within the sensor that do not react as designed to illumination. Such reactions may be permanently on, causing a hot pixel, or permanently off resulting in a dead pixel. This creates a static pattern that may be used to successfully match an image to its source camera [40]. Many modern cameras facilitate hot and dead pixel tracking algorithms to ensure that these pixels are hidden prior to Bayer interpolation.

Dark Current (DSN)

All image sensors regardless of construction have a thermally induced signal present in all images referred to as the dark current or "Dark Sensor Noise" (DSN). DSN is often referred to as Fixed Pattern Noise (FPN) however, in this work we will move away from this notation since it is dependant on temperature. FPN would be a more accurate description for PNU in our forensic context hence, some confusion exists if we use this terminology. DSN signal arises from the thermal energy of the sensor within the PN junction of the silicon causing electrons to excite through the lattice structure into the subsequent amplifier and analogue-to-digital conversion pipeline. In a method that pre-dates the Lukáš methodology it has been shown that this stochastic dark current signal

can be used as a suitable reference pattern for the identification of tape video cameras [32]. However, as this signal is a high spatial frequency signal, its effects are not removed by the high-pass filter nor the subsequent PRNU estimation. DSN remains an open question for isolation in images that contain it. However, it can be suppressed through the subtraction of a dark frame prior to the image processing stage of the image capture pipeline or through cooling [10]. [41] further extended the work by applying a hybrid method of identification using DSN and PRNU in combination for greater precision. However, this method did not explore the temperature dependency of DSN and how it may effect the precision or accuracy of the positive match obtained.

Photo Response Non-Uniformity (PRNU)

Research published in 2005 by Lukáš, Goljan and Freidrich (Lukáš *et al*) [6, 11, 12] demonstrated that by exploiting this PNU a digital image can be identified back to a specific digital camera. This was achieved through the analysis of noise contributed by Photo Response Non-Uniformity instead of dark current. The confusion in terminology as described earlier is avoided by adopting the same definition as in [11] whereby PRNU is defined as noise due to PNU and low frequency defects such as dust and scratches on the lens or imaging sensor. By passing the PRNU through a high-pass filter an approximation for the PNU can be obtained. Hence, a forensic fingerprint can be isolated for a specific camera and image. As in [41], the effects of temperature have not been considered. It is also worth noting that if the images have been subjected to a dark frame subtraction in camera, the PRNU finger prints will contain a deeply attenuated DSN contributed to PNU.

Since both DSN and PRNU are caused by differences in an image sensor such as the individual silicon substrate doping and the variable size of the photodiode it is often referred to collectively as Sensor Pattern Noise or SPN.

3.2.2 Electronics

Banding/Seam Noise

To improve the readout speed of CCD sensors, multiple on-chip amplifiers may be used. Similarly, the number of transistors can be increased in CMOS designs. However, the addition of non-identical amplifiers reading sections of the image sensor array comes at the expense of streaks called banding or seam noise [29]. Extreme cases can be seen in CCD arrays divided into quadrants or rows where each quadrant or row is read out independently. This noise is not included in the additive signal model discussed in Chapter 4, but its effects will be seen passed directly through the high-pass filter. Due to proprietary designs it is unknown what effect this will have on CMOS sensors that deviate from the patent [25] by sharing amplifiers between active pixels. Manufacturers are aware of such noise and go to great lengths to reduce it through the use of Correlated Double Sampling (CDS). However, some non-uniformity would remain.

Random Processes

Additional random noises are present within the additive signal model. Sources include amplifier noise, voltage or timing frequency and incomplete resets of pixel wells back to zero. These sources of noise are attenuated through frame averaging [10].

3.2.3 Lens Design

Lens aberrations that can appear within an image included pin cushion and barrel distortion, chromatic aberration, coma, astigmatism, and spherical aberration. These are third-order optics or more commonly known as Seidel aberrations [42]. The most common type of lens to correct for these aberrations is an anastigmat, which is a lens made up of multiple elements. These elements are designed to work in unison to reduce the effects of Seidel aberrations on the

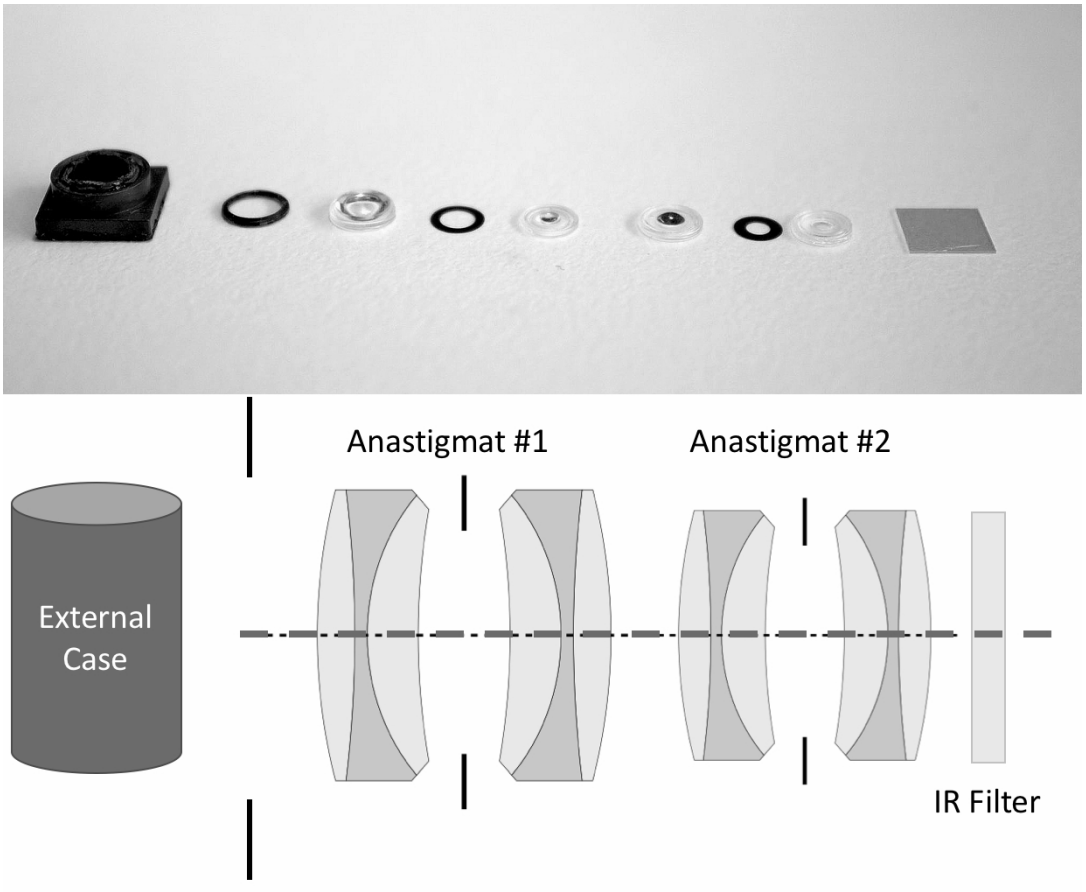

Figure 3.2: The inner parts of the Sony IMX219 dual anastigmat lens as used in this chapter (above) with its graphical representation (below). The individual lens components are seen from left to right and include stops, lenses and finally an infrared filter.

image.

In this chapter we use Sony IMX219PQ CMOS cameras with a built in dual anastigmat lens as seen in Figure 3.2. We are able to compare and contrast the results between several of these lenses. Similar work has been done in [16] where the lens on a dSLR was substituted for ones of similar design. This work showed that the lens was not statistically significant within the noise residue to uniquely identify a specific lens. This was due to lenses of similar design being used. Our work in this chapter is unique as we remove the lens contribution completely through the use of pinhole lenses. In doing so we are able to analyse the lens contribution to the noise residue directly.

3.3 Forensic Implications of the Digital Image Pipeline

The digital image pipeline comprises of the operations that the digital signal undergoes after conversion by the analogue to digital converters to create the output file from the camera. Scaling, cropping, cloning or resaving is not traditionally included in this pipeline and are left as implications of the image itself. However, with the increasing ubiquitous nature of all-in-one image processing packages on chip, these operations can increasingly be done on the camera and therefore, may need to be considered.

3.3.1 Compression Artefacts

Image file compression artefacts from within the firmware have already been shown to survive the filtration process [16]. This creates a source of error when definitively matching to an image sensor. To avoid this source of error, raw images should be used where ever possible in creating reference patterns and noise residues. However, not all candidate images under test will be in raw image format. A solution was proposed in [43] source which averaged macro blocks of half the size of the JPEG discrete cosine transformation (DCT) macro block to create an averaged noise residue. This averaged noise residue suppresses the effects of the DCT edge effects. In our work we consider only raw images to avoid the impacts of lossy quantisation and downsampling.

3.3.2 Camera Noise

Each image is first passed through a high-pass filter prior to PRNU estimation. This results in low-frequency scene content being suppressed but high-frequency remaining in the noise residues upon computation. As a result, high-frequency content is considered in each reference pattern calculation. To suppress this content in source camera verification applications, techniques such as thresholding

have been developed [43]. However, images that contain large amounts of dark, saturated or high-frequency regions are more likely to be incorrectly identified using this method.

Through the digital processing pipeline of the image capture process additional noise is added to the model through "camera noise" [10]. This "camera noise" is added via digital corrections such as white balance and gamma correction.

3.3.3 Metadata

When an image is saved more than 460 additional metadata tags of information can also be saved in parallel, embedded within the binary file structure of the image. The most common format for this data is the EXIF 2.3 file format [44]. This standard allows images to correctly render between platforms. Tags saved alongside the image can include location data, image size, a smaller thumbnail of the image and additional information relating to make and mode [45]. Inconsistencies within the metadata can be linked to image tampering or improper chain of custody from the original image. Fields such as the make and model of the camera can be used to link the image to a class of camera, but this does not match it to a unique camera. There are additional issues since the metadata can be manipulated with any common hex editor [46].

3.4 Forensic Implications of the Image Environment

The image environment includes the physical constraints upon the image and camera. This includes violations of physics within an image, such as something that clearly cannot belong, shadows and reflections that do not exist, geometry of the image that are impossible and any environmental conditions of the original scene. In part, this is dominantly in the domain of conventional photographic

forensic analysis.

The appearance of dust within the noise residue is a contentious issue. Previous works have cited that dust creates a low frequency spatial response within the image that is able to be filtered out from our high-pass filter [12] however, this is not the case. The appearance of dust in images can be modelled as a function of exit pupil position, window thickness, focal length, f-stop and position within the image plane [47]. As the f-stop of the camera varies the frequency response of the dust varies. For lenses of low f-stop, sensor dust appears as low frequency noise. However, as this number increases high frequency components readily appear. This has been used successfully as a method to solve the closed set problem [48] by understanding how the dust changes with f-stop. Thus, lens dust as opposed to sensor dust is more likely to appear as high-frequency noise within our noise residues however, the presence of sensor dust cannot be excluded.

Additional environmental effects are theorised within the noise residue but have yet to be documented. Such affects include temperature and voltage levels due to power supply variations.

The appearance of shadows has been used to indicate forgeries previously [49]. However, it has not been used to prove the uniqueness of an individual camera. It is proposed that the exposure time will have an effect on the sensor pattern noise methods mentioned above due to the number of electrons either self induced or created from photons at a set time. Thus, the lighting within a scene may be of forensic importance when establishing uniqueness of individual cameras.

3.5 Conclusion

In summary, three promising areas have been identified from the literature. There is an intermixing of PRNU and DSN that shows promise in identifying

cameras uniquely. However, this has not been suitably analysed in the context of competing objectives. There has not been robust study on the interaction between PRNU and DSN to determine if DSN is contaminating a PRNU signal when measuring PNU for camera uniqueness. Likewise, the interaction of lens effects on the uniqueness of the camera's fingerprint cannot be discounted. Finally, there has not been any discussion of the formulation of triage tools for camera identification, that is, tools that can be run in short amounts of time with limited resources. Such tools can trade off accuracy for quicker run times so long as there are secondary tools to process evidence after the fact. This is the focus of this work. In the next Chapter we will take a critical look at these identified areas with an exploratory study to frame the novel work which is to follow.

Chapter 4

Rethinking Image Sensor Noise for Forensic Advantage: An Exploratory Study

4.1 Abstract

Sensor pattern noise has been found to be a reliable tool for providing information relating to the provenance of an image. Conventionally sensor pattern noise is modelled as a mutual interaction of pixel non-uniformity noise and dark current. By using a wavelet denoising filter it is possible to isolate a unique signal within a sensor caused by the way the silicon reacts non-uniformly to light. This signal is often referred to as a fingerprint. To obtain the estimate of this photo response non-uniformity multiple sample images are averaged and filtered to derive a noise residue. This process and model, while useful at providing insight into an image's provenance, fails to take into account additional sources of noise that are obtained during this process. These other sources of noise include digital processing artefacts collectively known as camera noise, image compression artefacts, lens artefacts, and image content. By analysing the

diversity of sources of noise remaining within the noise residue, we show that further insight is possible within a unified sensor pattern noise concept which opens the field to approaches for obtaining fingerprints utilising fewer resources, with comparable performance to existing methods.

4.2 Introduction

In this chapter we contextualise the work which will follow by taking a closer look at the existing literature and apply a critical review. Sensor pattern noise (SPN) is a reliable tool for tracking the provenance of images [12]. Through the use of high-pass filtering, a unique signal can be extracted from an image consisting of Photo-Response non-uniformity (PRNU) noise. This signal is unique to the image sensor and is capable of discrimination across cameras of the same make and model. This discrimination is because the PRNU is defined as the pixel to pixel variance in output intensity of an image sensor when illuminated with a constant light source. The PRNU is the light-sensitive signal caused by Pixel Non-Uniformity (PNU) within a discrete image sensor. It is statistically unlikely for two image sensors to have the same PRNU fingerprint. This capability has been demonstrated with a false acceptance rate of 0.0024% and a false rejection rate of 2.4% making PRNU comparison an attractive tool where other evidence can also be used to verify the outcome [8]. The PRNU approach was further reinforced experimentally by [49] showing that the probability of the wrong camera with a positive match to an image with the same PRNU is 1/100,000.

Since images in the real world are often never illuminated with a constant light source, solving the blind source camera identification problem in this manner requires large sample sizes of images specially crafted to ensure scene contamination is minimised. Processing the large sample of images is either time consuming or requires large amounts of computing resources to ensure efficacy. These resources are not always available for forensic investigators in the field

who need efficient tools to quickly and accurately quarantine evidence. There are further challenges in maintaining chain of evidence for embedded cameras, such as in contemporary smart phones and the emerging field of wearable technologies.

Through careful analysis of the current sensor technology in terms of optical effects, semiconductor physics and the environment image sensors operate in, this chapter considers the current methodology for measuring the unique PRNU signal and shows that other options exist for extracting the unique signal that may provide more accurate results and lead to the development of more efficient tools.

4.3 Basic operation of an Image Sensor

The fundamental principle of collecting a digital image has not changed since the first experiments involving selenium-coated metal plates [50]. Since then the progression from plates to tubes [51] (realising the vision of [52]), to Charged Couple Device (CCD) arrays [53] [54] and currently to CMOS imaging sensors (CIS) [55] [26] has seen the quality of the image improve, but the principle remains the same. Photons are converted to electrons in a PN junction of a photosensitive material through the recombination of holes and electrons via the photoelectric effect. In the current state of the art pinned photodiode (PPD) conversion of photons to electrons is done in the heavily P doped layer of the PN diode. This is because the PPD architecture results in the depletion layer being almost the entire width of the P+ region [56].

The PPD is the preferred architecture for modern CIS (Figure 4.1) due to several significant advantages over its predecessors [10]. The PPD exhibits lower noise, lower dark current, higher sensitivity and broader dynamic range than traditional photodiodes or CCDs. As CMOS technology advances we have seen the image sensor shrink in size. However, due to the limitations of CMOS

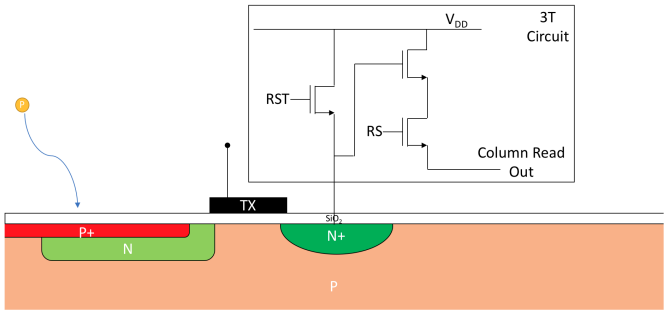

Figure 4.1: PPD CIS with a three transistor circuit built into the pixel. Each transistor is for a specific function. RST resets the PPD back to full positive voltage at the end of the read cycle to decrease readout noise. RS is used to select the correct pixel in combination with the column bus. TX is used to transfer the charge from the photodiode to the readout node. When a photon P strikes the heavily P doped region P+, the photoelectric effect causes the voltage to decrease across the PN junction.

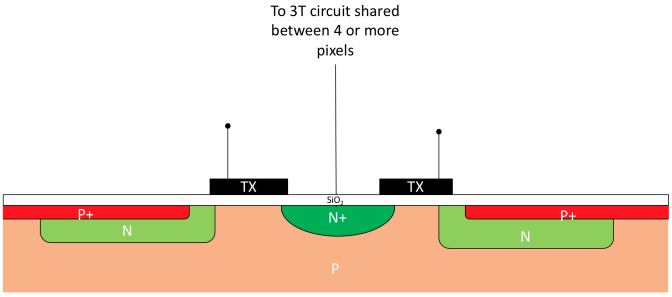

Figure 4.2: The Shared Pixel Concept results in four or more pixels sharing common readout circuitry allowing pixel pitch to approach the $1\mu m$ limit. It is theorised that sharing readout circuitry increases Fixed Pattern Noise in macroblocks of a size matching the number of pixels sharing the same circuitry.

architecture pixel size has been unable to effectively make pixels smaller than 3 µm without sharing the on-pixel readout circuity between multiple pixels. This shared pixel concept has allowed pixels to approach the practical limit of 1.0 µm [10]. This technology dominates the current generation of mobile phone image sensors and results in a biased increase of fixed pattern noise (FPN) corresponding to the macroblocks of pixels sharing the same transistors.

A principle driving factor behind the inability to shrink the photo-sensor area is due to the limitations imposed by the signal-to-noise ratio (SNR) [10]. If consideration is isolated to photon shot noise, the statistical variation of photons striking the sensor, it can be shown that the absorption of incoming photons

by a pixel is easily modelled as a Poisson process [10]. These photons are also characterised by a noise component σ_{ph} which is known as shot noise:

$$\sigma_{ph} = \sqrt{\mu_{ph}} \tag{4.1}$$

The flux of μ_{ph} photons results in μ_e electrons stored in this pixel since the photoelectric effect causes direct integration of photos to electrons also characterised by a noise component of variance σ_e^2, proportional to μ_e.

Assuming a hypothetical noise-free image sensor and noise-free electronics, the performance of the image sensor based system will be limited by photon shot noise. The maximum signal-to-noise ratio can be described as follows:

$$\left(\frac{S}{N}\right)_{MAX} = \frac{\mu_e}{\sigma_e} = \frac{\mu_e}{sqrt\mu_e} = \sqrt{\mu_e} \tag{4.2}$$

From this equation, it can be seen that the CMOS process does not determine the minimum size of the pixel. Instead, the number of electrons that can be stored in the pixel successfully while overcoming any noise issues is the determining factor [56].

Even with these noise limitations however, efforts to shrink pixels continue unabated with new technologies combining CCD and CIS techniques with integrated pixel optics to achieve "subapertures" as small as 0.75 μm in size [57].

Accurate noise models, analysis of image sensors regarding noise, and attempts to reduce noise, are thus important areas of research to maximise the efficiency of ever-shrinking image sensors.

4.4 Rethinking the noise model for Forensic Advantage

In this Chapter we are contextualise the existing literature and exploring the current methodology for improvement to see if additional forensic indicators

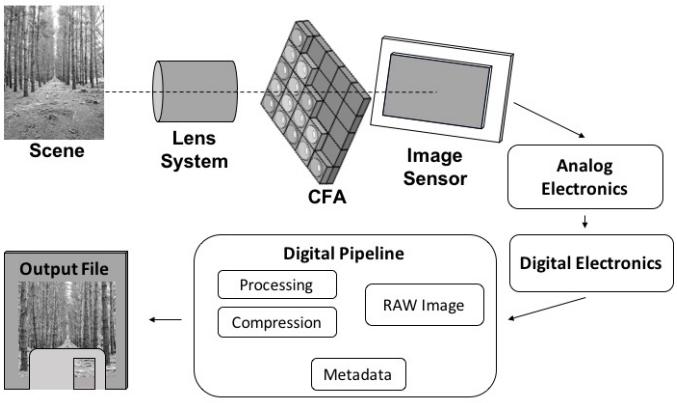

Figure 4.3: The image capture process referred to as the image pipeline contains two discrete sections, the analogue and the digital. Each element within the pipeline can be exploited to solve the camera identity problem. The analogue pipe consists of the lens optical system including the colour filter array and microlens system, the image sensor and the analogue readout electronics. The digital pipe commences from the output of the analogue to digital converters (ADC) and involves all the in-camera digital processes the discrete digital signal transverses before finally being saved as an image file.

may be exposed. Currently, the pixel size is not determined by the limitations of CMOS technology but rather the physical capacity for electrons within the N-well region of the photo-detector, be it a photo-gate, photo-diode or pinned photo-diode [56]. This limitation is seen with current CIS unable to breach the 1.0 μm pixel pitch limit [58] even with CMOS fabrication currently pushing beyond the 1nm scale. The number of electrons that can fit in the pixel is an important observation that will be revisited.

An abstract model of noise within image sensors can be developed by first focusing on what is known as the image pipeline (Figure 4.3). This pipeline is the process through which an optical image is converted and processed as an electronic signal to result in a digital image capable of being saved in the multiple formats commonplace today. Each element of the pipe adds an element of noise to the signal resulting in an additive noise model [10]. Through careful analysis of this pipeline, a noise model has been developed (Figure 4.4).

For a single image, the discrete sources of noise can be modelled as an additive combination of sensor pattern noise, lens optical effects, digital processing

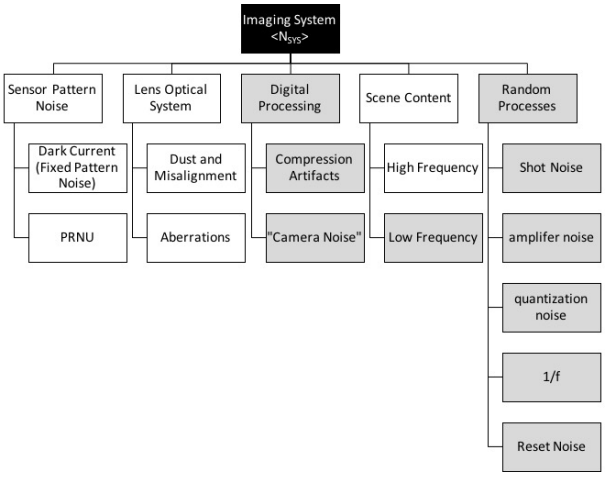

Figure 4.4: The noise residue model as proposed in our work based on the system noise equations from [10]. The dark grey boxes indicate sources of noise that can be easily removed. Random processes are traditionally removed through frame averaging [10] while RAW format images remove digital processing artefacts [16]. The low-frequency components of the scene content and all other sources of noise are removed due to the high-pass filter that the images are passed through to obtain the noise residue in the current unique PRNU signal fingerprinting method.

artefacts, scene content and random process [10]. To analyse the noise model for forensic advantage, the focus is linked to the areas that are related to the image sensor itself, namely the optical effects caused by integrated filters and lenses, noises caused by semiconductor physics of the sensor and integrated "on-chip" electronics, and the impact of the environment the sensor operates within. Such a focus allows the image sensor to uniquely describe the camera and not the parallel processes an image runs through before saving.

To determine which noise dominates a complete SNR analysis must be undertaken [10]. An SNR analysis is not the focus of this Chapter but can be seen in Chapter 6.

4.4.1 Optical Effects

To isolate the image sensor within the model, the first step is to ensure all other contributions of noise from the image pipeline have been eliminated. It is seen in Figure 4.3 that before entering the sensor, light first must pass through a

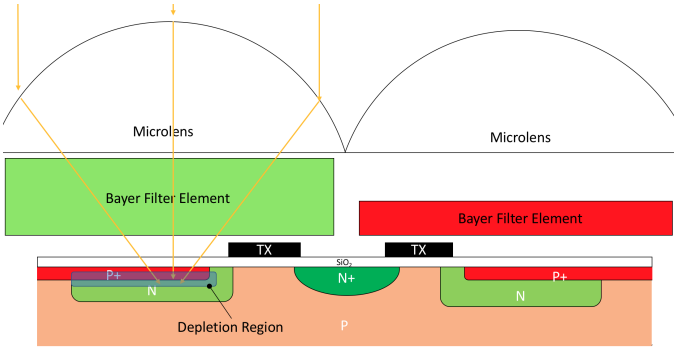

Figure 4.5: A shared pixel concept CIS with CFA elements and microlens attached.

lens system. Lens systems are not without error. Aberrations in multi-lens design and the lens itself include spherical aberration, coma, astigmatism, the curvature of field, distortion and chromatic aberration (a particular case of spherical aberration). These are commonly referred to as the primary or third-order Seidel Aberrations after the work of Ludwig von Seidel in 1857 [42]. Each aberration causes the light rays travelling to deviate in some manner from the optical axis of the lens resulting in optical noise which can be confined to either a pixel, group of pixels or the whole image. The relevant mathematical proof behind each aberration has been well explored in the literature, and many texts have been written on the topic [59].

In addition to the lens system, each image sensor has integrated by design an optical colour filter array (CFA) to ensure colour images can be obtained from broad wavelength light-sensitive silicon. To focus light onto the photosensitive area of the pixel, each pixel also includes a microlens (Figure 4.5). Should any of these elements be incorrectly manufactured additional noise will be introduced to the system per the same aberrations as above.

Finally, due to physical properties of light, namely Planck-Einstein's Formula, each discrete photon carries different levels of energy according to its wavelength λ:

$$E_{ph} = \frac{hc}{\lambda} \tag{4.3}$$

where h is Planck's constant $6.626 \times 10^{(-34)} Js^{-1}$ and c is the speed of light. This energy results in longer wavelengths penetrating deeper into the sensor before being absorbed [10], affecting photon shot noise.

Optical effects have already been shown to be useful for forensic advantage using discrete lenses and CFA processing artefacts as the identifier. This identification has been achieved primarily through the use of radial lens distortions [60] and CFA interpolation algorithms [61]. What has not been shown is how variance in the CFA elements construction may affect penetration of photons to the sensor substrate below. Additionally, aberrations within the integrated microlens have yet to be included in the consideration of the overall noise profile since the sensor contains these elements that physically cannot be removed without destruction. This integrated microlens provides a point of difference that may be exploited for forensic advantage or otherwise contaminate the noise profile of the underlying silicon.

To illustrate the optical effects a side by side comparison of pixel intensities across a single row of an image taken with two separate lens systems is shown in Figure 4.6. In this graph, the top figure represents a row 1024 of a 2048x2048 image taken by an integrated lens. The bottom section displays the same row as taken with a pinhole lens. The pinhole image was taken with a suitable exposure time to ensure that the amount of light entering the sensor was the same. It is clear that the optical effects are removed since the variation of the pixel intensities is decreased in the pinhole image. This is most obvious towards the centre of the row where the intensity of the pixel is mostly uniform for the pinhole, however it increases for the lens. Such an aberration would be seen in an image as vignetting.

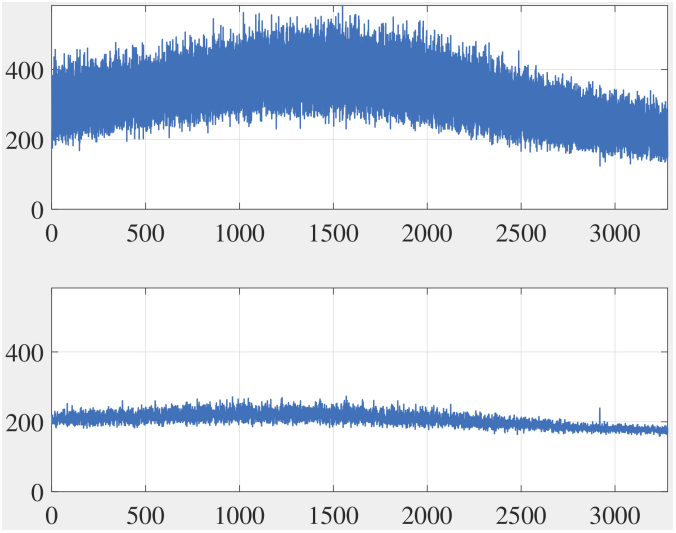

Figure 4.6: Comparing image line 1024 of a 2048x2048 image we see that an image taken with a lens (top) shows aberration effects with the light concentrated towards the centre of the image. Replacing the lens with a pinhole (bottom) removes these aberrations as demonstrated from the decreases in pixel to pixel variance and smooth response across the row.

4.4.2 Semi-Conductor Physics

The basic operation of a photodiode has been described above in section 4.3. The primary process is to fill the N-well region of the photodiode with electrons in proportion to the number of photons that have excited the sensor. Under normal operation, however, the number of photon-induced electrons is combined with dark current electrons caused by the physical properties of the PN junction. Three primary sources generate this dark current: irregularities in the silicon structure, diffusion current due to Fick's law and depletion region current which follows Ohm's Law [62].

The various sources of dark current are complicated to model. This complexity is also in part due to issues with generation in multiple regions as dark current is not just generated in the photosensitive region. These regions include the depletion region, the field-free region and the surface of an oxide layer interface, as well as dark current increasing exponentially with temperature [10].

With much work devoted to the subject, it is often enough to model these

interactions by simplifying DSN (D_{e^-}) to the following [10]:

$$D_{e^-} = \frac{J_D A_D t_{int}}{q} \tag{4.4}$$

Where A_D is the detector area, t_{int} is the integration or exposure time, q is the charge of an electron $q = 1.6 \times 10^{-19}$ coul and J_D is the dark current density which is proportional to:

$$J_D \propto T^2 e^{\frac{(E_t - E_G)}{kT}} \tag{4.5}$$

where k is Boltzmann's constant, $k = 1.38 \times 10^{-23}$ J/K, T is the temperature in degrees Kelvin and $(E_t - E_G)$ is the difference in bandgap energies for the impurity carrier and the primary carrier respectively.

From here it is possible to estimate the dark current at a specific temperature from a known image sensor at a given exposure time.

These dark current electrons n_{DARK} will be combined with the photon generated electrons $n_{PE}$to fill the N-well region:

$$n_{PE} + n_{DARK} = n_{WELL} \tag{4.6}$$

Since no silicon wafer is without defect and no two pixels are uniformly the same it is seen that the dark current will be measurably different between two pixels, however, is usually treated as uniform and quasi-stable for a sensor as a whole [63].

At the heart of the operation of an image sensor is the N-well region filling with electron generated photons thanks to the photoelectric effect at the depletion region between a PN junction at the N-well region. Since the size of this well differs from pixel to pixel, and sensor to sensor, it is possible to create a unique signal or fingerprint from the PRNU noise. This concept is the work of [12] which focuses on how N-well of each pixel can be filled to an equal

amount via photonic energy. Each pixel is then read out via the well described processes and ultimately saved as an image. The slight variation of each pixel is measured on a pixel to pixel basis due to the differences in the ability of the PN junction of the photosensitive region to recombine photons.

It has been stated that dark current can be ignored for forensic purposes due to dark-frame removal [12], the subtraction of a frame exposed without opening the shutter of the same length of time immediately before taking an image. However, since the N-well region can be filled with electrons via dark current generation (equation 4.6), it is theoretically possible to measure a unique PNU signal in the same manner with the dark current being the excitation source rather than photons.

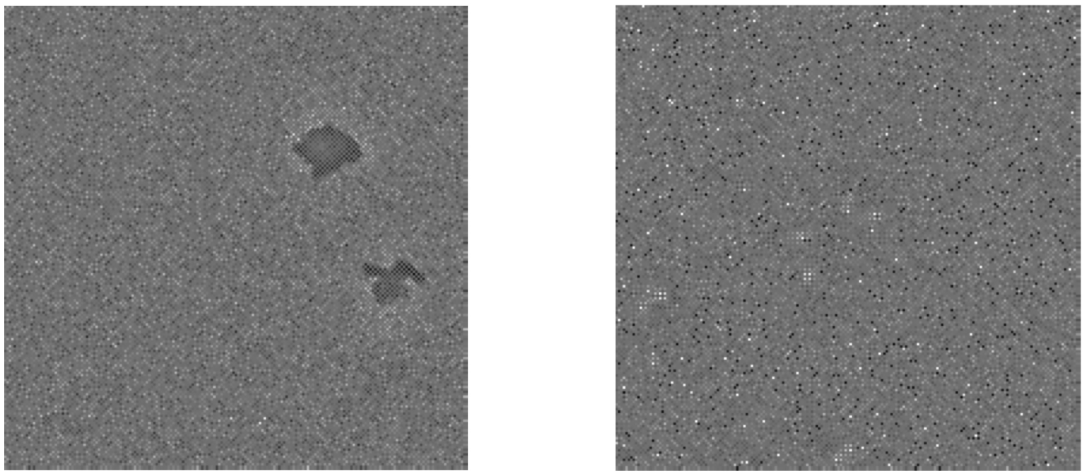

Figure 4.7: A side by side comparison of the green layer of the fingerprint obtained using PRNU through a pinhole (left) and dark current (right). The effects from sensor dust are clearly visible in the pinhole image while these are absent in the dark current equivalent section. Kurosawa hot pixels are apparent in the dark current fingerprint as salt and pepper noise on top of the fingerprint.

Since dark current density increases exponentially with temperature and proportionally with exposure time it is theoretically possible to completely saturate the N-well region with electrons generated purely from dark current, especially if the pixel pitch is small, as seen in mobile devices. By controlling these two parameters, it is proposed that a valid unique fingerprint can be obtained from

Table 4.1: Correlation of 100 image PRNU reference pattern vs single dark current fingerprint: Camera One

Temp (°C)	0° Rotation	90° Rotation	180° Rotation	270° Rotation
20	0.0219	1.30e-03	2.00e-03	1.70e-03
45	0.0408	-8.68e-04	1.28e-05	3.50-05

Table 4.2: Correlation of 100 image PRNU reference pattern vs single dark current fingerprint: Camera Two

Temp (°C)	0° Rotation	90° Rotation	180° Rotation	270° Rotation
20	0.0335	1.10e-03	2.00e-03	7.23e-05
45	0.0740	-7.56e-04	1.28e-04	-2.64-08

Table 4.3: Correlation of 100 image PRNU reference pattern vs single dark current fingerprint: Flipped PRNU

Temp (°C)	0° Rotation	90° Rotation	180° Rotation	270° Rotation
20	1.30e-03	-8.01e-04	7.67e-04	1.30e-03
45	8.733-04	-1.20e-03	-7.77e-05	-9.31-04

a sensor using dark current electrons alone. Such a fingerprint is demonstrated in Figure 4.7. Demonstrating the reliability of such a fingerprint in a forensic context is beyond the scope of this Chapter and will be demonstrated in Chapter 7. However, to demonstrate that the fingerprints are indeed similar some observations are made, using the toolbox provided in [8] and the method of dark frame removal discussed in Chapter 7 Within the dark current fingerprint the Kurosawa hot pixels [32] need to be suppressed for an accurate comparison. This results in a salt and pepper noise artefact present within the fingerprint. Additionally, since light is not used to generate the fingerprint there is no contamination from dust as seen in the PRNU reference pattern.

Demonstrating that the dark current fingerprint is correlating to the PRNU fingerprint a set of correlations is calculated for a single image dark current fingerprint at T=20°C and 45°C against a 100 image PRNU reference pattern (Table 4.1). The PRNU reference pattern is rotated 90°, 180° and 270° as a proxy for a deliberate mismatch to ensure correlation is indeed occuring with

the reference pattern and not an arbitary artefact of the sensor design. This is repeated for another camera in table 4.2 with the results confirming the previous demonstration. Finally, to ensure that the correlation is between the excitation of the silicon and not the read out of the sensor design itself half the PRNU reference pattern is swapped with the other half of the reference pattern to create a deliberate mismatch while maintaining colour filter rotation. These results are shown in table 4.3 with no significant correlation detected. These results demonstrate our hypothesis that a dark current fingerprint can be generated which may form as a substitute for the current PRNU methodology. A full analysis is left for Chapters 6 and 7.

4.5 Micrometer Imagery

To illustrate these concepts we have discussed above a cross-sectional image of a Sony IMX219PQ [64] image sensor that was taken under a scanning electron microscope. Using an FEI Dual Beam Helios Nano Lab 600 [65] scanning electron microscope, two excavations were made into a Sony IMX219PQ CIS. Since the CIS is conductive, no sample preparation is required before scanning. First, a layer of platinum is deposited above the area to be excavated to prevent fracturing (Figure 4.8). After the platinum is deposited a process of staged cuts are made using a gallium ion beam to create an excavated area through the sensor that can be imaged (Figure 4.9).

Using a magnification of 20,000x, a current of 0.17nA and voltage of 10kV, images are then obtained of the top layers of the integrated CIS containing the pinned photodiode. Since our study is not concerned with the readout circuitry, we exclude it from our observations. The process is repeated for a diagonal cross section to ensure multiple pixels across CFA regions are obtained.

In Figure 4.10 a layered PPD architecture is seen as expected. This PPD architecture uses a shared pixel concept with multiple transfer points (shown

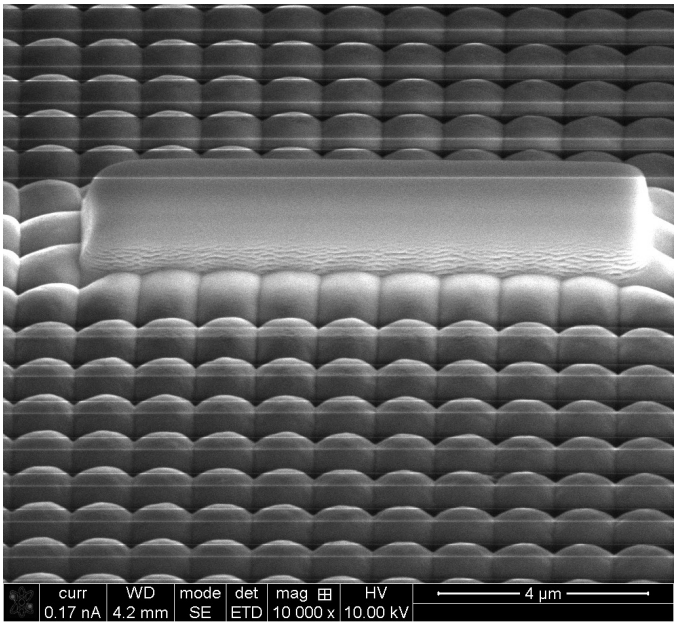

Figure 4.8: Platinum (shown here as a growth on top of the micro-array) is deposited on the CIS to prevent micro-fractures forming during the excavation process.

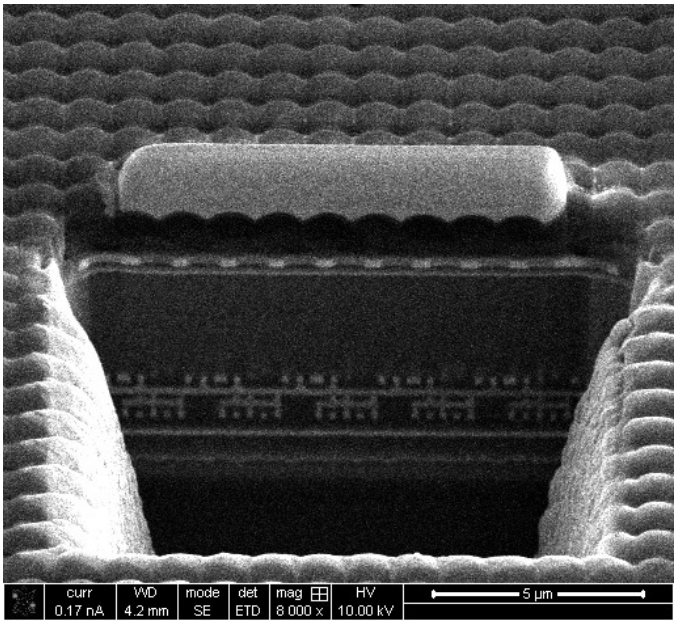

Figure 4.9: The excavated region of the CIS is shown after the Gallium ion beam has been used to step out the material present in the region of interest. Several passes are used to obtain a smooth, polished cross-section.

as TX). Using Energy-dispersive x-ray spectroscopy, the architecture can be determined in detail. Elements detected in the EDX analysis include Platinum,

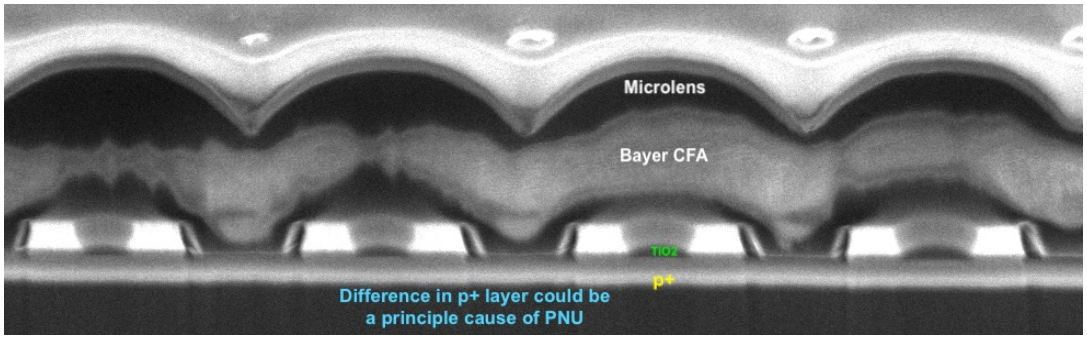

Figure 4.10: A diagonal cross-sectional view of the Sony IMX219PQ CIS. Four pixels are shown. The pinned photo-diode shared pixel architecture is visible. The Pinning layer is marked P+.

Carbon, Gallium, Oxygen, Silicon, Tungsten, and Titanium. The presence of gallium and platinum must be excluded since they are used in the SEM processes outlined above. However, using reasonable assumptions, the areas of the CIS in the image as shown can be reverse engineered. An isolation oxide layer directly below the PN junction made from titanium dioxide is observed as part of the structure. This TiO2 layer electrically isolates the PN junction from the underlying substrate and also isolates any photons from further penetrating into the underlying substrate [10].

To explain the structure and operation we refer to [64]. Light first enters the sensor via the microlens array and is then filtered using a Bayer filter. The IMX219PQ sensor has traditional "R, G, and B primary colour pigment mosaic filters" CFA [64]. These filter elements are not uniform in their construction, and it is seen that even cells of the same colour have different widths (Figure 4.10). From Equation 4.3 it is clear that this will result in different wavelengths being filtered out on a pixel by pixel basis rather than just the three principal components being isolated by the chemical composition of these layers. This filtering will cause chromatic distortion. While the cause of variation in the CFA layer is impossible to determine from this image, an indication is given from the P+ pinning layer directly below. Since the CMOS process manufactures each layer on top of the previous layer, variations in the layers below will cause issues

in the layers above. It is seen that the width of the pinning layer is different from pixel to pixel in the cross-sectional view not just in width but also in length. This pinning layer will affect the performance of the photosensitive PN region and even the dark current of each pixel.

Since there are variations between each pixel, it may be possible to isolate and hence exploit these variations, to create better processes to isolate a unique fingerprint for the sensor.

4.6 Conclusion

SPN has shown to be a promising area of research for answering provenance questions relating to imagery. It still suffers from reliance on large data sets ideally constructed from flat fielded images and a-priori information that is not always apparent or readily available to forensic investigators in the field. By rethinking the noise model of a digital camera, SPN can be isolated as an element that is primarily dependent on the physical silicon that each image sensor is built from, regardless of technology. From this analysis, it can be seen that there are alternative ways to create the unique fingerprint that will not rely on large data sets or mass computational resources. Indeed, by drawing focus to dark current an opportunity arises to explore the temperature bias which is present within to see how this affect may impact upon the sensor pattern noise methods. Before this can begin however, a study as to the origins of SPN must be undertaken to confirm the source of the noise. Such a microscopic analysis is the subject of Chapter 5. DSN must then be appropriately isolated within the current SPN methodologies. This is the topic of Chapter 6. Finally, an analysis of temperature effects resulting from DSN is presented in Chapter 7.

Authorship Statement:

Title of Paper:	Reverse Engineering the Raspberry Pi Camera V2: A study of Pixel Non-Uniformity using a Scanning Electron Microscope
Publication Status:	Submitted for publication
Publication Details:	Submitted to Digital Investigation 10/Jan/2019. Under Review 15/Jan/2019.

Name of Principal Author:	Richard Matthews
Contribution to paper:	Collected all data, Performed analysis, interpreted data, wrote manuscript and acted as corresponding author.
Overall Percentage:	85%
Certification:	This paper reports on original research I conducted during the period of my Higher Degree by Research candidature and is not subject to any obligations or contractual agreements with a third party that would constrain its inclusion in this thesis. I am the primary author of this paper.

Signature

Date

Co-Author Contributions

Certification: By signing the Statement of Authorship, each author certifies that:

1. the candidate's stated contribution to the publication is accurate (as detailed above);
2. permission is granted for the candidate to include the publication in the thesis; and
3. the sum of all co-author contributions is equal to 100% less the candidate's stated contribution.

Name of Co-Author:	Dr Matthew Sorell
Contribution to the Paper:	Supervised development of work, helped in data interpretation and manuscript evaluation.

Signature Date

Name of Co-Author:	Dr Nickolas Falkner
Contribution to the Paper:	Supervised development of work, helped to evaluate and edit the manuscript.

Signature Date

Chapter 5

Reverse Engineering the Raspberry Pi Camera V2: A study of Pixel Non-Uniformity using a Scanning Electron Microscope

5.1 Abstract

In this chapter we reverse engineer the Sony IMX219PQ image sensor, otherwise known as the Raspberry Pi Camera v2.0. We provide a visual reference for pixel non-uniformity by analysing variations in transistor length, microlens optic system and in the photodiode. We use these measurements to demonstrate irregularities at the microscopic level and link this to the signal variation measured as pixel non-uniformity used for unique identification of discrete image sensors.

5.2 Introduction

Sensor pattern noise (SPN) has been accepted as a viable method to identify a unique camera responsible for taking a specific image. These methods rely on the non-uniform nature of individual pixels, known as pixel non-uniformity

(PNU), to establish a unique reference pattern. There exists a gap in the literature which clearly explains the cause of PNU, especially with the purpose of informing jurors in mind. Sensor pattern noise (SPN) methods based on PNU are important for intelligence communities, law enforcement communities and can have additional applications for photographers wishing to establish ownership without relying on metadata or additional watermarks. While SPN methods are accepted by the forensic community (an important Daubert criterion)[1] there is a risk that a lay juror with no mathematical background may be confused by the evidence presented in a court setting. This can be confounded by issues such as the *CSI effect* where a juror expects Hollywood science to replace real forensic methodology.

In this chapter we explore some of the physical characteristics of the IMX219PQ image sensor, providing direct evidence of variation which may cause SPN. We reverse engineer the design, and analyse three features of an image sensor under a scanning electron microscope: transfer gate length, variations within the microlens optic system (LOS) and variations within the photodiode region. It is hypothesised that the variations within these features are principally caused by tolerances in the manufacturing process, can visually be seen under significant magnification, and may contribute to PNU.

5.3 Related Work

The existing literature asserts, without apparent experimental validation, a blanket statement for the source of PNU [12]. "PNU is caused by the inhomogeneity of silicon wafers and other imperfections during the manufacturing process." The focus of the literature since has been directed on improving the method first identified as distinct from identifying the underlying source. A gap

[1]The Daubert criterion relate to a set of five factors to determine the admissibility of forensic evidence. The five factors are: a testable theory, peer review and publication of the theory, a known error rate for methodologies, the existence of operating standards and if it has reached widespread acceptance. [66].

exists to address this underlying assumption as to the source of PNU within the pixel unit of an image sensor. Clarifying this assumption is important for forensic identification purposes should the literature be challenged in a legal setting.

We focus on three feature categories which may cause the PNU used to uniquely identify each sensor. These are: variations within the length of the transfer gate, within the micro lens optical system (LOS) and within the photo diode itself. The justification for this approach is given in the related works below.

[67] provides an analysis of key geometric properties within the structures of an image sensor and how this affects the charge transfer efficiency (CTE). Variable CTE values for discrete pixels will cause PNU. The geometric aspects investigated by [67] include the photodiode size, the transfer gate length and the sense node (SN) storage area. The SN is also referred to as a floating diffusion (FD). The two terms are able to be used interchangeably. In both cases, the region refers to a highly-conductive region without resistive connection to allow the storage of charge, in effect a capacitor. [67] showed that in all instances of geometric variation it was the length of these critical geometries which affected the CTE of the device. Incomplete transfer between photodiode and SN also causes image lag and noise on an individual pixel [68]. This provides justification to measure the lengths of the transfer gate as well as the photo diode as a possible source of PNU.

Differences in the transfer gate are also responsible for dark current variations. Dark current is generated in the transfer gate by the silicon to silicon dioxide interfaces or by defects below the surface of the gate itself [68]. We shown in Chapter 7 the use of dark current for thermal identification of image sensors. Dark current has also been used in isolation and in hybrid methods for image identification alongside PRNU [41]. Measuring differences within the

transfer gate thus provides additional motivation as larger gates will provide greater surface area interactions for dark current generation.

In Chapter 6 we show the contamination of lens effects within the SPN methodology. In [69] the non-uniform output of a photodiode was presented. [69, Fig. 2 c] shows the non-uniform output of the diode while being excited by a 7V laser through various incident angles. The output of the photodiode was measured to vary between 305mv and 208mv depending on the incident angle of the laser. Given the non-uniform output demonstrated in this work it is hypothesised that this could be a contributor to PNU in image sensors. Assuming this is a contributor of PNU in image sensors, it is theorised that this would manifest via misalignment within the micro LOS of a sensor focusing or filtering photons to different areas of the depletion region of the photodiode. This would be distinctively different to PNU being caused by variance in doping levels within the photodiode or the size of the photodiode during manufacture. Such misalignments should be possible to visually see under cross-sectional analysis through the use of a scanning electron microscope. This provides justification to examine the micro LOS of the image sensor.

5.4 Research Methodology

Using a Sony IMX219PQ [70] image sensor as the test subject imaging was performed under an FEI Dual Beam Helios Nano Lab 600 scanning electron microscope [65]. The Helios allows imaging down to 1nm at 15kV. Minimal preparation of the sample is required before imaging since the image sensor is made primarily of silicon and hence, is conductive to the electron beam. The IMX219PQ comes as a package board from the Raspberry Pi Foundation. The sensor is de-constructed to obtain the silicon wafer in isolation to the peripheral circuit and attached to the FEI imaging platform by way of adhesive conductive dot. The platform is tilted to 52° to enable imaging and machining by the gal-

lium focused ion beam. Under magnification, a layer of platinum was deposited above the area to be excavated to prevent fracturing (Figure 5.1a). After the platinum is deposited a process of staged cuts were made using a gallium ion beam to create an excavated area through the sensor that can be imaged (Figure 5.1b). The gallium ion beam is capable of machining down to 5nm allowing precise cuts to be made. This is a destructive process.

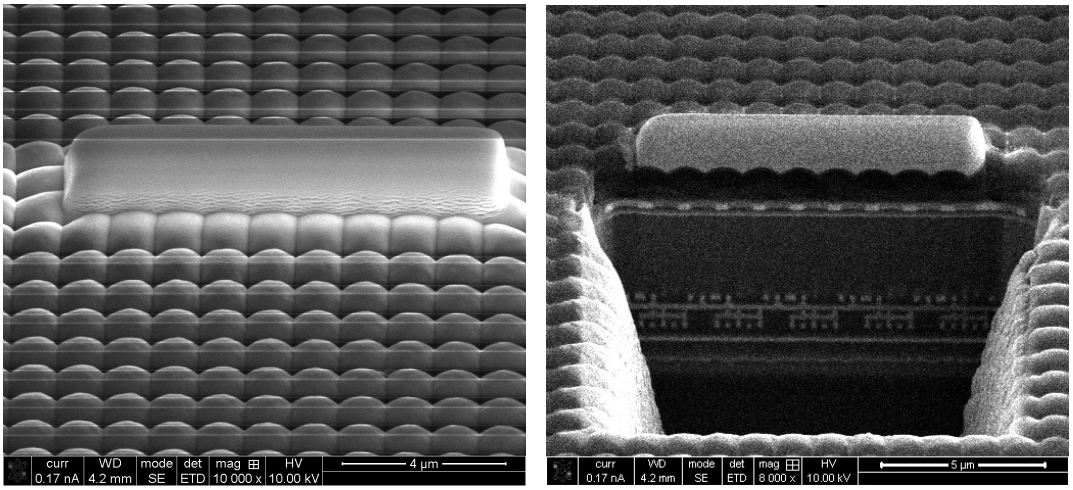

(a) (b)

Figure 5.1: (a) Platinum (shown here as a growth on top of the micro-array) is deposited on the CIS to prevent micro-fractures forming during the excavation process. (b) The excavated region of the CIS is shown after the Gallium ion beam has been used to step out the material present in the region of interest. Several passes are used to obtain a smooth, polished cross-section.

Using a magnification of up to 100,000x (400nm scale), a current of 0.086 - 0.17nA and voltage of 5-15kV, images are then obtained of the top layers of the integrated CIS containing the pinned photodiode and the associated supply and readout circuitry. Only the top silicon wafer is studied.

5.5 Data Collection and Analysis

5.5.1 Reverse Engineering

Using [68], Figure 5.2 and 5.3 presents the layers of the CIS with each region identified. The sensor is a back illuminated sensor (BIS) with a pinned photodiode (PPD). The P+ pinning layer can be seen in Figure 5.3. In Figure 5.2 the width of the sensor is measured as approximately 6um. This is consistent with the provided literature from Sony [71] which also indicates a dual wafer design. This is confirmed in these images with the bonding surface between the two wafers indicated in Figure 5.2 at the appropriate distance from the top of the micro LOS. In the micro LOS the structure can be seen as a main lens, passivation layer, Bayer filter and then a minor sub lens nestled in between the nodes of the wire grid. The photodiode region is identified and isolated between two layers of P doped semiconductor used to prevent cross talk. The isolation regions are located directly beneath the wire grid used for optical isolation. This is seen more clearly in Figure 5.3 where the microscope is focused onto the read out circuit layer of the image sensor.

Using reference images from [68], the Bayer filter elements visible in Figure 5.3 are identified as green and red. This is made out as the red filter elements are thinner than green with the blue elements being thicker and filling almost the entire layer. The transfer nodes (TX) are visible within the image. From here it is possible to identify the individual transfer, M1 reset (RST), M2 source follower (SF) and M3 column select transistors within the Metal 4 layer. The wiring for each of these nodes is then routed to the underlying metal layers to provide read out access to the circuit, most likely on the peripheral or underlying silicon wafer. The TX wires are seen within the Metal 2 layer while it is assumed that the Vcc, select and column bus tracks are visible in Metal 1.

Using the information identified above in conjunction with [72] and [68] an

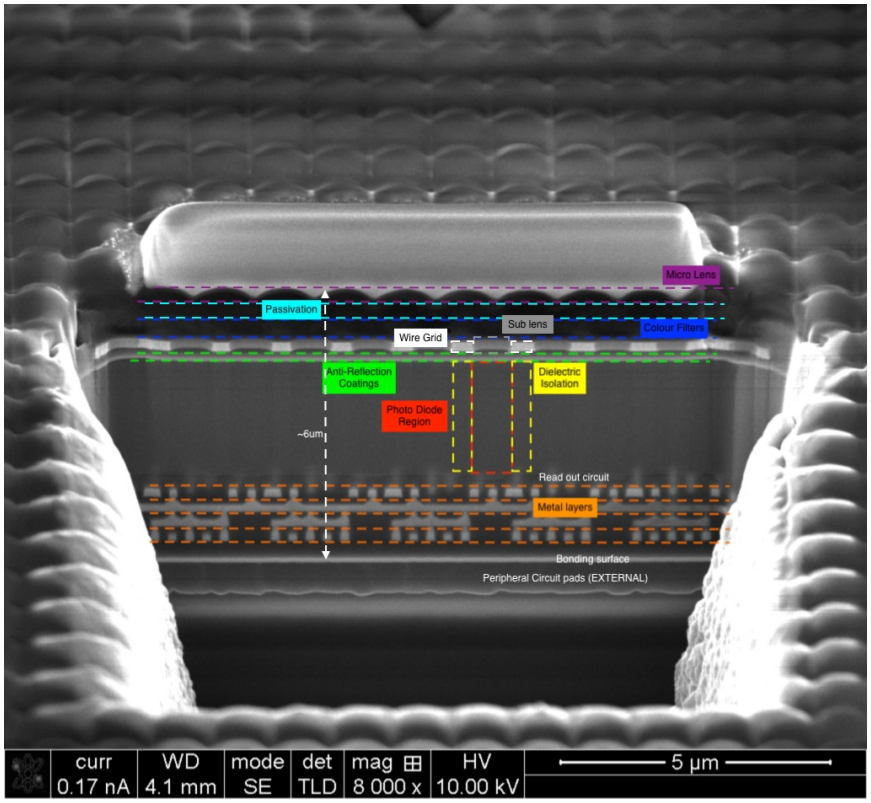

Figure 5.2: A horizontal cross-section of the IMX219PQ sensor. Each region of the sensor is clearly identified.

equivalent circuit can be identified for the Sony IMX219PQ BIS pixel unit. From examining [72] we see that the sensor has the capability to store defective pixels in one of three modes: single pixels, single adjacent pixels by Bayer element and individual blocks of 2x4 adjacent pixels. Understanding how the sensor stores defects provides insight to the readout structure. It follows that the sensor has a pixel unit comprising of 2x4 photodiodes sharing a single readout circuit. Using [68] the pixel unit is comprised of a circuit of eleven transistors for every eight photodiodes. Using the familiar nomenclature of average number of transistors per pixel we see the IMX219PQ is a 1.375T (11 transistors per 8 pixels) design. This is indicated in Figure 5.4.

We suspect that the clover leaf pattern is utilised as per previous Sony iterations, in particular the sensor (Sony IMX145) in [68]. Unlike the equivalent

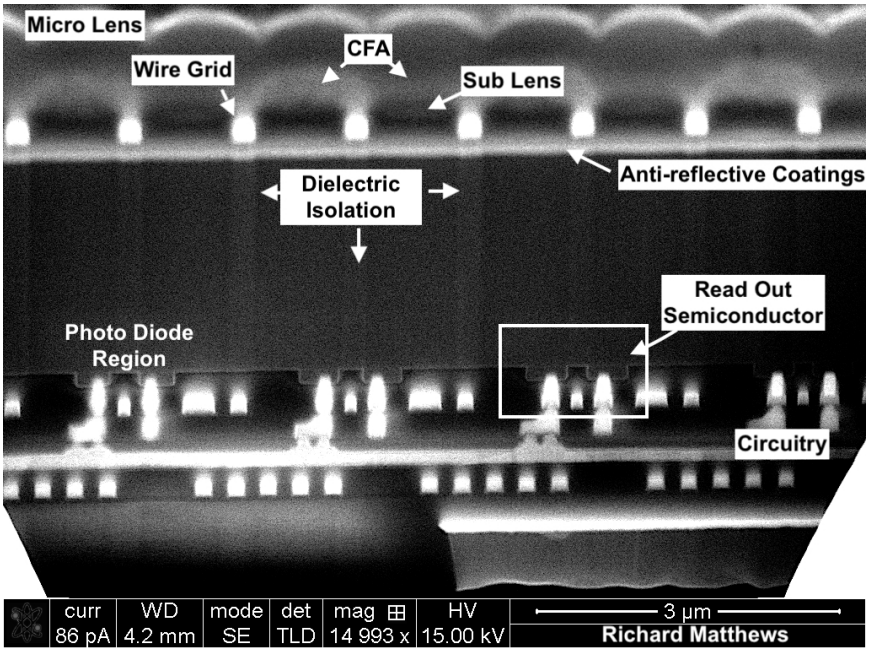

Figure 5.3: A secondary cross-section of the IMX219PQ sensor. The structure of the photodiode and circuit is identified within the image.

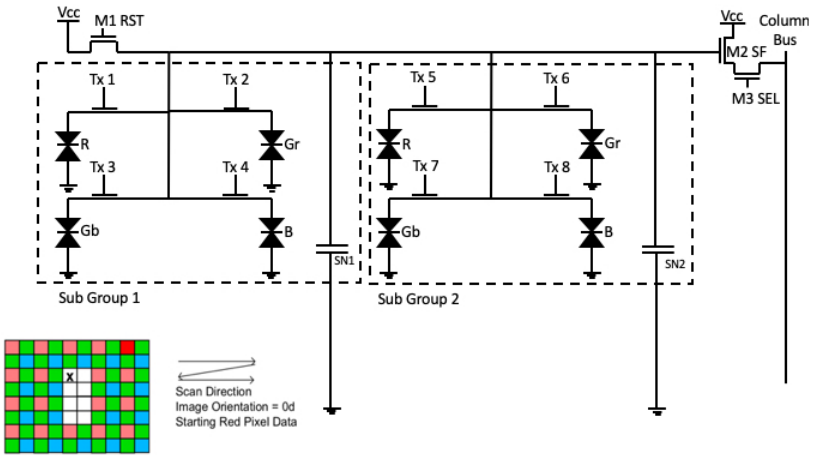

Figure 5.4: The equivalent circuit for the IMX219PQ pixel unit. Inset shows the scanning direction for read out of the IMX219PQ sensor when identifying a 2x4 pixel defect on the sensor taken from [72].

circuit shown in [68, Fig. 9] we show only two sense node locations corresponding to the sense node in each of the two pixel subgroups noting the work of Fontaine in [68, Fig. 10] showing these two locations in the centre of the clover leaf. We note that the charge for each photodiode when read out will be distributed on

both of these nodes in parallel due to Kirchoff's Current Law. The readout circuitry is an important distinction to clarify as it forms a significant source of dark current. Sensors that demonstrate a different readout structure (3T, 4T, 2T, 1.75T) provide a possible source of difference for forensic identification. The dark current of such sensor configurations should be measured in future work. The clover leaf pattern should also be confirmed by imaging the bottom of the sensor.

5.5.2 Transfer Gate

Measurements were taken of the readout node of the photo diode using the SEM built in measurement tool. These were then verified manually by printing images to scale and measuring by hand. These results are shown in Table 5.1.

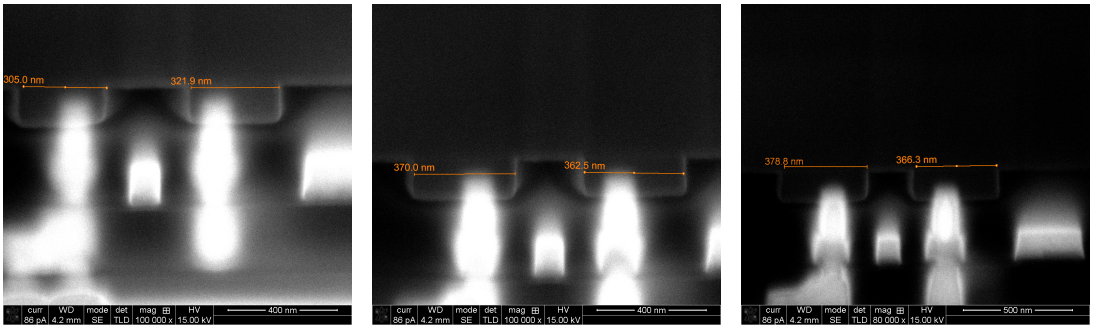

(a) (b) (c)

Figure 5.5: The length of six transfer gates are taken across three separate pixel units. For the image above, odd gates are green, even gates are red. (a) Transfer gates 1 and 2. (b) Transfer gates 3 and 4. (c) Transfer gates 5 and 6.

Table 5.1: Transfer Gate Length

Pixel	SEM Measure (nm)	Manual Measure (nm)	Average (nm)
1	305	308	307
2	322	329	326
3	370	370	370
4	363	364	364
5	379	380	380
6	366	378	372

There is variation with all transfer nodes measured. The mean of all six transfer nodes is 353nm. Measuring the variance to the mean from each transfer node we obtain a double sided tolerance of +27nm and -46nm. Extrapolating, this leads to a feature size of 350nm with an engineering tolerance of +/-50nm. The polysilicon layer has an average thickness of 160nm with metal 4 being approximately 280nm in thickness. This is consistent with the 130nm lithography process design rules in [73] noting we have labelled our metal layers in reverse order. This measurement is not consistent throughout the layer with the layer increasing and decreasing in thickness throughout the images obtained. This thickness variation will cause minor geometric changes to the features of the circuit. These thickness variations will become more pronounced in top layers as the variations stack.

5.5.3 Micro Lens Optical System

Two Green-Red Bayer elements are overlaid in Figure 5.6. In 5.6a the microimagery is presented for the two immediate, same colour, neighbouring elements with noticeable variations in the structure of these two identical Bayer elements. The stained blue shows a large segment missing to the right whereas the stained yellow is slightly thicker. The cropped images are run through a Canny edge detector in FIJI [74] to provide a binary gate to compare the two filter elements against. This result of the Canny edge detector is presented in 5.6b. White is where element 1, previously tinted yellow, is presented. Dark grey is element 2 previously tinted blue. Dark white is where both elements are, and light grey is where only element 1 is present. This shows the contrasting differences between the two CFA elements with a hole in element 2 positioned above the optical block (metal grid). These minor variations are likely to create optical aberrations known as Seidel aberrations affecting where individual photons will strike the depletion region of the photodiode [17, 42].

The Bayer filter is not the only region that is observed to have irregularities

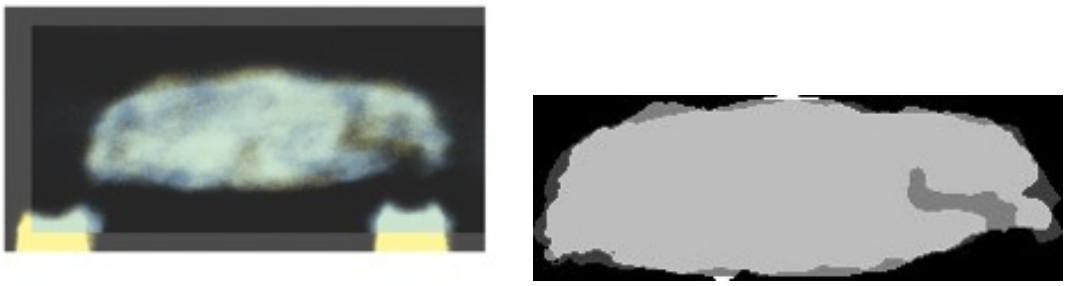

(a) (b)

Figure 5.6: (a) Overlay of the two Green-Red Bayer filter elements. (b) The overlay of the two Green-Red Bayer filter elements as a binary image using FIJI [74].

which will cause optical aberrations. Sectioning off the top layer of the micro LOS provides access to the passivation layer in between the micro lens and the Bayer elements. Holes in the passivation layer are visible directly above the wire grid elements as shown in Figure 5.7. This is another defect within the structure of the sensor that is not uniformly distributed on every pixel. Once again, the formation of holes within the upper layers of the micro LOS are likely to cause aberrations [17, 42].

5.5.4 Photodiode Variations

Four photodiodes and their length are shown in Figure 5.8. We note the presence of a charging artefact due to the highly conductive metal layers causing a smearing effect into the photodiode region on the image. Measurements are taken well away from this artefact to avoid any contamination. Measurements are taken from the SEM and then confirmed via manual scaling as per section 5.5.2. These measurements are displayed in Table 5.2. All measurements show variation from photodiode to photodiode.

The mean photodiode length is measured as 894nm with a range of +/-14nm. The nominal pixel length is stated as being 1120nm (1.12um) [72]. Measuring the length of the isolation in between the photodiode regions we can obtain a measurement for the average pixel length. The P dielectric isolation is manually

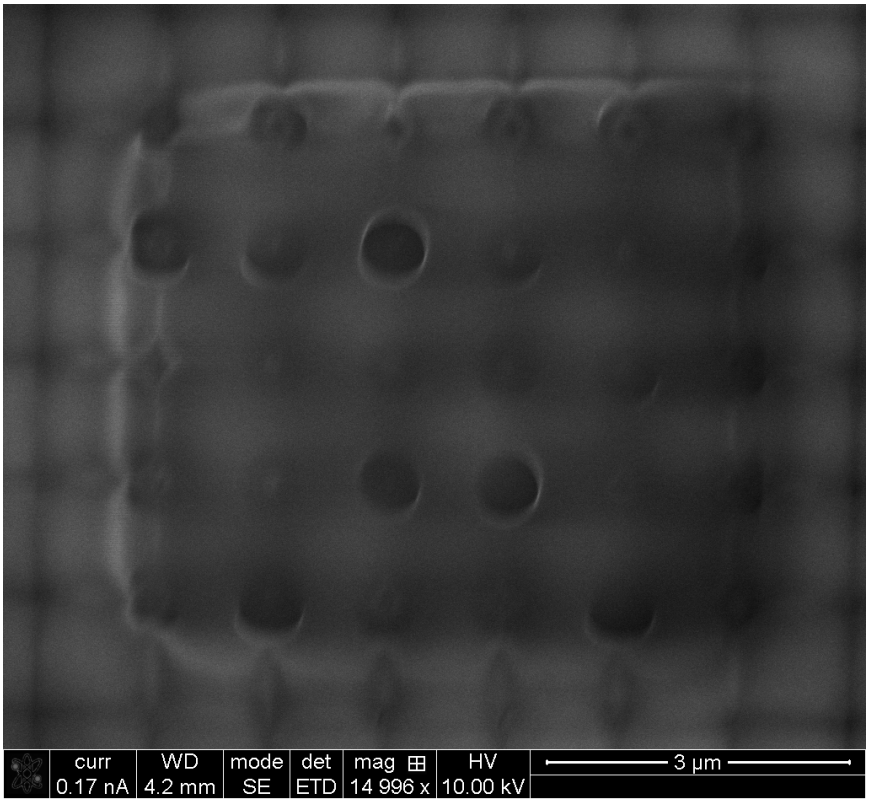

Figure 5.7: Sectioning the top lens layer of the IC reveals the passivate later above the Bayer elements below the micro lenses. Bubbles are evident above the wire grid in random locations on the surface of the chip.

Table 5.2: Photodiode length

Photodiode	SEM Measure (nm)	Manual Measure (nm)	Average (nm)
1 Gr	910	899	905
2 R	890	873	882
3 Gr	880	879	880
4 R	910	905	908

measured as above and displayed in Table 5.3. A mean measurement is obtained as 240nm. Adding the two mean measurements together obtains an average pixel length of 1134nm (1.13um). The four pixels in Figure 5.8 are manually measured to obtained a length of 451nm. This provides a mean measurement of 1127.5nm (1.13um). These measurements indicate that the pixel length is slightly larger than stated in the documentation but, likely within manufacturing tolerance of

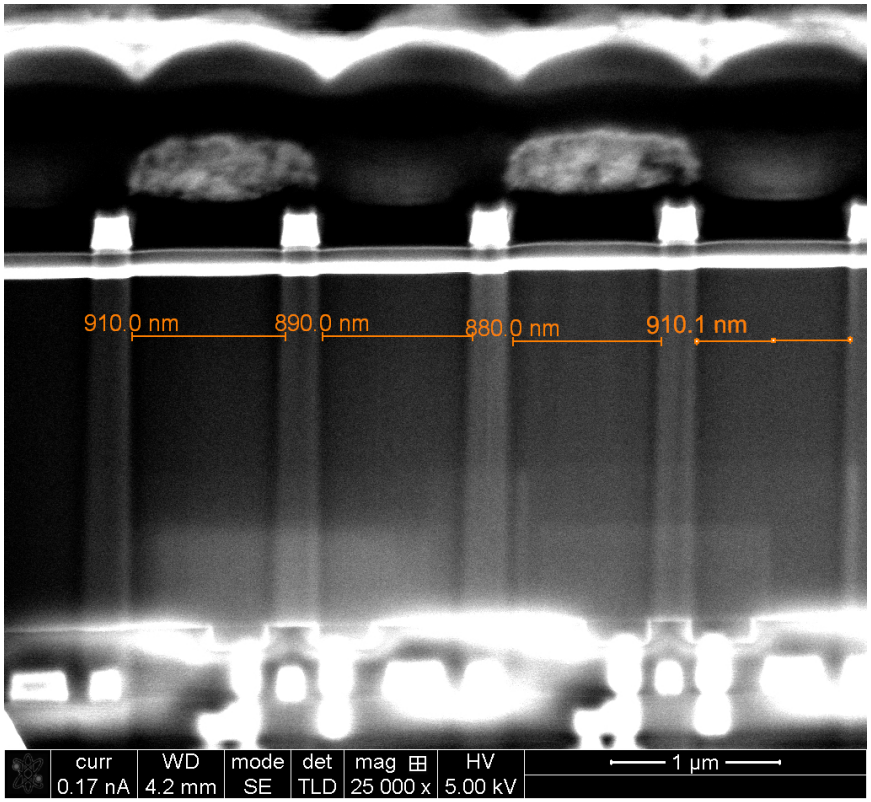

Figure 5.8: Four photodiodes from two separate pixel units compared for length.

1%.

Table 5.3: Isolation Length

P Isolation	Manual Measure (nm)
1 Gr	232
2 R	234
3 Gr	264
4 R	228

The variation in sizes across pixels is likely to be a significant contributor to PNU on the sensor as different sized photodiodes will have different light sensitivity and dark current behaviour.

5.6 Discussion

Dark current and Photo Response Non-Uniformity noise are leading candidates in SPN methods for identification of discrete image sensors from a candidate photo. [41] and [12] are both indications of how this method can be used with great success. The defects shown in Sections 5.5.2 and 5.5.4 are the features within the image sensor and the electrical circuit which are likely candidates to cause the non-uniform characteristics of both Dark Current and Photo Response non-uniformity used for unique identification.

Lens aberrations are known to link images to cameras [60]. Shown in Section 5.5.3 are irregularities in the micro LOS that are inseparable from the image sensor. Lens aberrations normally link an image to a LOS that is able to be separated from a camera. In the case presented here, the defects within the micro LOS are inseparable from the sensor itself and as such should provide a forensic link to the image sensor as opposed to an external LOS.

It is important to note that when we and the literature have referred to manufacturing defects we are not referring to quality control issues in the typical sense. Where defects would normally cause the scrapping of the sensor or entire wafer, the defects we discuss are minimal and still allow the sensor to operate within the designed engineering tolerance. It is this variability within tolerance that is being exploited here for forensic identification. While this trace is treated as unique it is also important to note that this has not been proven. The largest scale test of this method has been done by [8] where it was found, using the current state-of-the-art method, PCE identification has a false acceptance rate of less than 3 in 125,000. As this work has been conducted with the juror in mind, it is important to highlight this distinction for the purposes of the Daubert criterion.

5.7 Conclusion and Future Work

In this chapter we have demonstrated pixel non-uniformity within the silicon structure of the image sensor at the microscopic level. We have demonstrated discontinuities between discrete layers within the image sensor. While these discontinuities do not affect the overall image performance capabilities of the sensor they do contribute to a layer of additive noise known as PNU. Particular attention has been paid to the transfer gates and the associated read out circuitry. This work has drawn attention to the variability of physical characteristics of the electronic circuits on an imaging sensor to visualise how sensor pattern noise may, at least in part, be explained. We have not considered the variation in semiconductor performance due to chemical-level variability such as doping concentration and contamination, nor have other read-out circuitry configurations been analysed, which are matters for future study. Our exploration of the physical dimensional variability may also be useful in explaining, in part, the origins of sensor pattern noise to a lay audience.

Authorship Statement:

Title of Paper:	An Analysis of Optical Contributions to a Photo-Sensor's Ballistic Fingerprints
Publication Status:	Published
Publication Details:	*Digital Investigation*, vol. 28, pp 139-145, 2019. [Online]. Available: https://-doi.org/10.1016/j.diin.2019.02.002

Name of Principal Author:	Richard Matthews
Contribution to paper:	Collected all data, Performed analysis, interpreted data, wrote manuscript and acted as corresponding author.
Overall Percentage:	85%
Certification:	This paper reports on original research I conducted during the period of my Higher Degree by Research candidature and is not subject to any obligations or contractual agreements with a third party that would constrain its inclusion in this thesis. I am the primary author of this paper.

Signature

Date

Co-Author Contributions

Certification: By signing the Statement of Authorship, each author certifies that:

1. the candidate's stated contribution to the publication is accurate (as detailed above);
2. permission is granted for the candidate to include the publication in the thesis; and
3. the sum of all co-author contributions is equal to 100% less the candidate's stated contribution.

Name of Co-Author:	Dr Matthew Sorell
Contribution to the Paper:	Supervised development of work, helped in data interpretation and manuscript evaluation.

Signature Date

Name of Co-Author:	Dr Nickolas Falkner
Contribution to the Paper:	Supervised development of work, helped to evaluate and edit the manuscript.

Signature Date

Chapter 6

An Analysis of Optical Contributions to a Photo-Sensor's Ballistic Fingerprints

6.1 Abstract

Lens aberrations have previously been used to determine the provenance of an image. However, this is not necessarily unique to an image sensor, as lens systems are often interchanged. Photo-response non-uniformity noise was proposed in 2005 by Lukáš, Goljan and Fridrich as a stochastic signal which describes a sensor uniquely, akin to a "ballistic" fingerprint. This method, however, did not account for additional sources of bias such as lens artefacts and temperature.

In this chapter, we propose a new additive signal model to account for artefacts previously thought to have been isolated from the ballistic fingerprint. Our proposed model separates sensor level artefacts from the lens optical system and thus accounts for lens aberrations previously thought to be filtered out. Specifically, we apply standard image processing theory, an understanding of frequency properties relating to the physics of light and temperature response of sensor dark current to classify artefacts. This model enables us to isolate and account for bias from the lens optical system and temperature within the current model.

6.2 Introduction

Much work has been done to solve the open and closed set camera identification problem [12, 16, 40, 43, 48]. One of the most promising methods used to identify an image uniquely to not just a particular make or model of camera but the unique image sensor itself is that of photo-response non-uniformity noise (PRNU) or sensor pattern noise (SPN) [12]. While blind source camera identification has been used for some time as a reliable and accepted method for legal purposes [33], there are untested scenarios within the existing literature that provide a level of uncertainty. It is widely accepted best practice to identify any source of error within forensic tools and provide methods for their mitigation [75]. There still remains questions regarding the science of the method due to high-frequency components of the image remaining within either the image fingerprint, the camera reference pattern or both. These high frequency components include but are not limited to image compression artefacts [43], dark current [10], amplifier noise [10], and lens and optical effects [16] including dust [48]. These high frequency components can corrupt the fingerprint if their energy dominates the unique signal and are significantly uncorrelated to the sensor. In this chapter we aim to isolate a source of error from blind source camera identification and, applying principles of signal processing, demonstrate the energy distribution to the various traces that the SPN method is capable of isolating.

While much is known about the mathematical design of lenses, only recently have image analysts begun to study their unique geometric effects to solve the camera identity problem [60, 76]. Lens aberrations have successfully been used in image linking [60] and identifying copy paste forgeries [76]. This is because lenses create artefacts in an image known as Seidel Aberrations [42]. These aberrations describe how each ray of light travelling through a lens deviates in some manner from the optical axis and is unique to a lens system due to the

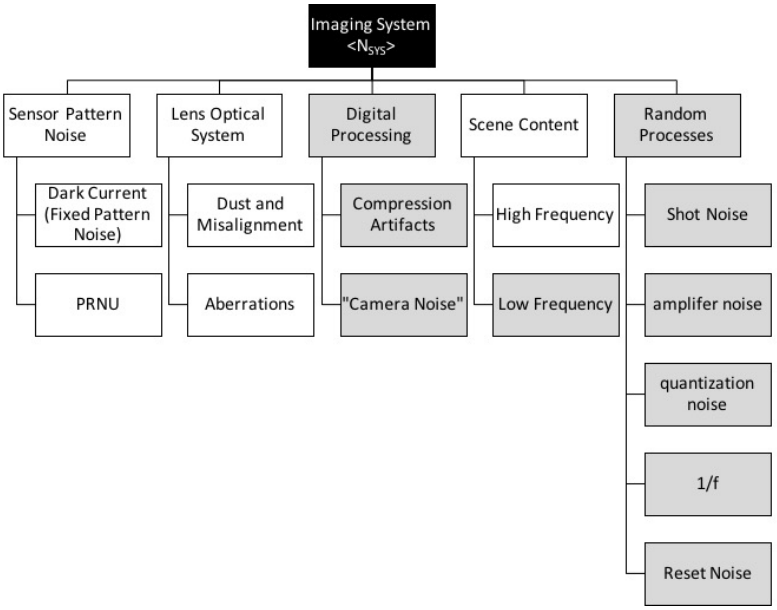

Figure 6.1: The noise residue model as proposed in our work based on the system noise equations from [10]. The dark grey boxes indicate sources of noise that can be easily mitigated. Random processes are mitigated through frame averaging [10] while RAW format images remove digital processing artefacts [16]. Camera Noises introduced through computer algorithms such as demosaicking, dynamic range adjustments and downsampling are controlled through correct choice of camera hardware values prior to imaging [10]. The low-frequency components of the scene content and all other sources of noise are removed due to the high-pass filter that the images are passed through to obtain the noise residue.

multiple lenses used in combination [59]. While this method is successful at lens identification, it provides little information about the specific image sensor in question since lens systems are easily substituted.

While an abstract model of noise within image sensors has been developed as seen in Figure 6.1, to determine which source dominates a complete signal-to-noise ratio analysis must be undertaken [10]. In this chapter, we begin this work by limiting ourselves to evaluating the contribution of the lens within a noise residue to ascertain if contamination is possible with lens substitution. The next section provides an overview of how the noise residue is obtained and describes the work that has already been done in isolating the contaminating effects within this fingerprint. In Section 6.3 we describe a new noise model for the noise residue based off the work of [10] that is more inclusive of the

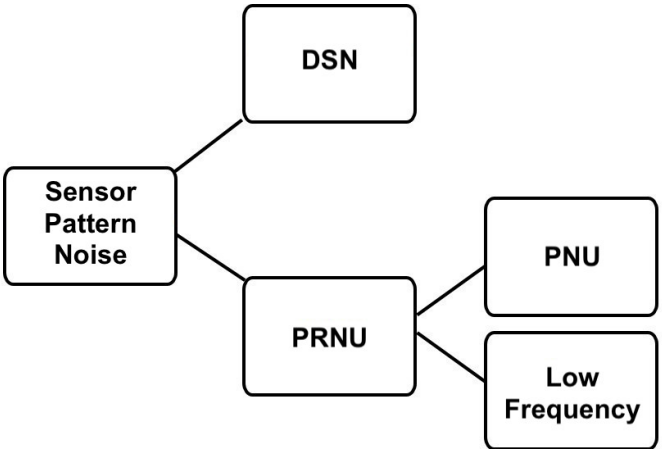

Figure 6.2: The additive noise model as proposed by Lukáš *et al* in their seminal work [12]

high-frequency leakage seen in [12]. We describe our lens isolation experiments in Section 6.4 in which we use a physical filter to remove all contributions from Seidel aberrations. The results of these experiments are discussed in Section 6.5 before concluding in Section 6.6.

In the sections which follow we consider all operations as element-wise matrix operations unless specifically expressed otherwise. Boldface is used to denote $m \times n$ vectors. The product between two vectors is assumed to be the vector product $\mathbf{x} \odot \mathbf{y} = \sum_{i=1}^{n} \mathbf{X}[i]\mathbf{Y}[i]$ where i is the i'th element of the vector. $\|\mathbf{X}\| = \sqrt{\mathbf{X} \odot < X >}$ is used to denote the argument of the vector $\mathbf{X}$, and the mean value of the vector $\mathbf{X}$ is indicated by$< \mathbf{X} >$. Correlation between two vectors is the cross correlation:

$$corr(X, Y) = \frac{(\mathbf{X} - < \mathbf{X} >) \odot (\mathbf{Y} - < \mathbf{Y} >)}{\|\mathbf{X} - < \mathbf{X} >\| \odot \|\mathbf{Y} - < \mathbf{Y} >\|}$$

6.3 Background

We model the signals contained within a single image as an additive signal model based on [10] and shown in Figure 6.1. This expands upon the model proposed by [12] as shown in Figure 6.2.

Quoting levels of noise in terms of electrons at the level of image sensor output, the noise magnitude is the root mean square value and the sources are expressed as the root sum of the squares and added in quadrature where appropriate we obtain the following:

$$< \mathbf{N_{SYS}} >= \sqrt{< \mathbf{n_1^2} > + ... + < \mathbf{n_i^2} > \overline{+ ... + < \mathbf{n_N^2} >}}$$

Where $< \mathbf{n_i^2} >$ is the variance of noise source i and $< \mathbf{N_{SYS}} >$ is the standard deviation measured in RMS units for the entire system.

Substituting for the various sources of noise identified in Figure 6.1 :

$$\begin{aligned} < \mathbf{N_{SYS}^2} > = & < \mathbf{n_{RANDOM}^2} > + < \mathbf{n_{IMAGE}^2} > \\ & + < \mathbf{n_{DIGITAL}^2} > + < \mathbf{n_{LOS}^2} > \\ & + < \mathbf{n_{SPN}^2} > \end{aligned} \tag{6.1}$$

Since SPN is the signal we wish to isolate we deviate from traditional noise models to include the image as a noise source where $\mathbf{n_{IMAGE}}$ is the high and low frequency components of the scene being imaged, $\mathbf{n_{DIGITAL}}$ are the noise sources due to the digital processing pipeline, $\mathbf{n_{LOS}}$ is the Lens Optical System (LOS) , $\mathbf{n_{SPN}}$ is the contribution from SPN being the addition of dark current (FPN) and PRNU:

$$< \mathbf{n_{SPN}^2} > = < \mathbf{n_{FPN}^2} > + < \mathbf{n_{PRNU}^2} > \tag{6.2}$$

and $\mathbf{n_{RANDOM}}$ is the sources of noise able to be mitigated through frame averaging represented by:

$$\begin{aligned} < \mathbf{n}^2_{\mathbf{RANDOM}} > = & < \mathbf{n}^2_{\mathbf{SHOT}} > + < \mathbf{n}^2_{\mathbf{A}} > \\ & + < \mathbf{n}^2_{\mathbf{ADC}} > + < \mathbf{n}^2_{\frac{\mathbf{1}}{\mathbf{f}}} > \\ & + < \mathbf{n}^2_{\mathbf{RESET}} > \end{aligned} \tag{6.3}$$

For our usage, we agree with the findings of [10] as shown in our theoretical model of the noise sources contained within the noise residue after following the de-noising method in [12].

We break down the signals within our of noise residue as being comprised of three main areas: SPN or those due to the sensor, those due to the LOS, and the high-frequency components of the scene content. We illustrate this in Figure 6.3. From the sensor, we follow the model as proposed in [12] and break the Sensor level noise down to PRNU and Dark Current. For ease of modelling, we also include dust on the sensor as per [12] noting that dust modifies the PRNU response since light is blocked from the sensor. The LOS is comprised of two levels. These are lens dust or misalignment, and Seidel aberrations caused by design errors during lens manufacture. Both aspects are high-frequency components only due to the filter f that the system is run through to obtain the noise residue.

To simplify the model, acknowledging we introduce a source of possible error in doing so, we focus our attention on the sections of the model that positively correlate with an individual image under test (IUT). [12] using [10] identified that the only sources of noise not reduced through frame averaging were dark current and PRNU. This was further refined in [16] to eliminate compression level artefacts through the use of raw images. LOS aberrations and components of the scene remain (Figure 6.3). The scene components are limited to only the spatial high-frequency components since the image has been high-pass filtered. The model when a reference pattern is compared to a IUT fingerprint is therefore

considered as follows:

$$\begin{aligned} < \mathbf{N_{SYS}^2} > = < \mathbf{n_{SPN}^2} > + < \mathbf{n_{LOS}^2} > \\ + < \mathbf{n_{W_{ref}}^2} > + < \mathbf{n_w^2} > \end{aligned} \tag{6.4}$$

Where $\mathbf{n_{W_{ref}}}$ is the contribution of high-frequency elements from the reference pattern due to the insufficient suppression from frame averaging and $\mathbf{n_w}$ is the high-frequency scene components of the IUT. Given that these two sources are uncorrelated we further reduce our model to:

$$< \mathbf{N_{SYS}}^2 > = < \mathbf{n_{SPN}^2} > + < \mathbf{n_{LOS}^2} > + < \mathbf{n_V^2} > \tag{6.5}$$

From this model, we can determine the contribution of the LOS aberrations within the system to the correlation energy $< \mathbf{N_{SYS}^2} >$. We achieve this through the use of a physical filter (a pinhole lens) thus removing LOS aberrations from the system altogether.

$$< \mathbf{N_{SYS}^2} > = < \mathbf{n_{SPN}^2} > + < \mathbf{n_V^2} > \tag{6.6}$$

Given $< \mathbf{n_V} >$ is uncorrelated, the resulting correlation will be directly proportional to a combination of FPN and PRNU. We assume the definition of this as SPN as per [10]. This is the basis of the original method as seen in [12] with differences as explained here. [12] acknowledged that pattern noise is *any noise component that survives frame averaging* and focused on only one part of this theoretical model, pixel non-uniformity noise (PNU). From our use of the model as proposed in [10] it is clear that lens aberrations are involved unless otherwise filtered, which frame averaging does not achieve. [12] assumed the positive match from their method was directly proportional to PNU defined as a sub layer of PRNU caused by the different sensitivity of pixels to light. We

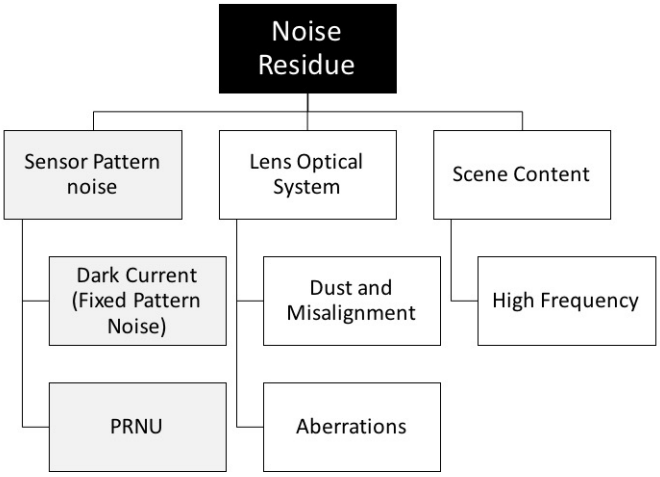

Figure 6.3: The groupings of noise remaining in our noise residue. The grey indicates the sensor specific noise.

do not agree as shown from the theoretical break down above hypothesis that Dark Current and the LOS must be included with appropriate weight.

Dark current is generated in multiple places within an image sensor. Generally, three sources of dark current contribute to the total generated by a sensor. These sources are typically the depletion region through the swapping of minority carriers, the diffusion of carriers in the field-free region at saturation (drift current) and on the surface of any oxide layer interface. A complete study of dark current is beyond the scope of this chapter but can be read in [77]. Previous work by [32] has presented a hypothesis that dark current could be an effective tool for matching images to a source camera. However, this work is often reduced to pixel defects for matching images as demonstrated in [40]. We propose that even with pixel defects isolated and removed, dark current is a unique trace in itself. This philosophy has previously been proposed. In [41] the concept of a hybrid model was explored where the individual traces of PRNU and DSN were combined to create a new method that ultimately "had higher discrimination capability than the method using pixel non-uniformity when the number of recorded image [sic] was small". By isolating lens effects and dark current from the PRNU trace we illustrate why this is the case, further demonstrating the

need for more work to understand the science behind the sensor pattern method for uniquely solving the blind source camera identification problem.

6.4 Methods

Six Sony IMX219PQ CMOS image sensors (CIS) with integrated lenses were used in our analysis. The lenses were carefully removed from the sensor and placed into a 3D printed jig. The jig was designed explicitly so that each image was slightly out of focus. This assists in removing high-frequency image components from our analysis. Only three sensors were used in our experiments as three sensors were damaged during the lens removal process. This gave us six lenses and three image sensors. Images were taken of a fixed intensity white LED light source evenly focused through a sheet of white opaque perspex to create an evenly illuminated light box. This suppressed contamination from high-frequency image content being passed through the high-pass filter of our PRNU estimator.

Pinholes were manufactured using 3D printing. A 1.5mm diameter aperture was designed at a distance of 3mm to ensure the focal ratio of the lens was kept consistent at f/2.0. This enabled intensity of the light striking the sensor to be kept consistent across the pinhole and standard lenses resulting in a consistent integration time of 1/1008 seconds. Ensuring integration time was consistent meant that no scaling effects occur between pinhole and lens image sets, and keeps dark current constant. The temperature was kept at a constant T=30 °C to further ensure the effects of dark current were controlled. Varying either the exposure light intensity or the temperature should result in an increase of dark current, hence, it is important that these variables are kept constant for comparison.

Each image was preprocessed before filtering. We separated each colour filter array element into a separate array. Each image was cropped to 1024x1024

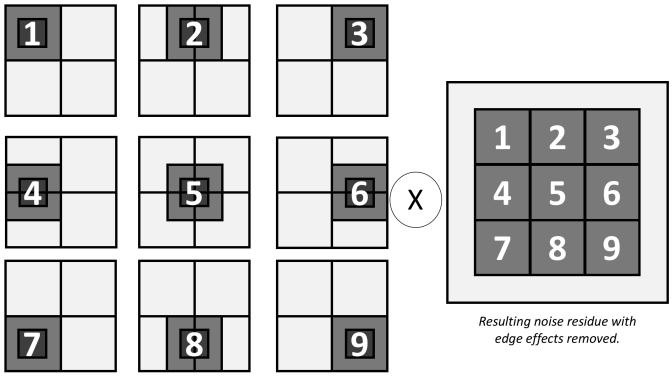

Figure 6.4: The overlapping method to reduce edge effects from the wavelet coring method. The dark regions in each square (left) indicate the calculated region of the filtered noise residue retained in each pass corresponding to their effecting location in the resulting noise residue (right). The method results in m+1 x n+1 passes being performed as opposed to the original m x n.

image offset by 38 pixels from the top left-hand corner. This enabled us to obtain a broad cross-section of the image and would emphasise any lens effects such as vignetting. The resulting four arrays were turned into zero mean signals before being processed by the wavelet coring filter [49]. We used the same wavelet coring filter as proposed in [12] with one minor difference. Instead of using advancing squares in the m x n MAP estimate we used overlapping squares, doubling the number of calculations required. We then rejected the outer edges of the m x n pixel arrays to ensures edge effects are discounted from the final analysis. The m x n arrays are then stitched back to create the final PRNU analysis for each CFA array. This process is shown in Figure 6.4. Finally, we merge each PRNU estimation for each CFA array back to a single array for the PRNU estimation of the entire sensor. We then correlate each CFA to its corresponding CFA in the image under test. Our final correlation value is then taken to be the average correlation value across each of the four CFA sub arrays.

150 images were taken using each of the three cameras with each of the six lenses attached in turn. From each set of 150 images, 50 were randomly divided into a reference pattern, while the remaining 100 formed an image set to correlate against the reference patterns. An additional set of images was captured at the

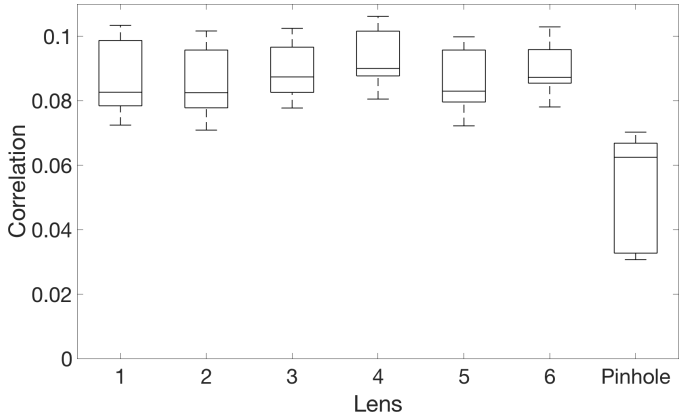

Figure 6.5: Box plot of all cameras reference patterns of the lenses correlated against lens image sets not corrected for dark current.

same exposure time, temperature and illumination using a pinhole designed to have the same f-number as the original lenses. This gave us seven sets of images per camera and 21 discrete reference patterns.

6.5 Results and Discussion

Results of the lens image sets (3600 images) correlated against each of the seven reference patterns are shown in Figure 6.5. Figure 6.6 shows the result of these same reference patterns correlated with the remainder images captured using the pinhole lens on each camera (300 images). Only images known to be from that camera are shown in these figures as uncorrelated results are uniformly distributed about the origin and hence are omitted for clarity.

The results in Figure 6.5 show the lens reference patterns with similar means and ranges. Our results are approximately 0.02 larger than those first reported in [12] which we attribute to the additional steps taken to eliminate edge effects in our denoising filter. Each of the lens sets shows statistically similar results. The range, mean, maximum and minimum values are consistent within an overall range of 0.025 to 0.031 across the six lenses. The pinhole set, however, has a range of almost twice that at 0.040 with the maximum value below the minimum value of any one lens. This suggests statistical invariability across

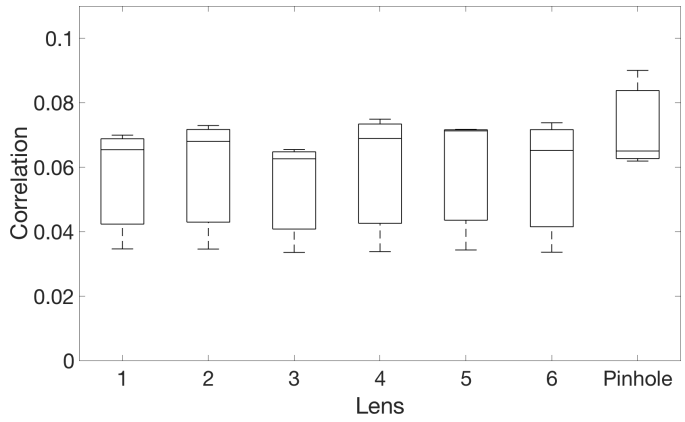

Figure 6.6: Box plot of pinhole image reference patterns correlated against pinhole image sets not corrected for dark current.

lenses manufactured of the same type, however, reinforces the hypothesis that high-frequency lens artefacts are included in the noise residues used to create both individual fingerprint and reference patterns.

The lens sets have a median value of 0.085 and mode of 0.083. There is a difference of less than 0.007 within the means for the lens sets showing that they are consistent. The pinhole set has a mean of only 0.062. This is a clear difference between the average means of the lens sets and the mean of the pinhole set at 0.023, but the pinhole is still capable of statistically matching to the right camera. The pinhole correlation showed a broader range than each of the lens sets with a majority of the data falling within the interquartile range and skewed towards the higher values, whereas each of the lens sets is skewed towards the lower end of the range.

An interesting observation is that the uncorrelated pinhole image set is positively skewed whereas the correlated lens image sets are negatively skewed. This observation extends to figures 6.6 and 6.7 with the exception being the pinhole image set matched to a pinhole reference pattern corrected for dark current with dark frame removal in Figure 6.8. It may be possible to identify or profile a device such as a pinhole by comparing means of statistically significant sample sizes in this manner.

Comparing Figure 6.5 to Figure 6.6 it is apparent that the means of the lens reference patterns reduce to be in line with the pinhole reference pattern when correlated against pinhole image sets taken from the same camera. This aligns with the hypothesis that the lens reference patterns contain additional signal energy from the high-frequency components of the lens passing through the signal filters in the process of obtaining the noise residues.

Using the average correlation from the lens sets in Figure 6.5 (since they are consistent) and Equation 6.5 above we can calculate the overall correlation energy of the SPN with the effects of the lens included.

$$\begin{aligned} < \mathbf{N_{SYS}^2} > - < \mathbf{n_V^2} > = < \mathbf{n_{SPN}^2} > + < \mathbf{n_{LOS}^2} > \\ = 0.0865 \end{aligned} \tag{6.7}$$

Using the averages of all results contained in Figure 6.6 we are able to calculate the correlation energy of the SPN without effects of the lens present:

$$\begin{aligned} < \mathbf{N_{SYS}^2} > - < \mathbf{n_V^2} > - < \mathbf{n_{LOS}^2} > = < \mathbf{n_{SPN}^2} > \\ = 0.0666 \end{aligned} \tag{6.8}$$

Substituting this result back into 6.5 we can obtain a result for the correlation energy of the LOS alone.

$$\begin{aligned} 0.0666 + < \mathbf{n_{LOS}^2} > = 0.0865 \\ < \mathbf{n_{LOS}^2} > = 0.0199 \end{aligned} \tag{6.9}$$

This figure corresponds to the effects of the LOS based on measurements with dark current influence in the sensor.

Since many modern-day cameras correct for dark current, each of the images

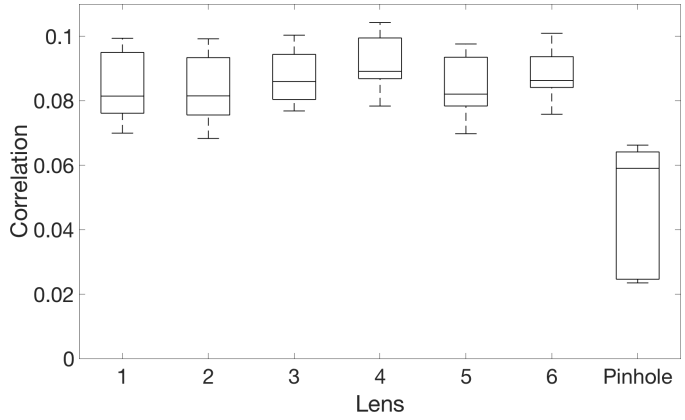

Figure 6.7: Box plot of all camera reference patterns of the lenses correlated against lens image sets corrected for dark current.

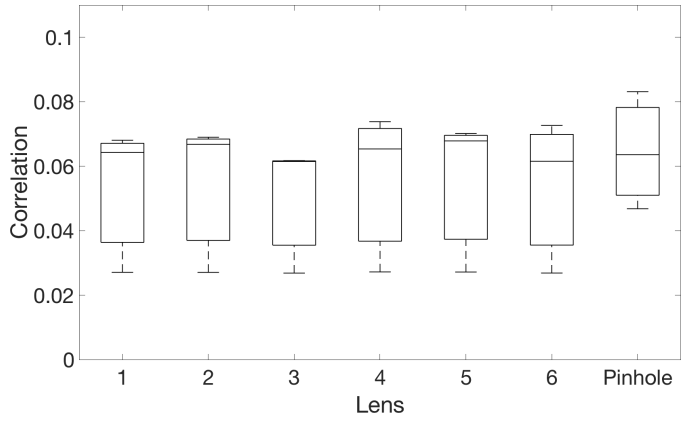

Figure 6.8: Box plot of pinhole reference patterns correlated against pinhole image sets corrected for dark current.

was also corrected for dark current through the use of a dark current frame removal. This was to ensure dark current was not contaminating our results. As seen in Figures 6.7 and 6.8 the range of the correlation scores are reduced however the overall result remains. The correlation is significantly reduced upon removal of the lens.

The pinhole set with dark current removal shows good uniformity with the mean centred about the range of the set. Since lens effects and dark current have been removed, the correlation should be acting upon only the correlated PRNU within the image. This shows a Gaussian distribution as expected with the mean centred around the mean of the lens results. When our reference

pattern is constructed only with pinhole images and is correlated with images taken using a lens we are no longer correlating against the high-frequency lens artefacts seen within the lens reference patterns. This is a clear result from Figures 6.6 and 6.8.

We can use this result to further estimate the effects of dark current within the correlation energy by repeating the calculations above and also check the figure we have obtained for the LOS.

Using the average correlation from the lens sets in Figure 6.7 (since they are consistent) and Equation 6.5 above we can calculate the overall correlation energy of the PRNU only with the effects of the lens included but without dark current.

$$\begin{aligned} < \mathbf{N^2_{SYS}} > - < \mathbf{n^2_V} > = < \mathbf{n^2_{SPN}} > + < \mathbf{n^2_{LOS}} > \\ = 0.0844 \end{aligned} \tag{6.10}$$

Using the averages of all results contained in Figure 6.8 we are able to calculate the correlation energy of the PRNU alone:

$$\begin{aligned} < \mathbf{N^2_{SYS}} > - < \mathbf{n^2_V} > - < \mathbf{n^2_{LOS}} > = < \mathbf{n^2_{SPN}} > \\ = 0.0644 \end{aligned} \tag{6.11}$$

Substituting this result back into 6.5 we can obtain a result for the correlation energy of the LOS alone.

$$\begin{aligned} 0.0644 + < \mathbf{n^2_{LOS}} > = 0.0844 \\ < \mathbf{n^2_{LOS}} > = 0.0200 \end{aligned} \tag{6.12}$$

Figure 6.6 corresponds to the effects of the lens only within the sensor and

is consistent for our measurements with dark current as calculated in Equation 6.9. Comparing the results of Equations 6.7 and 6.8 with Equations 6.10 and 6.11 we see that dark current (FPN) corresponds to a contribution of 0.0022 to a correlation of 0.0865.

Given these values represent power correlation amplitudes we are able to convert them into signal to power ratio terms using the following:

$$SNP_{dB} = 10log_{10}\frac{P_{signal}}{P_{total}} \tag{6.13}$$

Where the identifier is either PRNU, dark current or combination of them both. These values are summarised in Figure 6.9.

It is possible to treat each of PRNU, dark current and the LOS as unique identifiers hence, the signal. Conversely, we can think of the high frequency image content within our residues as the noise. Switching our definition of the signal and noise in such a manner enables us to calculate SNP values for each identifier in a forensic context. These values are summarised in Figure 6.9. We see that the uncorrelated high-frequency components of the reference patterns dominate with a signal to power value of 91.4% of the total signal power. PRNU has the strongest of the individual identifiers with a signal to power value of 6.44% however, the highest identifier value corresponds to the combination of PRNU, dark current and LOS with a value of 8.7% of the total power of the signal. This is clearly contrary to assumptions made in [12] that the method is matching only to the PNU as a subsection of PRNU since the best match is made with a combination of all the identifiers measured. We can also see that PRNU accounts for nearly 75% of the extended fingerprint's power. This is compared to the LOS at 23% and Dark Current at only 2.5%. This observation provides an explanation as to why the work of [12] was successful although all sources of correlated power were unaccounted for in their method.

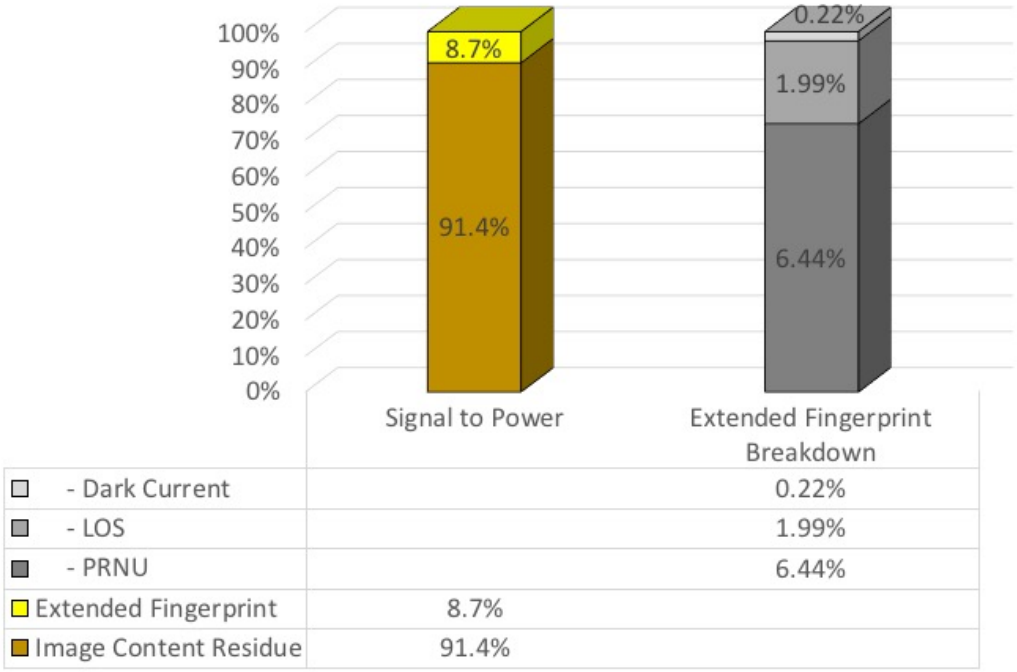

Figure 6.9: Signal power expressed as a ratio of total power levels of each identifier contained within our extended fingerprint.

Dark current was measured to be an appreciative 0.2% of the total range of the image when held constant at T=30 °C. This is expected to increase with temperature as seen by the theoretical models in [10] and will be explored in Chapter 7. It is also noted that should the intensity of light decrease the amount of power that the dark current has compared to other sources of power in the image would inversely increase. This has not been experimentally shown due to limitations of the lighting apparatus used when conducting this initial study but, we note the theory illustrated in [10]. By removing the lens, we were able to eliminate the source of stochastic variance and isolate the deterministic component of the lens optical system and measure the contribution of the LOS to be 2.0%. We note that some variance due to lens aberrations will still be present due to the involvement of the micro-lens array on the sensor itself. Some sensors use a dual micro-lens design. These aberrations from the micro-lens are unique to each sensor and hence form a significant source of the PRNU.

Likewise, some aspects of the camera noise [10] is unique to each camera but were excluded from our noise residue model since we were only concerned with the image sensor. In reality, since these camera noises are unique their effects may be seen within a sensor fingerprint but have not been attributed above.

While cameras of a similar make and model have been evaluated here to eliminate possible sources of experimental error it is worth noting that we expect that other cameras should exhibit similar breakdowns with the amount of power scaling in proportion with the quality of the sensor. Scientific grade sensors with low dark noise by design should show very little dark current contamination whereas we expect low grade CMOS cameras for integrated mobile applications designed without built in dark current correction to have some of the worst. This expectation is consistent with the results shown here. The Sony IMX219 sensor used in this work has built in dark current correction at the silicon level [70] , however, still shows evidence of a contribution, albeit small, of signal power attributed to this forensic trace.

6.6 Conclusion

While we do not dispute that the method first proposed by Lukáš *et al* is capable at blindly identifying images uniquely to their source camera, our work has shown that there is more to understand behind this methodology than first described. The additional factors are acting upon the correlation seen need to be understood before it can be used as a reliable methodology to solve the blind source camera identification problem for legal purposes. We have shown that dark current and the LOS contribute a non-insignificant amount of energy to the correlation. While an amount of energy in the correlation is contributed by the lens aberrations, the method shown here is not statistically capable of uniquely identifying a particular lens of similar design. An area of counter forensic method however is left as a proposal to disrupt the SPN

fingerprint methods by designing a lens with extreme high-frequency aberrations to corrupt the SPN. This reinforces the initial findings of Knight *et al.* Herein, our method demonstrates an additional protocol step of lens isolation using a pinhole camera should the suspect camera be available to the investigator. This chapter demonstrates that this critical step of image verification should be taken to increase the certainty of a positive match particularly in the context of charges relating to the production of photographs using professional grade dSLR cameras where multiple lenses are interchangeable. Such a step can increase the certainty of a positive match and aim to verify the results of the forensic investigation. Forensic investigators must be aware of the result of this step demonstrating the significance that the lens system may play particularly when using SPN to solve the open set blind source camera identification problem.

Authorship Statement:

Title of Paper:	Determining Image Sensor Temperature Using Dark Current
Publication Status:	Submitted for Publication
Publication Details:	Submitted to Digital Investigation 16/Dec/2018. Under Review 10/Jan/2019

Name of Principal Author:	Richard Matthews
Contribution to paper:	Collected all data, Performed analysis, interpreted data, wrote manuscript and acted as corresponding author.
Overall Percentage:	85%
Certification:	This paper reports on original research I conducted during the period of my Higher Degree by Research candidature and is not subject to any obligations or contractual agreements with a third party that would constrain its inclusion in this thesis. I am the primary author of this paper.

Signature

Date

Co-Author Contributions

Certification: By signing the Statement of Authorship, each author certifies that:

1. the candidate's stated contribution to the publication is accurate (as detailed above);
2. permission is granted for the candidate to include the publication in the thesis; and
3. the sum of all co-author contributions is equal to 100% less the candidate's stated contribution.

Name of Co-Author:	Dr Matthew Sorell
Contribution to the Paper:	Supervised development of work, helped in data interpretation and manuscript evaluation.

Signature Date

Name of Co-Author:	Dr Nickolas Falkner
Contribution to the Paper:	Supervised development of work, helped to evaluate and edit the manuscript.

Signature Date

Chapter 7

Thermal Effects of Dark Current on Blind Source Camera Identification

7.1 Abstract

The state of the art method for fingerprinting digital cameras exploits the non-uniform output of an array of photodiodes due to the distinct construction of the PN junction when excited by photons. This photo-response non-uniformity (PRNU) noise has shown to be effective but ignores knowledge of image sensor output under equilibrium states without excitation (dark current). The dark current response (DSN) traditionally has been deemed unsuitable as a source of fingerprinting as it is unstable across multiple variables including exposure time and temperature. As such it is currently ignored even though studies have shown it to be a viable method similar to that of PRNU. We hypothesise that DSN is not only a viable method for forensic identification but, through proper analysis of the thermal component, can lead to insights regarding the specific temperature at which an individual image under test was taken. We also show that digital filtering based on the discrete cosine transformation, rather than the state-of-the-art wavelet filtering, provides significant computational gain albeit with some performance degradation. This approach is beneficial for

triage purposes.

7.2 Introduction

In this chapter, we examine the relationship between temperature, dark current (DSN) and its effect on the accepted sensor pattern noise (SPN) methods using a discrete cosine transformation (DCT) filter instead of the computationally intensive wavelet filter. We achieve this using a lens cap applied during our image capture process to eliminate the interaction of light with our image sensor. We calculate the correlation across the temperature range of 10°C to 50°C in 5°C increments before calculating a theoretical model for each of the cameras used in our experiments. This model is then used to contrast the photo-response non-uniformity (PRNU) SPN method against a DSN SPN-only method similar to the hybrid SPN method in [41].

A reliable method of linking media to their source camera is through the analysis of pixel non-uniformity (PNU) sensor noise to generate a photo-response non-uniformity (PRNU) trace often referred to as a fingerprint [12]. When tested across the limited range of -7.9°C to 29.5°C it has been observed that this method is not affected by temperature [13]. [12] goes as far as to state that PNU "is not affected by ambient temperature or humidity" due to the simple fact that PRNU is the dominant trace component of PNU.

Sensor Pattern Noise (SPN) methods for solving the blind source camera identification problem has already been shown to be a valuable tool for both insurance providers and law enforcement. In [78] it was shown that SPN for a scanned image differs to that of a genuine photograph. Such a method has applications for insurance fraud when detecting scanned images vs genuine images of goods; for example when attempting to prove ownership. PRNU has previously been ruled out as a useful tool for policing insurance fraud concerning vehicle collisions due to the inability to link a camera to a particular vehicle [79]. In [41]

five separate cases are given which shows the practical application of SPN methods for law enforcement ranging from sexually based offences to those resulting in death.

Even though SPN is considered to be a robust and mature tool for linking images to cameras, has undergone significant peer review, has calculable potential error rates and has reached a level of general acceptance within the digital forensic community there are still questions regarding some features of the physics behind the method. [41] expanded upon the method above to generate a PNU hybrid trace model based on the inhomogeneous nature of both PRNU and Dark Current (DSN). In [80] it was demonstrated that DSN exhibits signal power which adds to the overall correlation energy during the original SPN methods even when using sensors that have DSN correction methods. Since it is accepted that DSN is heavily temperature dependent, we investigate whether the current SPN methods are immune to temperature bias.

The rest of the chapter is organised as follows. In Section 7.3 we document the prior efforts in this field and highlight our novel contribution. In Section 7.4 our methods and experimental set-up is documented. The results of our experiments are presented in Section 7.5 before being discussed in 7.6. Finally, future work is presented, and the chapter is concluded in Section 7.7.

7.3 Related Work

A reliable method of linking images to their source camera is through the analysis of pixel non-uniformity (PNU) sensor noise to generate a PRNU trace often referred to as a fingerprint [12, 41]. The basic premise of these methods is to apply a high pass filter to an image which isolates a noise residue directly related to the non-uniform nature of how the sensor outputs an electrical signal. This non-uniform output is due to manufacturing defects such as misalignment and inconsistent silicon dopant across a wafer during production [81]. An example

of this can be seen in Figure 7.1.

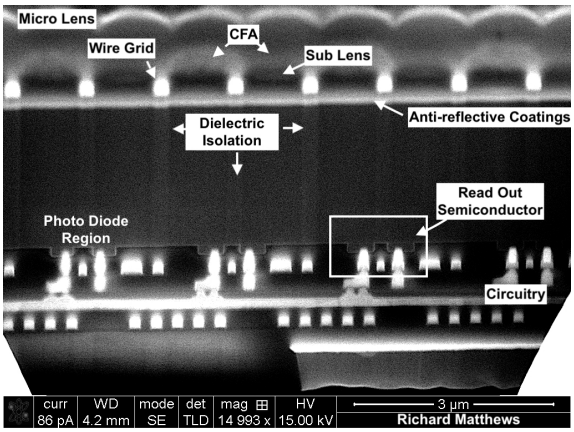

(a)

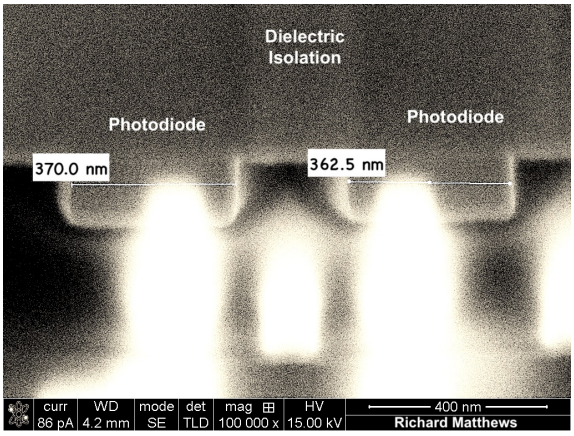

(b)

Figure 7.1: (a) A cross section of a CMOS image sensor. (b) Inconsistencies within the diode region can be visually observed between neighbouring pixels. While this will not effect the overall function of the sensor this is an example of pixel non-uniformity (PNU).

A photo-diode consists of a junction of positively and negatively charged semiconductor material to form a depletion region. When a photon enters this depletion region it produces an electron-hole pair by transferring the energy of the photon to an electron resulting in the electron moving to a higher valence band or even becoming a free electron. We refer to these free electrons generated from photon energy as e^-_{PH}. e^-_{PH} is stored in the N-well semiconductor region of the photodiode which causes the depletion region to shorten.The associated hole left by e^-_{PH} moves to ground via the P-type semiconductor. We refer to electrons

generated due to the swapping of minority carriers without external excitation as dark electrons e^-_{DARK} the movement of which promotes dark current. The n-well region is gradually filled to capacity N_{max} by the combination of these electrons at which point the depletion region is removed:

$$N_{max} = N_{e^-_{PH}} + N_{e^-_{DARK}} \tag{7.1}$$

This combination of e^-_{PH} and e^-_{DARK} results in a sensor output PNU that is linked both to the sensor's PRNU and DSN. We have discussed how DSN is included in the SPN noise model in our previous work [81]. In the previous Chapter (Chapter 6), we have also shown that the state of the art method for generating noise residue traces based on PRNU [82] contains additional forensic information in the form of lens aberrations and dark current even when dark current removal or suppression techniques are employed on the integrated circuit (IC) [83,84]. This result verified the work previously highlighted in [16,41] where it was shown that additional information could be obtained via a hybrid SPN DSN method to solve the blind source camera identity problem in a real-world setting.

To isolate the PNU effects, a three-stage process is used. The first stage is applying some form of filter to obtain a noise residue via the formula:

$$Y = I - f(I) \tag{7.2}$$

where Y is the noise residue obtained containing the SPN signal and $f()$ is the filter used to isolate the noise in the image. The second is the estimation stage where the SPN is estimated from a set of noise residues to remove the effects of random variables. Finally, the third stage is the post-estimation phase where the SPN can be enhanced for more accurate and precise camera identification.

Focusing on the first stage of this process much work has been done in the area of signal processing to provide alternative filters than the original filter based on a wavelet corring method seen in [12]. The work of [85] demonstrated the need for accurate highpass filtering since an image can contaminate the estimated PRNU if it contains significant high spatial frequency content such as edges, lines, contours and texture. Similarly, in the work of [83, 84] edge effects of the image are taken into account before filtering to ensure effects such as ringing are taken into account within the estimate. A well-written summary of the state of the art regarding different filter techniques is discussed in the background work of [86] before proposing an improved locally adaptive DCT (LADCT) filter and documenting its effectiveness.

This noise residue is also susceptible to high-frequency patterns such as those generated through JPEG compression [16, 87]. JPEG compression, being a lossy compression algorithm, will remove high-frequency components and thus lowers a potential correlation match between source and reference. All of this additional information is of value to a forensic investigation as it enables a more confident match to be established between camera and image in the context of the blind source camera identification problem when correctly accounted for. Understanding how to account for these additional sources of potential bias, however, is left to a suitably trained investigator and reinforces the already established work as seen in [12, 43, 87].

When tested across the limited range of -7.9°C to 29.5°C it has been observed that this method is not affected by temperature [13]. However, the theory as shown in [10] indicates that DSN is not immune to temperature and in fact bears an exponential relationship due to the relationship between dark current density and temperature following the equation:

$$J_D \propto T^2 e^{\frac{(E_t - E_G)}{kT}} \tag{7.3}$$

The Scientific Working Group on Digital Evidence (SWGDE) has previously released an error mitigation framework [75], which introduces a basic strategy to identify and mitigate sources of likely error within digital forensic tools. Among the quality control and tool testing measures described is finding "untested scenarios that introduce uncertainty in tool results." In this chapter, we conduct tool testing of the SPN method in high-temperature environments to determine if the method is immune, particularly to the range in temperature seen in vehicles during an Australian Summer. In this scenario, the dashboard of a car is known to fluctuate from 19°C due to climate control, to more than 60°C. This is known from the practical experience of the first author working in a proprietary context for the automotive industry.

7.4 Research Methodology

To obtain a dark current signal which is uncoupled from other signals a series of steps are followed based on the image pipeline model of a digital camera. We use three Sony IMX219 CMOS digital image sensors mounted onto a Peltier plate temperature controlled device. The image sensors have built-in low dark current by design [70] through the use of correlated double sampling both before and after the Analogue to Digital Converter [88]. Through the use of an Arduino controlled Peltier plate device we vary temperature between 10°C and 50°C in 5°C increments. This Peltier plate is attached to a metal plate which extends into thin fingers of metal that the IC of the image sensor is secured onto using a custom 3D printed enclosure and thermal paste. The IC itself is located onto the metal finger rather than the PCB of the camera to ensure the temperature of the sensor is captured as opposed to the temperature of the PCB the sensor is mounted upon. To measure the temperature of the sensor an MCP9808 solid state temperature sensor is mounted on the reverse side of the metal finger underneath the sensor IC. This setup is shown in Figure 7.2.

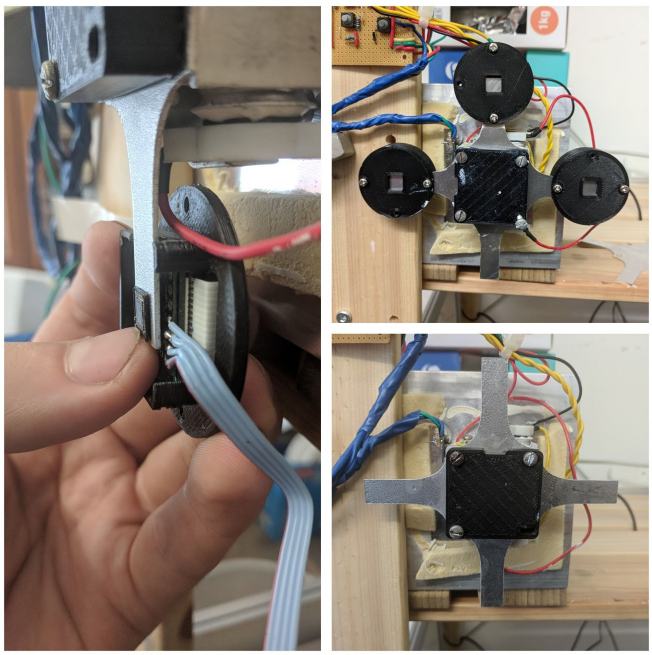

Figure 7.2: The Arduino controlled Peltier plate device used for controlling the temperature of the cameras. Seen here is the mounting position used for the image sensor to obtain an accurate reading of the sensor as opposed to the PCB. The black mounting square (shown here) was replaced with an aluminium block for thermal sinking purposes before imaging was conducted.

The aperture of the camera is covered with several layers of black electrical tape to ensure no photons are allowed to enter the imaging column. Covering the aperture ensures only dark frames are captured. Using a python script, we set exposure time to a constant t = 1/1008s, and the effects of internal amplifiers are controlled by setting a predetermined long wait time during the setting up of the camera to allow the gains to reach a stabilised temperature before setting the ISO light sensitivity to 800. Future implementations of this experiment should take advantage of the additional code to be included in a future release of the Raspberry Pi camera distribution [89] to allow the manual setting of the Analogue and Digital gains [90]. Each image is saved as a JPEG with 100QF setting with appended BAYER raw information to the end of the JPEG file. JPEG is used due to a limitation of the Raspberry Pi Camera API. While it is noted that JPEG at QF100 is not the same as lossless JPEG, the

appended BAYER raw information is extracted to obtain a RAW format image using DCRAW [91]. This BAYER raw format thus avoids all onboard processing steps of the digital pipeline within the image pipeline model of the Raspberry Pi Camera model [84]. To extract the RAW information from JPEG file it is converted to TIFF using DCRAW as per [16] using the command:

dcraw -D -T -4 -W filename

For each temperature interval, an image set of 100 dark frames is taken per camera. We prepare a noise residue for each dark frame by filtering each image using a high-pass filter in the discrete cosine domain to extract the high-frequency components using Matlab. This filter is similar to the one seen in [86] however we only employ a simple image mask as demonstrated in Figure 7.3. A cut off frequency of 150/1136pi is chosen to match the seminal work of [12]. This mask is applied purely in the DCT domain as an implementation of "goldilocks" filtering. The hypothesis is that simple filters run in quicker time with fewer resources required and thus can serve as a useful tool for processing of large evidence datasets.

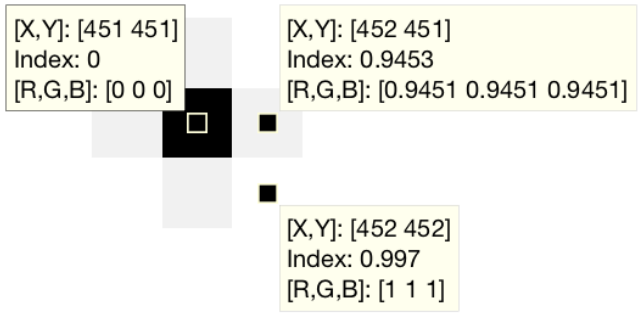

Figure 7.3: The Gaussian high pass filter with cut off frequency (150/1136)pi in the DCT domain. The cut off frequency is chosen to replicate that of the wavelet corring method of [12].

The effectiveness of the DCT filter is demonstrated in figure 7.4. Pixels that are greater than 95% full value are considered to be saturated and are ignored

as hot pixels [32, 41]. Excluding saturated pixels ensures we are matching the unique DSN as opposed to the current literature of saturated pixels. The DSN noise residues are then averaged to obtain a single reference pattern for each temperature interval. It is noted that 100 dark frames may be excessive and a smaller number is potentially viable, however, this is excluded from this study.

We then correlate the reference pattern against a different set of illuminated flat field images captured at 30°C and the same exposure time as the dark frames. The flat field images were taken using six discrete interchangeable lenses per camera resulting in a total of 300 images per camera, 50 per lens, per camera. A total of 2,700 correlations were made across the three cameras between the lens images and the dark current reference patterns. It is observed that the lens affects the data (Figures 7.5); to offset this effect the raw data across all lenses are treated as a single data set for each camera. This raw data is presented as box plots in Figures 7.6. The result of these correlations is then averaged for each camera to obtain a single result per temperature interval. These results are shown in figures 7.8, 7.9 and 7.10.

7.5 Data Collection and Analysis

The results of the comparative test between the wavelet coring method and the proposed DCT method used in the rest of this chapter is displayed in Figure 7.4.

A comparison of how long each method took to execute is displayed in Table 7.1. This table when read in conjunction with Figure 7.4 shows a computational gain with a loss of correlation. Such a trade off is of benefit for large data sets.

Table 7.1: Run Times of Filter Methods

Filter Run	Wavelet (s)	DCT (s)	Delta (s)
Set 01	630	272	-358 (-57%)
Set 02	832	315	-517 (-62%)

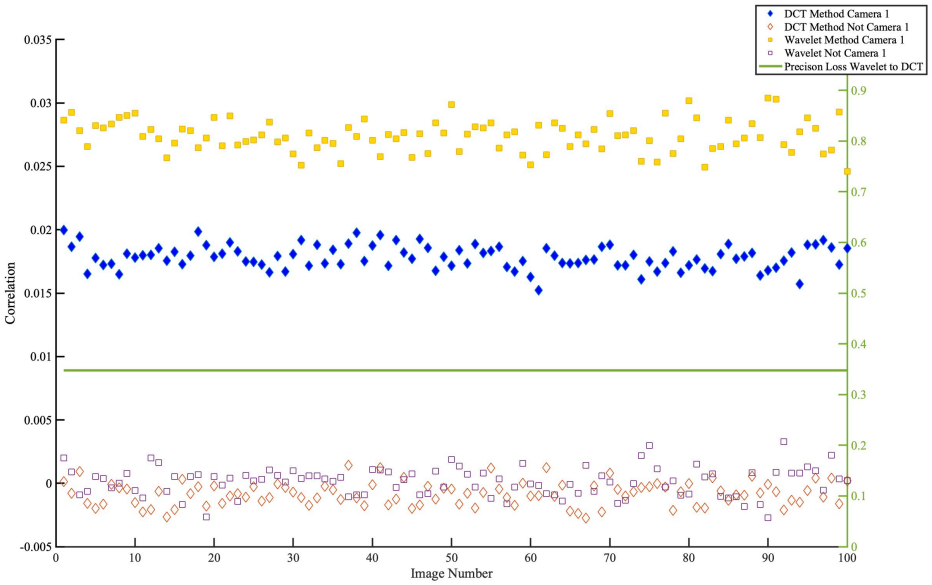

Figure 7.4: A typical comparative example of the accepted wavelet filter as shown in [12] compared to our DCT Gaussian filter.

Since a large-scale test of similar filters has already been conducted in [86] we refer to those results as to the suitability of this method. The results shown here are illustrated merely as confirmation that the tool, as built, is capable of performing the experiment as designed in the remainder of the chapter. We leave a complete, robust test of this "goldilocks" filtering method as future work.

The following observations are made. The DCT filter used may present itself as a viable method for triage since the DCT filter on average took between 4 and 6 minutes to execute whereas the wavelet method took between 10 and 14 minutes over the same image data and same resource assignment. The DCT method leads to lower correlation, but with negligible impact on the ability to classify the source camera. The variability in time is due to local resources assigned from the High-Performance Computer cluster beyond the control of the operator. The difference in execution times indicates a speedup of approximately 60%. The trade off is a loss of resolution with each trial having approximately 37% lower correlation. Such numerical values are quantified only for this specific

hardware and need to be considered across any resource being allocated.

The results of a single camera using the six different lenses are shown in Figure 7.5. This graph omits the correlations from the non matched camera for clarity. These omitted results are zero mean around the zero axes.

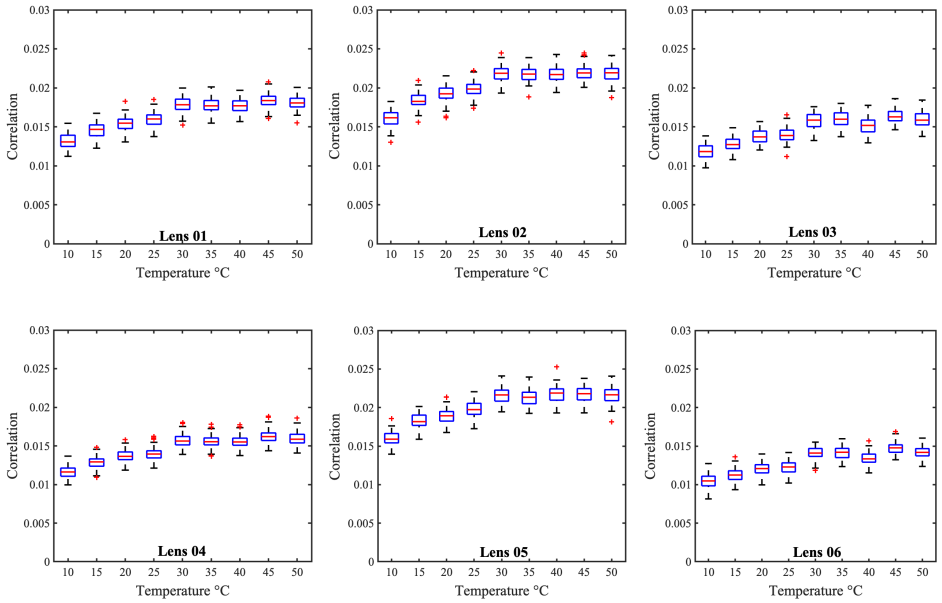

Figure 7.5: Correlation versus temperature plot for the various lenses across camera one. It is clearly evident that even with only a DSN reference pattern that the lens still plays a role in unique identification reinforcing the results of [81, 83, 84].

The results of each camera used in our method as a blind identified camera to a dark current reference pattern are shown in Figure 7.6. This graph omits the correlations from the non matched cameras for clarity. These omitted results are zero mean.

Using the theory presented in [10] we apply a model based on the dark current density model seen in Equation 7.3 to the measured results. This model has the exponential form $y = ae^{bt}$. Each model resolves with an adjusted R^2 value of .9449, .9787 and .9523 respectively for camera 1, 2 and 3. These models are shown in Figure (7.7) and then overlaid against the observed data in Figure 7.8, Figure 7.9 and Figure 7.10. There is a strong indication that the correlation is

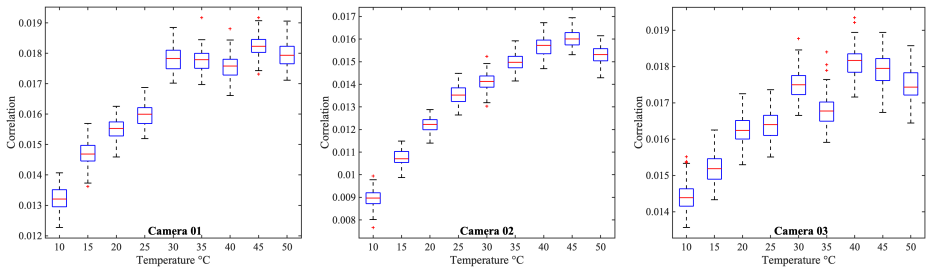

Figure 7.6: Correlation versus temperature plot across the three cameras.

related to the DSN as hypothesised. Taking the b value from each model we can approximate a value for the band gap energy $E_t - E_G$ for the cameras 1, 2 and 3 of 0.1896 eV, 0.3676 eV and 0.1268 eV. These values are consistent for band gap energies of silicon (1.1eV) and various dopant concentrations. Using this model we can identify that the correlation increases up to an approximately constant value. This constant value occurs when the temperature of the DSN reference pattern matches that of the image. Using this analysis, we can determine an approximate temperature for each image set. Camera 01 is identified as 30.5°C, Camera 02 is identified as 28.35°C and Camera 03 is identified as 30.15°C.

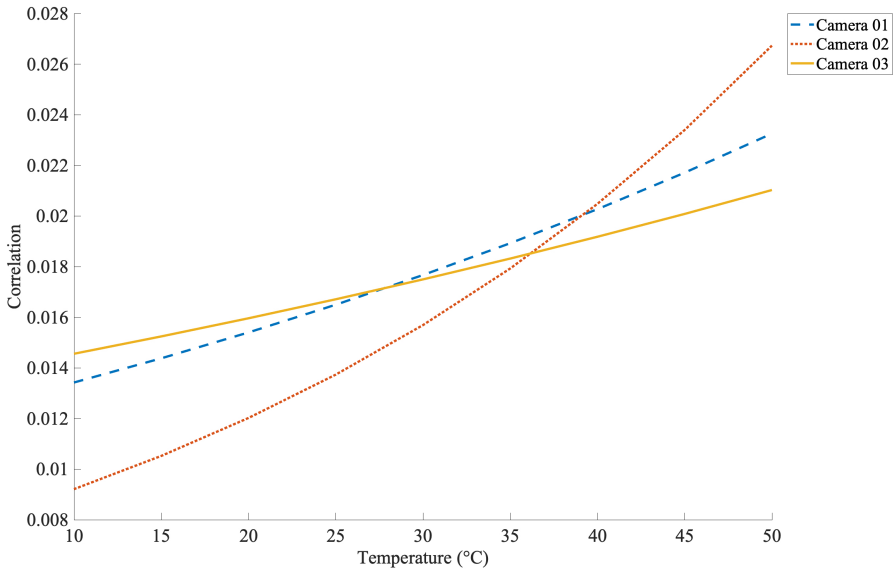

Figure 7.7: The three theoretical curves plotted against each other enabling an indication of the dopant strength to be determined.

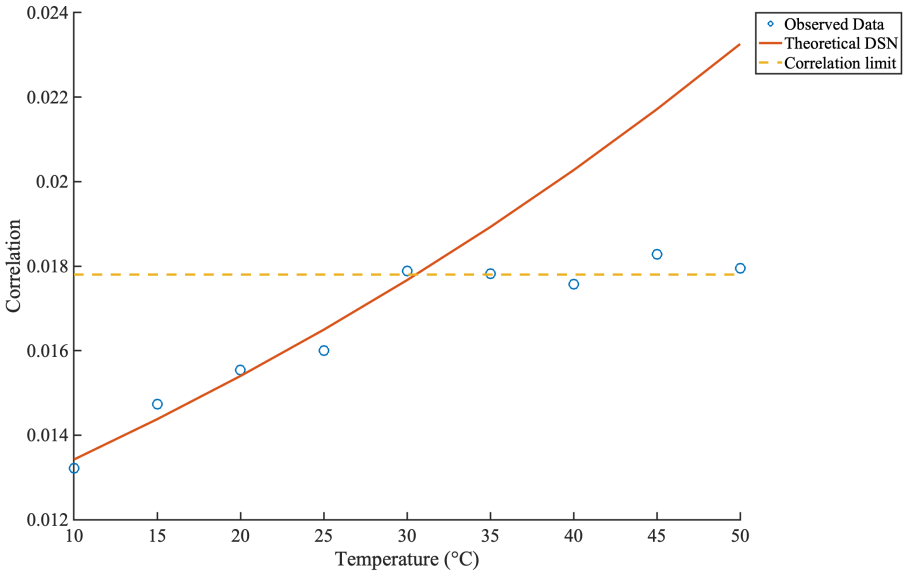

Figure 7.8: Correlation versus temperature plot for camera one showing the correlation increase in accordance with the theoretical model to a limit which corresponds to the temperature of the image sets under test. Camera 1 Identified Temperature 30.5°C

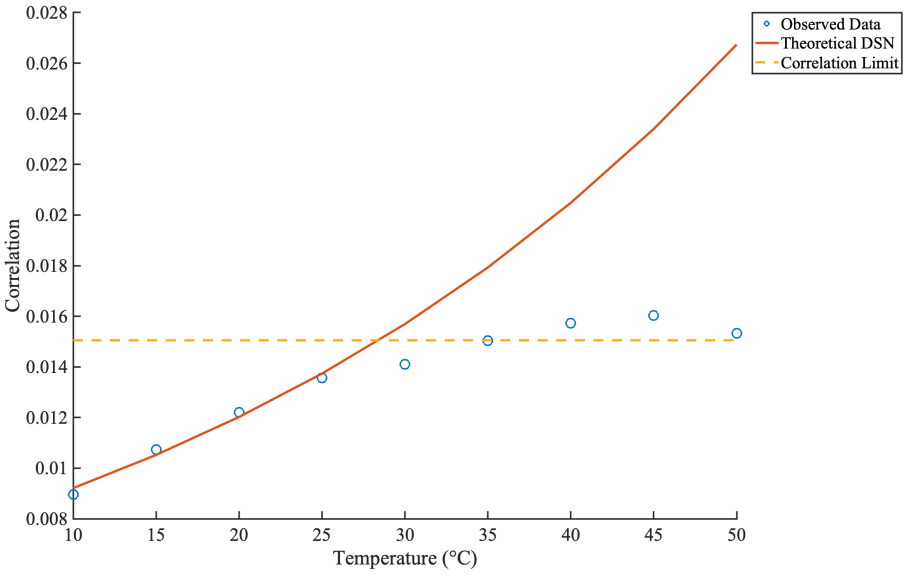

Figure 7.9: Correlation versus temperature plot for camera two showing the correlation increase in accordance with the theoretical model to a limit which corresponds to the temperature of the image sets under test. Camera 2 Identified temperature 28.35°C

It was observed that a prohibitively long time was required to take images at

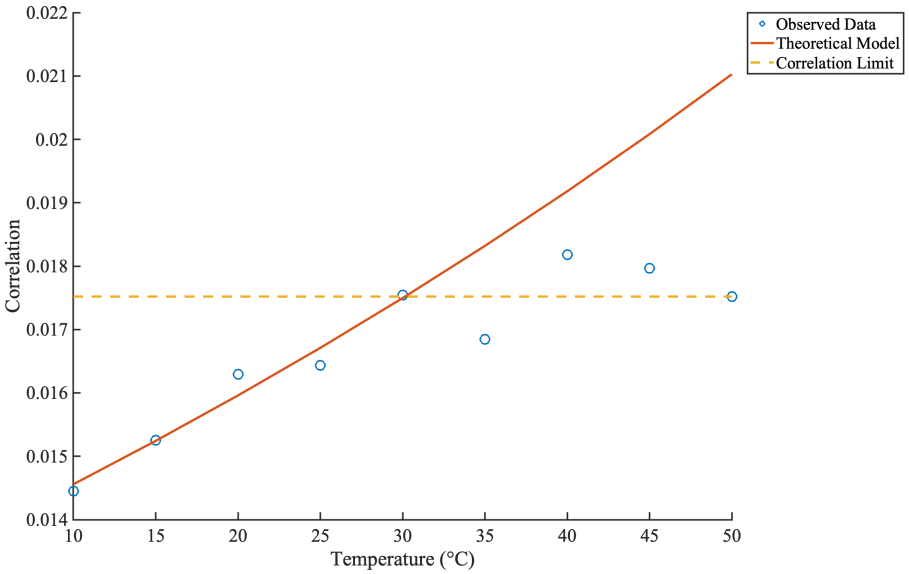

Figure 7.10: Correlation versus temperature plot for camera three showing the correlation increase in accordance with the theoretical model to a limit which corresponds to the temperature of the image sets under test. Camera 3 Identified Temperature 30.15°C

the exact temperature required for each set. As such, all images under test were taken over the range T=30°C+/-2 due to the thermal balance of the equipment used. The temperature sensor used for these experiments was an MCP9808. The sensor bounced around the setpoint due to several reasons including observed self-warming on the sensor during image capture and environmental conditions. As such, at the extremes of temperature, it would become difficult to wait for the experimental apparatus to set upon a fixed temperature. To ensure a prohibitively long time was not needed to acquire images, all images were taken over a maximum 4°C range of the target temperature. When averaged this could cause the expected temperature of the image set to be between 28°C and 32°C however, it is more likely than not that the average of the images would be 30°C. Unfortunately, the temperature of the images under test was not recorded in the EXIF metadata meaning the exact temperature could not be independently verified.

The MCP9808 temperature device used in these experiments has an overall

Table 7.2: Identified Temperature of Image Sets

	Identified Temp (°C)	Forensic Range (°C)	Actual Range (°C)
Camera 01	30.5	26.0 - 35.0	28.0 - 32.0
Camera 02	28.35	23.85 - 32.85	28.0 - 32.0
Camera 03	30.15	25.65 - 34.65	28.0 - 32.0

accuracy of +/-0.25°C. Accuracies should, therefore, add to obtain an overall error of +/-4.5°C of the expected target temperature of 30°C. Once this analysis is taken into account, we see that each camera has an accurate temperature result. We see that for each camera the forensic range should be as indicated in table 7.2. From here we see that the result from each camera is aligned to the actual range of the temperature taken during the image acquisition phase.

7.6 Discussion

In our work presented here, it is not the first time DSN has been used as a forensic trace. However, it is the first time that a temperature dependency has been observed and used for forensic inference. While the work of [32, 41] identified the use of DSN for unique forensic identification it is only now that we have further used the theory as presented in [10] to determine the temperature that the image sensor was at during image capture. Determining temperature using SPN methods is contrary to the existing narrative seen in [12, 13] who suggest sensor pattern noise methods are immune to temperature variance. This is particularly relevant since in our work we have used DSN reference patterns against noise residuals which are traditionally used for PRNU based methods. Our image sets thus contain both DSN and PRNU making up PNU.

Critically in this work, we have demonstrated once again a bias present within the noise residues which is linked to the lens system of the camera. Observing lens effects in such a manner reinforces the work of [80,83,84] showing that the PRNU component of the PNU is excited differently due to the path discrete photons travel through each lens element. This is, however, contrary

to the existing understanding of the SPN method whereby the image is tied uniquely to the image sensor with no contamination from sources which are not unique to the individual camera such as interchangeable lenses. Further investigation into this lens effect may lead to an understanding of why SPN based methods can provide discrimination of make and model and not just individual cameras as seen in [92]. Lenses may especially be relevant in [92] since mobile phone cameras are built with integrated lenses.

Whereas the current literature has shown a distinct direction in optimising filters used for sensor-based methods [86] to create more timely results we have began a new focus to enable faster processing times. Such an approach may sacrifice precision. Lower precision does not lower the usefulness of the tool. The quicker exclusions can be made in the field means a focused effort can be made in a laboratory environment on evidence that requires robust examination. This would counter the current practice of bringing most devices back to digital forensic laboratories and allow a more efficient expenditure of resources. Excluding devices is particularly relevant in the application of images on what [93] refer to as Type 2 and Type 3 mobile devices. These are devices in which large amounts of stored data including images which have the ability to store such data indefinitely. Efficient resourcing to allow time critical decisions is paramount when forensic intelligence is looked at in the military context where time can be of the essence due to the involvement of austere environments, sensitive and high profile targets and the resultant need for rapid execution [94]. By indicating how a simple, good enough "Goldilocks" filter can cut down on analysis times, we suggest such tools can be adopted into on-site triage packages resulting in a more focused application of search warrants and more efficient use of forensic capabilities in the future. More work is required to verify the capability of such filters.

Additionally, we expect that should a filter capable of obtaining the PRNU

in isolation be developed than this result will not be replicable as PRNU is indeed temperature invariant [12]. It is important to once again affirm that the noise residues being used in PRNU identification do not only contain PRNU, but are in fact SPN residues. This is a critical and important distinction to be made and is why our temperature identification methodology proposed her works.

7.7 Conclusion and Future Work

In this chapter, we have demonstrated a temperature bias in the method as first shown in [12] and expanded upon in [41]. This temperature bias present relates to the presence of dark current within an image and proves to be a useful forensic trace in its own right. We use this trace to isolate the temperature that an image is taken at independent of other sources such as EXIF metadata. This result is demonstrated across three CMOS image sensors of the same make and model and is experimentally linked to the dark current of the device. Further, even when engineering designs are implemented to minimise the effects of dark current at the sensor silicon level, the effects of temperature on the SPN methods are still apparent indicating dark current is never completely removed.

This study is, however, only an initial study into this physical phenomenon and should be conducted on a much broader sample. In the course of this study, we were exposed to a limitation in the ability of our lighting apparatus. This limitation resulted in an inability to vary the intensity of light that a scene was illuminated with. This work should be replicated using various exposure times and light intensity to measure the effects of dark current more thoroughly on the sensor pattern identification methods for the blind source camera problem. It is expected that light would also result in a variation in raw correlation obtained for each positive match. Such variances in correlation are expected to stack per the additive noise model and exacerbate the effects of either temperature or

light intensity.

Additionally, our small sample of image sensors means that this study is not an all-encompassing commentary on the issue of the thermal effect of SPN. Given the vast array of CCD sensors still in use, and the fact that their technology is significantly different to the active pixel CMOS sensors used in this study, verification on CCD sensors should be considered. Since the mobile imaging market is significantly increasing in size and complexity (for example Apple products with multiple sensors for a single image) a more extensive array of tests against CMOS sensors should also be conducted as future work. This initial study, however, has demonstrated a significant change in thinking to the current literature that SPN methods are immune to temperature dependency and thus, a new avenue of research is now opened to explore and exploit this phenomenon for forensic purposes.

Chapter 8

Discussion

8.1 Introduction

In this chapter the main findings of the thesis are summarised and contextualised within the existing literature. These findings fall into three main categories: applied signal processing theory, forensic indicators from manufacturing process variations, and findings for specific forensic indicators already used to solve the blind source camera identification problem. Each finding is discussed in turn with reference to the existing literature noting where the same ideas are reinforced and where new divergent theory has been discovered. By outlining where the theory diverges and converges the body of knowledge is moved closer towards a unified theory of sensor pattern noise for the identification of digital cameras in a forensic context.

8.2 Applied Signal Processing Theory - A new model for Pixel Non Uniformity

We start with a discussion of the signal processing methods that have been applied in this work that have previously not been seen or have been used to obtain other conclusions. The concept of sensor pattern noise (SPN) for

discrete identification of individual sensors is not original. It was introduced in the context of dark current in [32] and further elaborated upon in [41] in a hybrid template alongside photo response non-uniformity (PRNU) noise. PRNU was first introduced in the work of [12] some years prior where it was shown that PRNU could be obtained from the use of a noise free image obtained through the use of a de-noising filter subtractive cancelling everything but the noise remaining in an image under test (IUT). Through the work of Chapter 6 it has now been demonstrated that lens effects are also present within the noise residues used in these SPN methods. This reinforces the findings of [60] who demonstrated that lens aberrations were able to be used to uniquely identify source camera lenses. This is the first time however, that this has been done via SPN methodologies.

As discussed above, the existing literature has already demonstrated that SPN can be filtered to obtain forensic indicators which are unique to aspects of the camera including the sensor specifically. To uniquely identify a camera, matching an image to the image sensor provides a link that cannot be easily disrupted. Other methods of matching often link only to make or model of camera and not a discrete camera in its own right. To identify a sensor, SPN takes advantage of pixel non-uniformity (PNU). This work has demonstrated (Chapter 5) that PNU is made up of any defect within the ability of a sensor to convert photons to electrons in a repeatable fashion. From an electrical engineering perspective this can include any tolerance within the manufacture of layers which makes up the circuitry of a discrete sensor including the lens structures, Bayer filters, photodiode and associated read out circuitry. This is discussed further in Section 8.3.

While PNU is caused by any unique aspect of a sensor to convert light to charge, using the SPN method PNU is practically seen as any high frequency noise which survives filtering as described above. This method captures poten-

tial forensic traces such as PRNU, dark current and lens effects. It is worth nothing that the lens effects which make up PNU are from the micro lens and sub lens (if present) which focuses light into the individual photodiode as part of the sensor design and not the main lens which focuses light onto the sensor. This is divergent to the model as presented in [12]. Lens effects from the main LOS can still be present in the SPN method. However this is not a trace which makes up PNU. Non unique signals also survive this filtering process for discrete images such as random noise and high frequency image content. These non unique signals contaminate the correlation from a signal processing perspective and cause low correlation scores even when a positive match is detected. The impact of these non unique signals, what is effectively a random noise, can be reduced through the use of averaging multiple frames with dissimilar scene content.

Removing these unwanted signals through frame averaging is not the only way to obtain greater accuracy and precision. Through the use of appropriately designed filters a more accurate and precise estimation of the trace under examination can be isolated. This trace can be one of either PRNU, dark current or other individual aspects which make up PNU or it can be a combination of these unique traces to obtain greater statistical significance. Appropriately chosen filters can also be used to prioritise speed ahead of precision. Such prioritisation can be beneficial for applications such as forensic triage of large amounts of data. In addition to purpose built filters, methods in the signal processing discipline can be applied with great effect to clean and polish the existing SPN methods. Such methods include accounting for edge effects, a technique regularly implemented for Fourier transforms which has been used to great effect in this work.

It remains to be seen if smaller amounts of data can be used to create a robust forensic reference pattern for a unique sensor. The work to date suggests

that as the forensic certainty increases with each additional trace that can be obtained from the noise residue then the amount of unique data required to identify the sensor should decrease. This hypothesis remains to be tested.

8.3 Forensic Indicators from Process Variations

Image sensors, much like any consumer device, are made to a margin usually defined by cost. To make any device to this margin tolerances are required to be defined by the responsible design engineers. The tighter the tolerance, the more expensive the device is to make. Design tolerances are seen as the bounds setting the small variations in between sensors. These small variations can be exploited to uniquely identify one sensor over another. Much like any variation in manufacturer or material quality, these small variations can be visually inspected. Sensors that are outside of the defined tolerance are scrapped and not on-sold to consumers. From Chapter 5 we can see that variations can be seen on such areas of an image sensor as the Bayer filters, micro lens, photodiode and read out circuitry when examined under a scanning electron microscope.

If Bayer coatings are not uniform on each pixel unit on an image sensor it will cause some pixels to become hotter than others due to different wavelengths of light entering the photodiode. Different wavelengths being captured will cause different amounts of photons to enter an individual pixel than its neighbour at the "same" wavelength. Such differences reinforce the hot pixel theory for sensor identification [32] and provides a hypothesis as to why pixels can be hotter in some images but remain within normal values for others. The hypothesis to be tested is that the Bayer filter is not efficient or effective and is thus reacting differently as light is entering the photo diode through different sections of the filter. This should be further examined using point light sources at isolated frequencies. The same issue could also be seen in the filter masks used during the CMOS manufacturing process providing another source of process variation.

This work has began the process of establishing a cause for PNU as variations during the manufacturing process. To conclusively assert process variations as a cause of PNU, robust, large scale testing is required across a wider sample of image sensors from a wider range of manufacturers. In this work we have only examined one image sensor from one manufacturer. The process may differ by manufacturer and by discrete image sensor. Process variation would cause discrete changes which can be taken advantage of however, there has been no evidence presented in this work to suggest that. [95] recently showed that SPN methodologies can be used to identify image sensor make and model and not just a discrete sensor when analysed against large enough data. This would suggest that process variations are indeed a cause of forensic difference which can be used to advantage.

8.4 Specific Forensic Indicator Findings

In this work, one of the key concepts explored in the SPN methodology is that using different reference patterns keyed into different forensic indicators will yield different results from the IUT. As seen in 6, three of these traces are PRNU, lens effects and dark current. We now revise these traces in detail.

8.4.1 Photo Response Non-Uniformity

As demonstrated in 6, PRNU is the strongest of the three traces analysed. PRNU contains the most amount of signal power followed by lens effects than dark current. This supports that the PRNU approach to the SPN method is not just valid but is the correct approach to obtain the the strongest possibility for correlation. This work reinforces the validity of [12].

8.4.2 Lens Optical System

The lens system of a camera provided the second strongest signal in the analysis presented here. If this lens is static to the camera under test then it will

cause an increase in correlation however, if the lens is mismatched then the correlation will be negatively affected. Since PRNU dominates the SPN in the methodologies used in this work the correlation still performed a positive match even with mismatched lenses showing that an accurate match is possible even with mismatched lenses.

Extending this concept, the work discussed in Chapter 5 showed that the lens system unique to the image sensor itself is a likely contributor to PNU. Misalignment with the micro lens or sub lens structures can form additional aberrations in addition to the lens optical system of the camera. These aberrations cannot be easily removed or substituted between image sensor, camera makes and models even with the use of specialised hardware. As such it is likely that these will cause PNU on a sensor. Further examination is required.

8.4.3 Dark Current

The most significant finding of this work is that the temperature of an image can be determined through analysis of an image's dark current. By using a specifically constructed reference pattern containing only dark current at set reference temperatures the temperature of the image can be determined. This is documented in Chapter 7. Most importantly, it shows that SPN methods are temperature dependant correcting a misconception documented in [12, 13]. It also reinforces the work of [32, 41] which demonstrated that dark current can be used in conjunction with PRNU to obtain a positive match. The conclusions that have been documented however have been drawn from one make and model of image sensor. While dark current is present in all image sensors the conclusions that have been reached are only applicable to the Sony IMX219PQ image sensor that has been used in this work. This study should be extended to a wider sample including those from other manufacturers to ensure it is not a characteristic of a unique process variation. however, given the theory presented in [10], it is unlikely that these findings are isolated to a unique process

variation.

8.5 Conclusion

Several new areas of research have been opened up by this thesis with many more being reinforced. It is recommended to the community that future work is conducted to reinforce the findings, particularly with a focus to develop sound, effective and efficient triage tools and methods for the on-scene investigator. This is of particular importance to time critical investigations as those seen in austere environments that the military continually finds themselves operating in.

Chapter 9

Conclusion

This thesis has explored the science behind SPN methods used for camera identification in the context of the Blind Source Camera Identification problem. It has been demonstrated in Chapter 7 that it is possible to create a method which uses fewer resources than the currently accepted methods to solve this problem. Critically this was demonstrated in Table 7.1 through the use of a DCT filter with the same cut-off frequency as the existing literature. This method can be further refined to further reduce resources required. Dark current and lens effects have been shown to contaminate SPN. This is apparent even when DSN is reduced through on-chip methods. Since these noises contaminate the signal it is possible to use this to our advantage. A more precise match can be obtained by using these multiple sources of noise when correlating an image to a reference pattern. It has also been demonstrated that the temperature of an image at time of capture can be determined from careful analysis of the DSN correlated against reference dark images taken at known temperatures. Understanding SPN methods in this context will provide greater certainty to the law enforcement and intelligence communities moving forward.

Bibliography

[1] ECPAT International, *Towards a Global Indicator on Unidentified Victims in Child Sexual Exploitation Material*. INTERPOL, 2018.

[2] Department of Foreign Affairs and Trade, *Australia's International Cyber Engagement Strategy*. Commonwealth of Australia, 2017.

[3] Institute for Security Studies, *Riding the digital wave The impact of cyber capacity building on human development*. European Union, 2014.

[4] M. Kochavi, P. Richardson, and B. Shebar, *Dark Net: Exploit*. Showtime, 2016.

[5] Office on Drugs and Crime, *Protecting the Future: Improving the Response to Child Sex Offending in Southeast Asia*. United Nations, 2014.

[6] J. Lukáš, J. Fridrich, and M. Goljan, "Determining digital image origin using sensor imperfections," in *Electronic Imaging 2005*. International Society for Optics and Photonics, 2005, pp. 249–260.

[7] National Research Council *et al*, *Strengthening forensic science in the United States: a path forward*. National Academies Press, 2009.

[8] M. Goljan, J. Fridrich, and T. Filler, "Large scale test of sensor fingerprint camera identification," in *Media Forensics and Security*, vol. 7254. International Society for Optics and Photonics, 2009, p. 72540I.

[9] D. Wei and A. Bovik, "Wavelet denoising for image enhancement," in *Handbook of Image and Video Processing*, A. Bovik, Ed. Academic Press, 2000, ch. 3.4.

[10] G. C. Holst and T. S. Lomheim, *CMOS/CCD Sensors and camera systems, 2nd Edition*. SPIE Press, 2011.

[11] J. Lukáš, J. Fridrich, and M. Goljan, "Digital" bullet scratches" for images," in *Image Processing, 2005. ICIP 2005. IEEE International Conference on*, vol. 3. IEEE, 2005, pp. III–65.

[12] J. Lukas, J. Fridrich, and M. Goljan, "Digital camera identification from sensor pattern noise," *IEEE Transactions on Information Forensics and Security*, vol. 1, no. 2, pp. 205–214, 2006.

[13] Z. Ba, S. Piao, X. Fu, D. Koutsonikolas, A. Mohaisen, and K. Ren, "Abc: Enabling smartphone authentication with built-in camera," in *Network and Distributed System Security Symposium*, San Diego, United States of America, February 2018, pp. 1–15. [Online]. Available: http://dx.doi.org/10.14722/ndss.2018.23107

[14] J. Fridrich and M. Goljan, "Determining approximate age of digital images using sensor defects," in *IS&T/SPIE Electronic Imaging*. International Society for Optics and Photonics, 2011, pp. 788 006–788 006.

[15] K. San Choi, E. Y. Lam, and K. K. Wong, "Automatic source camera identification using the intrinsic lens radial distortion," *Optics express*, vol. 14, no. 24, pp. 11 551–11 565, 2006.

[16] S. Knight, S. Moschou, and M. Sorell, "Analysis of sensor photo response non-uniformity in raw images," in *International Conference on Forensics in Telecommunications, Information, and Multimedia*. Springer, 2009, pp. 130–141.

[17] F. A. Jenkins and H. E. White, *Fundamentals of optics*. Tata McGraw-Hill Education, 1957.

[18] E. Hecht, "Optics," *Addison Weley*, 2002.

[19] G. A. Lloyd and S. J. Sasson, "Electronic sstill camera," Dec. 26 1978, u.S. Patent 4,131,919.

[20] W. Boyle and G. Smith, "Information storage devices," Dec. 31 1974, patent 3,858,232.

[21] M. F. Tompsett, "Charge transfer imaging devices," Apr. 18 1978, patent 4,085,456.

[22] B. E. Bayer, "Color imaging array," Jul. 20 1976, uS Patent 3,971,065.

[23] J. Janesick, "Scientific charge-coupled devices," in *Damage*. SPIE - The International Society for Optical Engineering, 2001, ch. 8.

[24] S. Sasson, "Disruptive innovation: The story of the first digital camera," Oct. 2011, unpublished. [Online]. Available: https://vimeo.com/31404047

[25] E. R. Fossum, S. Mendis, and S. E. Kemeny, "Active pixel sensor with intra-pixel charge transfer," Nov. 28 1995, patent 5,471,515.

[26] E. R. Fossum, "Active pixel sensors: Are ccds dinosaurs?" in *Proc. SPIE Charge-Coupled Devices and Solid State Optical Sensors III*, vol. 1900, Jul 1993, pp. 2–14.

[27] P. D. Moor, "Stacked chip technology – overview of approaches to chip design," in *3D Stacked Chip Sensors – Is There Any Going Back From Here?* Image Sensors Americas 2014, 2014.

[28] R. Fontaine. (2017, June) A survey of enabling technologies in successful consumer digital imaging products: Part 2. Online. TechInsights. https://www.techinsights.com/about-techinsights/overview/blog/survey-of-enabling-technologies-in-successful-consumer-digital-imaging-products-part-2/.

[29] J. R. Janesick, *Scientific charge-coupled devices*. SPIE press, 2001, vol. 83.

[30] Panasonic, Fuji Film. (2013, June) Fujifilm and panasonic jointly develop an organic cmos image sensor technology using organic photoelectric conversion layer. Online. Fuji Film. http://www.fujifilm.com/news/n130611.html. Retrieved via the Internet Archive.

[31] Panasonic. (2018, February) Panasonic develops industry's-first 8k high-resolution, high-performance global shutter technology using organic-photoconductive-film cmos image sensor. Online. Panasonic. https://news.panasonic.com/global/press/data/2018/02/en180214-2/en180214-2.html.

[32] K. Kurosawa, K. Kuroki, and N. Saitoh, "Ccd fingerprint method-identification of a video camera from videotaped images," in *Image Processing, 1999. ICIP 99. Proceedings. 1999 International Conference on*, vol. 3. IEEE, 1999, pp. 537–540.

[33] "Strachan v HMA," 2009. HCJAC 3.

[34] N. Khanna, A. K. Mikkilineni, G. T. Chiu, J. P. Allebach, and E. J. Delp, "Scanner identification using sensor pattern noise," in *Security, steganography, and watermarking of multimedia contents IX*, vol. 6505. International Society for Optics and Photonics, 2007, p. 65051K.

[35] R. Caldelli, I. Amerini, and F. Picchioni, "A dft-based analysis to discern between camera and scanned images," *IJDCF*, vol. 2, pp. 21–29, 2010.

[36] M. Chen, J. Fridrich, M. Goljan, and J. Lukáš, "Source digital camcorder identification using sensor photo response non-uniformity," in *Security,*

Steganography, and Watermarking of Multimedia Contents IX, vol. 6505. International Society for Optics and Photonics, 2007, p. 65051G.

[37] N. Bartlow, N. Kalka, B. Cukic, and A. Ross, "Identifying sensors from fingerprint images," in *Computer Vision and Pattern Recognition Workshops, 2009. CVPR Workshops 2009. IEEE Computer Society Conference on.* IEEE, 2009, pp. 78–84.

[38] M. A. Berger, "Procedural paradigms for applying the daubert test," *Minn. L. Rev.*, vol. 78, p. 1345, 1993.

[39] M. Al-Ani and F. Khelifi, "On the spn estimation in image forensics: A systematic empirical evaluation," *IEEE Transactions on Information Forensics and Security*, vol. 12, no. 5, pp. 1067–1081, 2017.

[40] Z. J. Geradts, J. Bijhold, M. Kieft, K. Kurosawa, K. Kuroki, and N. Saitoh, "Methods for identification of images acquired with digital cameras," in *Enabling technologies for law enforcement and security*, vol. 4232. International Society for Optics and Photonics, 2001, pp. 505–513.

[41] K. Kurosawa, K. Kuroki, K. Tsuchiya, N. Igarashi, and N. Akiba, "Case studies and further improvements on source camera identification," in *Proc.SPIE*, vol. 8665, 2013, pp. 8665 – 8665 – 14.

[42] P. L. V. Seidel, *Über den Einfluss der Theorie der Fehler, mit welchen die durch Optische Instrumente gesehenen Bilder behaftet sind, und über die mathematischen Bedingungen ihrer Authebung.* Abhandlungen der naturwissenschaftlich-technischen Commission der Bayerischen Akademie der Wissenschafte, 1857.

[43] E. J. Alles, Z. J. Geradts, and C. J. Veenman, "Source camera identification for heavily jpeg compressed low resolution still images," *Journal of forensic sciences*, vol. 54, no. 3, pp. 628–638, 2009.

[44] *CIPA DC- 008-Translation- 2012 Exchangeable image file format for digital still cameras:Exif Version 2.3*, Standard of the Camera and Imaging Products Association Std., Rev. 2.3, December 2012.

[45] R. Matthews. (2017, June) Explainer: how law enforcement decodes your photos. Online. The Conversation. https://theconversation.com/explainer-how-law-enforcement-decodes-your-photos-78828.

[46] M. Sorell, "Digital camera photographic provenance," in *Handbook of Research on Computational Forensics, Digital Crime, and Investigation: Methods and Solutions.* IGI Global, 2010, pp. 104–129.

[47] A. Zamfir, A. Drimbarean, M. Zamfir, V. Buzuloiu, E. Steinberg, and D. Ursu, "An optical model of the appearance of blemishes in digital photographs," in *Digital Photography III*, vol. 6502. International Society for Optics and Photonics, 2007, p. 65020I.

[48] A. E. Dirik, H. T. Sencar, and N. Memon, "Digital single lens reflex camera identification from traces of sensor dust," *IEEE Transactions on Information Forensics and Security*, vol. 3, no. 3, pp. 539–552, 2008.

[49] H. Farid, *Photo forensics*. MIT Press, 2016.

[50] A. A. C. SWINTON, "Electric television," *Nature*, vol. 118, no. 2973, pp. 590–590, Oct 1926. [Online]. Available: http://dx.doi.org/10.1038/118590a0

[51] H. Iams and A. Rose, "Television pickup tubes with cathode-ray beam scanning," *Proceedings of the Institute of Radio Engineers*, vol. 25, no. 8, pp. 1048–1070, Aug 1937.

[52] A. A. C. SWINTON, "Distant electric vision," *Nature*, vol. 78, no. 2016, pp. 151–151, Jun 1908. [Online]. Available: http://dx.doi.org/10.1038/078151a0

[53] W. Boyle and G. Smith, "Buried channel charge coupled devices," Feb. 12 1974, uS Patent 3,792,322.

[54] ——, "Three dimensional charge coupled devices," Mar. 12 1974, uS Patent 3,796,927.

[55] K. Matsumoto, T. Nakamura, A. Yusa, and S. Nagai, "A new mos phototransistor operating in a non-destructive readout mode," *Jpn. J. Appl. Phys.*, vol. 24, no. 5, pp. L323–L325, May 1985.

[56] A. J. Theuwissen, "Cmos image sensors: State-of-the-art," *Solid-State Electronics*, vol. 52, no. 9, pp. 1401–1406, Sep 2008. [Online]. Available: http://linkinghub.elsevier.com/retrieve/pii/S0038110108001317

[57] K. Fife, A. El Gamal, and H.-S. P. Wong, "A 3M pixel multi-aperture image sensor with 0.7 μm pixels in 0.11 μm cmos," in *2008 IEEE International Solid-State Circuits Conference - Digest of Technical Papers*. IEEE, Feb 2008, pp. 48–594. [Online]. Available: http://ieeexplore.ieee.org/document/4523050/

[58] ePHOTOzine, "Complete guide to image sensor pixel size." [Online]. Available: https://www.ephotozine.com/article/complete-guide-to-image-sensor-pixel-size-29652

[59] F. A. Jenkins and H. E. White, *Fundamentals of optics*. Tata McGraw-Hill Education, 1937.

[60] K. San Choi, E. Y. Lam, and K. K. Wong, "Source camera identification using footprints from lens aberration," *Digital Photography II*, vol. 6069, p. 60690J, 2006.

[61] S. Bayram, H. Sencar, N. Memon, and I. Avcibas, "Source camera identification based on cfa interpolation," in *Image Processing, 2005. ICIP 2005. IEEE International Conference on*, vol. 3. IEEE, 2005, pp. III–69.

[62] E. W. Bogaart, W. Hoekstra, I. M. Peters, A. C. M. Kleimann, and J. T. Bosiers, "Very low dark current ccd image sensor," *IEEE Transactions on Electron Devices*, vol. 56, no. 11, pp. 2462–2467, Nov 2009. [Online]. Available: http://ieeexplore.ieee.org/document/5247096/

[63] R. M. Smith and G. Rahmer, "Pixel area variation in ccds and implications for precision photometry," in *High Energy, Optical, and Infrared Detectors for Astronomy III*, vol. 7021. International Society for Optics and Photonics, 2008, p. 70212A.

[64] Sony, "IMX219PQ Product Brief," https://www.sony-semicon.co.jp/products_en/IS/sensor1/img/products/ProductBrief_IMX219PQ_20160425.pdf.

[65] FEI, "Helios nanolab 450 / 450 s / 450 ml / 650 / 600i user operation manual v51," https://mc2.engin.umich.edu/wp-content/uploads/sites/227/2015/11/Helios.pdf, accessed 7/01/2019.

[66] "Daubert v. Merrell Dow Pharmaceuticals, Inc." 509 U.S. 579 (1993).

[67] S. Rizzolo, V. Goiffon, M. Estribeau, O. Marcelot, P. Martin-Gonthier, and P. Magnan, "Influence of pixel design on charge transfer performances in cmos image sensors," *IEEE Transactions on Electron Devices*, vol. 65, no. 3, pp. 1048–1055, March 2018.

[68] E. R. Fossum and D. B. Hondongwa, "A review of the pinned photodiode for ccd and cmos image sensors," *IEEE Journal of the Electron Devices Society*, vol. 2, no. 3, pp. 33–43, May 2014.

[69] A. Chandrakanta and H. Devassy, "The non-uniform characteristics of a photodiode," *International Advanced Research Journal in Science, Engineering and Technology*, 2017.

[70] Sony Semiconductor, Japan, "IMX219PQ data sheet," https://www.sony-semicon.co.jp/products_en/new_pro/april_2014/imx219_e.html, accessed 7/01/2019.

[71] ——, "IMX219PQH5 Module Design Reference Manual v2.2," https://github.com/rellimmot/Sony-IMX219-Raspberry-Pi-V2-CMOS/blob/master/IMX219PQH5_Module_Design_Reference_Manual_ver2.2_140425.pdf, accessed 7/01/2019.

[72] ——, "IMX219PQH5-C data sheet," https://github.com/rellimmot/Sony-IMX219-Raspberry-Pi-V2-CMOS/blob/master/RASPBERRY%20PI%20CAMERA%20V2%20DATASHEET%20IMX219PQH5_7.0.0_Datasheet_XXX.PDF, accessed 7/01/2019.

[73] S. Tyagi, M. Alavi, R. Bigwood, T. Bramblett, J. Brandenburg, W. Chen, B. Crew, M. Hussein, P. Jacob, C. Kenyon, C. Lo, B. McIntyre, Z. ma, P. Moon, P. Nguyen, L. Rumaner, R. Schweinfurth, S. Sivakumar, M. Stettler, and M. Bohr, "A 130 nm generation logic technology featuring 70 nm transistors, dual vt transistors and 6 layers of cu interconnects," in *Technical Digest - International Electron Devices Meeting*, 02 2000, pp. 567 – 570.

[74] J. Schindelin, I. Arganda-Carreras, E. Frise, V. Kaynig, M. Longair, T. Pietzsch, S. Preibisch, C. Rueden, S. Saalfeld, B. Schmid *et al.*, "Fiji: an open-source platform for biological-image analysis," *Nature methods*, vol. 9, no. 7, p. 676, 2012.

[75] Scientific Working Group on Digital Evidence, "SWGDE establishing confidence in digital forensic results by error mitigation analysis," https://www.swgde.org/documents/Current%20Documents/SWGDE%20Establishing%20Confidence%20in%20Digital%20Forensic%20Results%20by%20Error%20Mitigation%20Analysis, 2017, unpublished.

[76] M. K. Johnson and H. Farid, "Exposing digital forgeries through chromatic aberration," in *Proceedings of the 8th workshop on Multimedia and security*. ACM, 2006, pp. 48–55.

[77] R. Widenhorn, M. M. Blouke, A. Weber, A. Rest, and E. Bodegom, "Temperature dependence of dark current in a ccd," in *Sensors and Camera Systems for Scientific, Industrial, and Digital Photography Applications III*, vol. 4669. International Society for Optics and Photonics, 2002, pp. 193–202.

[78] A. E. Dirik, H. T. Sencar, and N. Memon, "Flatbed scanner identification based on dust and scratches over scanner platen," in *Acoustics, Speech and Signal Processing, 2009. ICASSP 2009. IEEE International Conference on*. IEEE, 2009, pp. 1385–1388.

[79] A. Mehrish, A. Subramanyam, and M. Kankanhalli, "Multimedia signatures for vehicle forensics," in *Multimedia and Expo (ICME), 2017 IEEE International Conference on*. IEEE, 2017, pp. 685–690.

[80] R. Matthews, M. Sorell, and N. Falkner, "An analysis of optical contributions to a photo-sensor's ballistic fingerprints," *arXiv preprint arXiv:1808.08684*, 2018, , "unpublished".

[81] ——, "Rethinking image sensor noise for forensic advantage," *arXiv preprint:1808.07971*, Submitted for publication.

[82] M. Goljan, M. Chen, P. Comesaña, and J. Fridrich, "Effect of compression on sensor-fingerprint based camera identification," *Electronic Imaging*, vol. 2016, no. 8, pp. 1–10, 2016.

[83] R. Matthews, M. Sorell, and N. Falkner, "Isolating lens aberrations within fixed pattern noise," in *Proceedings of the 3rd Interdisciplinary Cyber Research Workshop*. Tallinn, Estonia: Tallinn University of Technology, June 2017, pp. 21–24.

[84] ——, "Isolating lens effects from source camera identification using sensor pattern noise," *Australian Journal of Forensic Sciences*, pp. 1–4, 2019. [Online]. Available: https://doi.org/10.1080/00450618.2019.1569133

[85] C.-T. Li, "Source camera identification using enhanced sensor pattern noise," *IEEE Transactions on Information Forensics and Security*, vol. 5, no. 2, pp. 280–287, 2010.

[86] A. Lawgaly and F. Khelifi, "Sensor pattern noise estimation based on improved locally adaptive dct filtering and weighted averaging for source camera identification and verification," *IEEE Transactions on Information Forensics and Security*, vol. 12, no. 2, pp. 392–404, 2017.

[87] N. Khanna, A. K. Mikkilineni, and E. J. Delp, "Forensic camera classification: Verification of sensor pattern noise approach," *Federal Bureau of Investigation: Forensic Science Communications*, vol. 11, no. 1, January 2009.

[88] D. Bessette, "What is sony's exmor technology anyway?" https://www.framos.com/en/news/what-is-sony-s-exmor-technology-anyway, accessed 27-Nov-2018.

[89] D. Jones, "Picamera release-1.13," https://picamera.readthedocs.io/en/release-1.13/#, accessed 18-Nov-2018.

[90] R. Bowman, "Manually setting raspberry pi camera gains from within python," https://gist.github.com/rwb27/a23808e9f4008b48de95692a38ddaa08/, accessed 18-Nov-2018.

[91] D. Coffin, "Decoding raw digital photos in linux," http://www.cybercom.net/~dcoffin/dcraw/, accessed 18-Nov-2018.

[92] K. Akshatha, A. Karunakar, H. Anitha, U. Raghavendra, and D. Shetty, "Digital camera identification using prnu: A feature based approach," *Digital Investigation*, vol. 19, pp. 69–77, 2016.

[93] R. P. Mislan, E. Casey, and G. C. Kessler, "The growing need for on-scene triage of mobile devices," *Digital Investigation*, vol. 6, no. 3-4, pp. 112–124, 2010.

[94] L. Wilson, M. Gahan, C. Lennard, and J. Robertson, "The black sheep of forensic science: military forensic and technical exploitation," *Australian Journal of Forensic Sciences*, vol. 0, no. 0, pp. 1–13, 2018. [Online]. Available: https://doi.org/10.1080/00450618.2018.1541194

[95] S. Georgievska, R. Bakhshi, A. Gavai, A. Sclocco, and B. van Werkhoven, "Clustering image noise patterns by embedding and visualization for common source camera detection," *Digital Investigation*, vol. 23, pp. 22–30, 2017.